MeMoVolc short course, Santorini, 2015

Field guide to Santorini Volcano

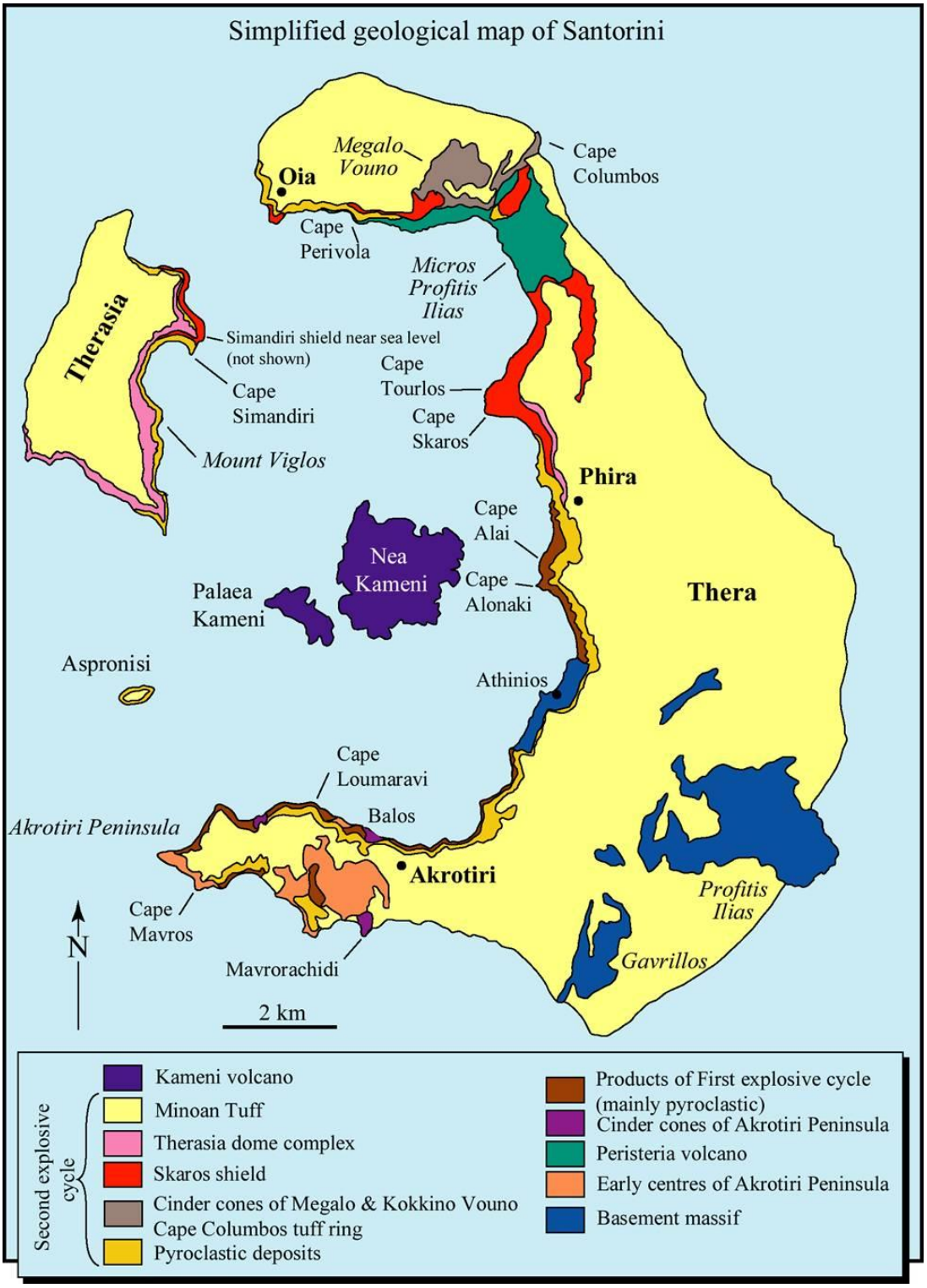

T.H. Druitt (LMV, Clermont-Ferrand, France), with contributions from
L. Francalanci (University of Florence, Italy) and G. Fabbro (EOS, Singapore).

INTRODUCTION

Santorini has fascinated and stimulated explorers and scholars since ancient times. Jason and the Argonauts were apparently visitors to the islands and described a giant called Talos. Molten metal flowed from his feet and he threw stones at them. The legend of Atlantis is plausibly based upon the great Bronze-Age eruption of Santorini. The geographer Strabo described the eruption of 197 BC in the following way:

'*…for midway between Thera and Therasia fire broke forth from the sea and continued for four days, so that the whole sea boiled and blazed, and the fires cast up an island which was gradually elevated as though by levers and consisted of burning masses…*'.

It was Ferdinand Fouqué (1879) who made the first detailed geological study of Santorini, distinguishing three layers in the deposits that buried Bronze-Age buildings. He postulated that the centre of the island sank beneath the sea during the eruption, and was one of the earliest scientists to come up with an interpretation of calderas with the basic elements of modern understanding. Fouqué also carried out some of the first systematic excavations of the prehistoric remains revealed by quarrying of the Bronze-Age deposits.

Numerous studies of Santorini volcanism have been carried out since Fouqué's times. Of particular significance was the work undertaken by Reck (1936), whose comprehensive treatise remains fundamental to modern re-appraisal.

The archaeological importance of Santorini became clear during 1967, when the Greek archaeologist Spyridon Marinatos first uncovered the buried Bronze-Age city of Akrotiri. Marinatos built on the experience of previous excavations by Fouqué and R. Zahn on the coast of southern Thera in order to locate the ancient site. He was motivated by a wish to prove his theory that the eruption of Santorini was the cause of the decline of the Minoan civilisation. Marinatos's theory is no longer considered tenable, but his efforts served to give us one of the richest and best preserved prehistoric cities in the world.

HISTORICAL AND GEOGRAPHICAL PERSPECTIVES

Lying in the southern Aegean sea, 107 km north of Crete, Santorini has played an important role in the cultural development of the region and has a history of occupation stretching far back in time. The traditional names of ***Strongyle*** (the round one) or ***Kallisti*** (the fairest one) reflect the shape and unquestionable beauty of the island cluster.

Although firm evidence of human occupation dates to only 3000-2000 BCE, obsidian finds show that the volcanic Cyclades were being visited by people from mainland Greece as early as the 7th millennium before Christ. By the time of the late-Bronze-Age eruption, an advanced people contemporaneous with the Minoan civilisation on Crete was established in the ancient town of Akrotiri, on the southern coast of the volcano. The eruption buried the town, possibly in the late 17th century BCE, and was followed swiftly by destruction of the Cretan palaces and decline of Minoan culture.

Following the eruption (and at least by the 13th century BCE) Santorini was resettled. The islands were occupied by the Phoenicians then, in the 9th century BCE, by the Lacedaemonians when they became an important stop-over on the east-west trading routes. By this time the name used was ***Thera***, after Theras of Autesion, an early Lacedaemonian leader. In the 2nd century BCE the natural fortifications of the coasts made the islands an important naval base for war campaigns. Following Roman occupation, Christianity reached Thera in the 4th century. From the 9th century until the spread of Christianity, the city of Mesa Vouno was the only urban centre on Thera.

The islands first became known as ***Santorini*** in the 13th century after the small chapel of Santa Irene, which is said to have been either at Perissa or on Therasia. At this time the islands were under Frankish Rule and suffered much from pirates and the feuds between local rulers. The seat of government at this time was the town of Skaro, which was destroyed by earth tremor in the 19th century. The ruins of Skaro are still visible perched on the top of Cape Tourlos, north of Fira. From the 16th to early 19th century the islands were under Turkish domination.

Figure 1. Santorini caldera

REGIONAL TECTONICS

Santorini is the southernmost volcanic centre of the Hellenic volcanic arc, which stretches between Greece and Turkey through the Aegean Sea (Fig. 2). The origin of the volcanism is the subduction of Ionian oceanic lithosphere beneath the Aegean Sea. The subducted slab dips at 10–20° from the Mediterranean Ridge towards the north, as shown by seismic tomography (Fig. 3) and the focal mechanisms of earthquakes between the slab and the overriding Aegean lithosphere (Papazachos and Nolet, 1997; Pearce et al., 2012; Piromallo and Morelli, 2003; Shaw and Jackson, 2010). The slab descends to a depth of 160-180 km at 35 mm/yr (Kalogeropoulos and Paritsis 1990). The subduction vector is N50-60ºE, so that the western (Ionian) trench is related to thrusting, while the eastern (Pliny and Strabo) trenches are dominantly strike-slip in nature (Le Pichon et al. 1979).

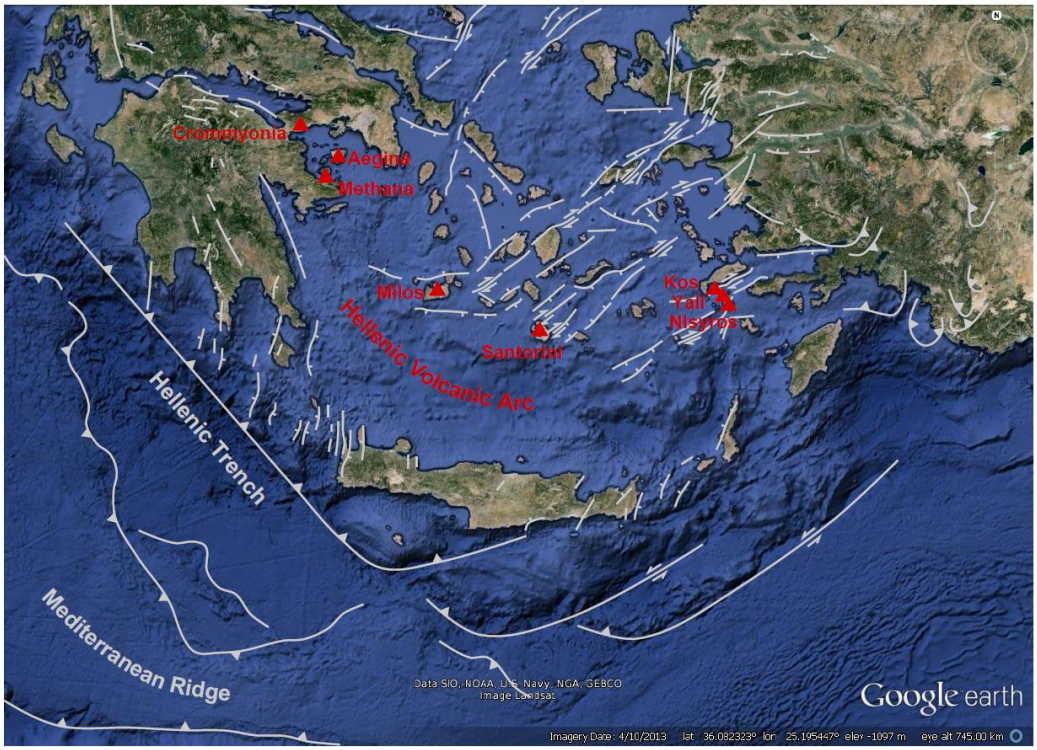

Figure 2. Map of the southern Aegean Sea. Volcanoes of the Hellenic arc are shown in red. Major faults compiled from Jackson (1994), Jolivet and Brun (2010) and Kokkalas and Aydin (2013).

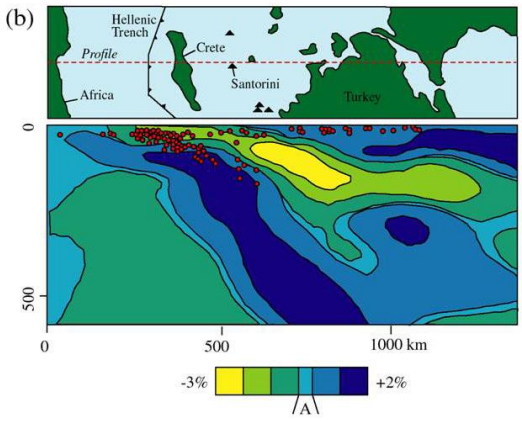

Figure 3. Tomographic images of P-wave velocity heterogeneity (Spakman et al. 1988).

The arc lies ~200 km behind the trench system.

The crust of the Aegean back-arc basin is continental (Makris 1978); thicknesses range from 20 to 30 km compared with 40-50 km under mainland Greece and Turkey, implying a stretching factor of two. Extension has been concentrated in the Cretan and Anatolian Troughs. Between these troughs, the Central Aseismic Plateau forms the relatively stable fault-bounded crustal block on which the Cyclades are situated. The arc volcanic centres are sited along the southern margin of the Central Aseismic Plateau in an extensional stress regime, as shown by normal fault-plane solutions.

The Aegean crust is usually described using a series of rigid blocks, or micro-plates (Jackson, 1994; McKenzie, 1970; Nyst and Thatcher, 2004). However the fact that some deformation occurs within these blocks shows that this model is not strictly valid (Benetatos et al., 2004; Floyd et al., 2010). Deformation in the Aegean is driven principally by two forces: the westwards extrusion of Anatolia along the North Anatolian Fault (McKenzie, 1972), and the southward retreat of the subduction zone by slab roll-back (Le Pichon and Angelier, 1979). Although Africa is currently converging with Eurasia at only 5 mm/yr, slab roll-back means that there is 35 mm/yr of convergence at the Hellenic trench (Nocquet, 2012; Reilinger et al., 2006, 2010). Figure 4 shows the velocity field for the eastern Mediterranean calculated by Nocquet (2012) using GPS measurements. This motion leads to deformation along three dominant trends (Benetatos et al., 2004): (1) north-south extension of the Aegean caused by slab roll-back; (2) trench-parallel extension close to the subduction zone, due to the

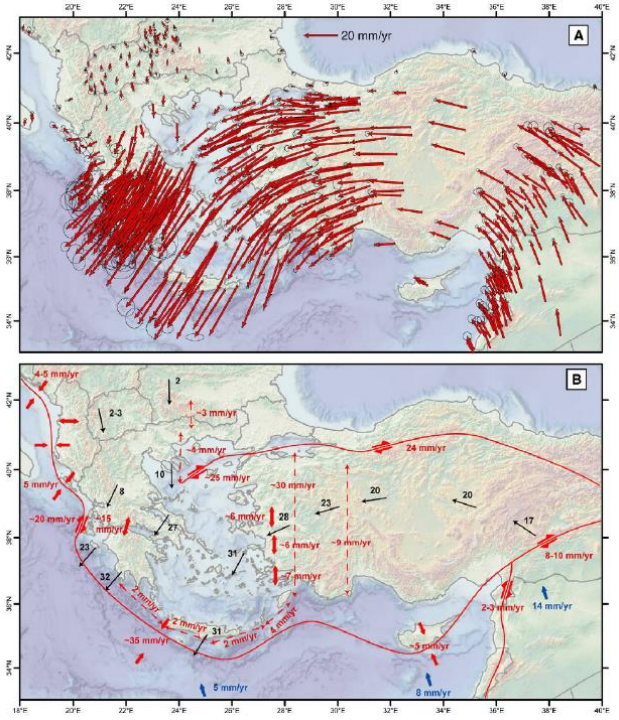

Figure 4. (a) Velocity field in a Eurasia fixed reference frame. (b) Kinematics sketch. Dashed double-arrow lines show integrated relative motion over a given area. Thin black arrows are velocities at selected locations. Taken from Nocquet (2012).

curvature of the trench; (3) right-lateral strike-slip motion, due to the motion of Anatolia and the Aegean relative to the Eurasian plate. The deformation is accommodated on large fault systems. Large earthquakes can occur on these faults, such as the 1956 Ms 7.6 Amorgos earthquake that devastated much of Santorini (Okal et al., 2009; Papadopoulos and Pavlides, 1992). The locations of the volcanoes of the Hellenic arc are controlled by the tectonic structure of the Aegean, lying on lines of weakness in the Aegean crust (Papazachos and Panagiotopoulos, 1993). Milos, Santorini and Nisyros all lie within pull-apart basins along major strike-slip faults (Kokkalas and Aydin, 2013). These same faults are interpreted to have played

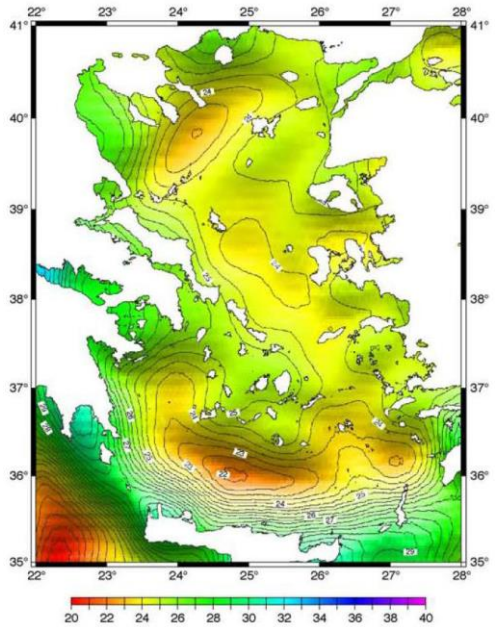

Figure 5. Crustal thickness in km from gravity measurements, isolines every 0.5 km, taken from Tirel et al. (2004).

an important role in controlling the locations of plutons from the Middle Miocene, by provided easy paths for their emplacement.

Extension of the Aegean started 36–25 Ma, and slowed after a tectonic reorganisation that took place in the Pliocene (Jackson, 1994; Jolivet and Faccenna, 2000; Walcott and White, 1998). There was another, short pulse of extension that occurred along the Hellenic Arc at 5.0-4.4 Ma, which led to rapid subsidence of 900m at Milos, and similar subsidence at Aegina (van Hinsbergen et al., 2004). The continental crust of the Aegean has been thinned from about 50km to 20–30km as a result of this extension, and is now about 25km thick under Santorini (Fig. 5; Karagianni et al., 2005; Tirel et al., 2004).

The crustal rocks revealed by this extension record two metamorphic events. There is a first stage of high-pressure, low-temperature metamorphism, related to convergence at the subduction zone. This is followed by a stage of low-pressure, high-temperature metamorphism, as the lithosphere is stretched due to slab roll-back (Avigad and Garfunkel, 1991; Jolivet et al., 2013; Lister et al., 1984; Trotet et al., 2001). The ages of these two metamorphic events get younger as you travel south through the Aegean, as a result of the progressive retreat of the subduction zone. In the Cycladic islands just north of Santorini, the high-pressure, low-temperature metamorphism took place during the Eocene. The low-pressure, high-temperature metamorphism here occurred during the Oligocene and the Miocene. The metamorphic rocks in the Cycladic isles can reach into the blueschist and eclogite facies, as well as containing granites from crustal melting.

HELLENIC ARC VOLCANISM

Volcanic activity in the Aegean started in the Oligocene, and occurred in two main phases with volumetrically subordinate volcanism in between (Fytikas et al., 1984). A first phase from the Oligocene until the Middle Miocene generated a broad belt of calcalkaline volcanism in the NE Aegean. In the middle Miocene a gradual change to more K-rich calcalkaline magmatism occurred, until in late Pliocene time when lavas and ignimbrites of this composition erupted all over the area. Volcanism then migrated to the south with time, due to retreat of the subduction zone (Jolivet and Brun, 2010; Jolivet et al., 2013).

Volcanism of the current island arc system began 3-4 My ago (Keller et al. 1990). Magma production at the western centres has been weak, probably due to the low regional extension rate of 2 mm/yr. Crommyonia and Aegina are small volcanic fields that had become inactive by early Quaternary time. Methana last erupted in about 250 BCE. Centres of the eastern arc (Santorini, Kos, Yali, Nisyros), where the extension rate reaches 26 mm/yr, are considerably more voluminous than those in the west. Volcanism at Kos began 3.4 My ago and

Table. Volcanic centres of the Hellenic Arc

Centre	Magmatic activity	Compositions	Historical activity
Crommyonia	3.9 - 2.7 Ma	Basalt to rhyodacite	None
Aegena	4.4 - 2.1	Basalt to rhyodacite	Weak hydrothermal activity
Methana	<0.9 Ma	Rhyodacite	258 ± 18 BCE lava effusion Weak hydrothermal activity
Milos	3 - 0.09 Ma	Basalt to rhyolite	80 – 205 CE phreatic activity Hydrothermal activity
Santorini	<0.65 Ma Multiple calderas Multiple large ignimbrites up to 60 km^3	Basalt to rhyodacite	1950 lava effusion Weak hydrothermal activity 2011-2012 inflation
Christiana	Unknown; >0.65 Ma	Andesite to rhyodacite	None
Kolumbo	Unknown	Andesite to rhyolite	1650 CE explosive eruption Strong hydrothermal activity
Kos-Nisyros-Yali	<3.4 Ma Multiple calderas 160 ka, 90 km^3 Kos Plateau ignimbrite	Basalt to rhyolite	1422, 1871-73, 1888 phreatic activity Strong hydrothermal activity 1995-2000 inflation

climaxed 160 ky ago with eruption of the ~90 km^3 Kos Plateau Tuff and collapse of a submarine caldera. The subaerial part of Nisyros has developed over the last 66 ky, with at least six explosive eruptions, formation of a subaerial caldera, and historical phreatic activity.

LOCAL TECTONIC FRAMEWORK

Santorini lies on a N50°E trending rift zone at a high angle to the volcanic arc (Nomikou et al. 2013). The main structures are two grabens (Anhydros and Anaphi Basins) separated by a horst (Santorini-Amorgos Ridge) (Fig. 6). To the southwest of Santorini lies the old (pre-650 ka) centre of Christiana, one ignimbrite of which occurs near the base of the volcanic succession on Santorini, and also on Anaphi (Keller et al. 2015). To the northeast lies a chain of 19 submarine cones, the summits of which lie between 18 and 450 m below sea level, deepening to the NE away from Santorini. The largest of these centres is Kolombo, which lies 7 km NE of Santorini and which last erupted in 1650. The crater from that eruption is 1.7 km in diameter, up to 500 m deep, and contains an active hydrothermal field with polymetallic chimneys of sulphides and sulphates. The 1650 eruption (described later) discharged about 2 km^3

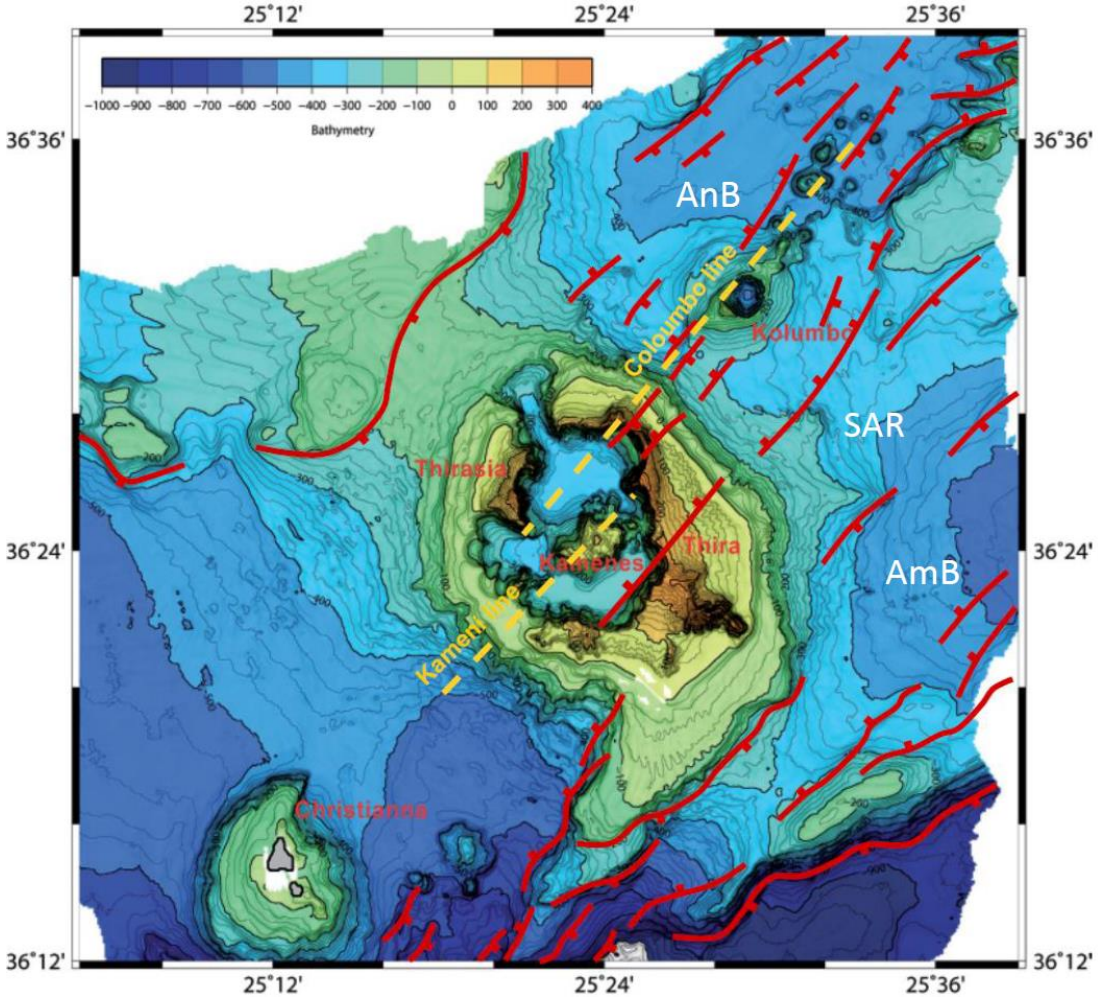

Figure 6. Santorini rift system. AnB: Anhydros Basin; AmB: Anaphi Basin; SAR: Santorini-Amorgos Ridge.

of rhyolitic magma. Modern-day microseismicity in the Santorini region is concentrated beneath Kolombo at depths between 6 and 9 km. An exception was in the unrest period of 2011-2012, when the seismicity focus migrated to Santorini.

STRUCTURE OF SANTORINI

Santorini is a complex of five islands. Thera, Therasia, and Aspronisi are arranged in a ring around a flooded caldera containing the islands of Palaea Kameni and Nea Kameni. The islands are all volcanic apart from the southeastern part of Thera, which is composed of basement lithologies of the Santorini-Amorgos horst. Basement does not crop out north of this, because it is downthrown within the Anhydros graben (Heiken and McCoy, 1984). The islands of Palaea and Nea Kameni postdate Minoan caldera collapse (3.6 ka), and are the subaerial expressions of a predominantly submarine lava shield.

The caldera is a 11 x 7 km composite structure resulting from at least four collapse events (Druitt and Francaviglia, 1992). It is bounded by subaerial cliffs up to 300 m high and consists of three flat-floored basins: a large northern basin 390 m deep, and two smaller ones (western, 320 m and southern; Fig. 8). The caldera is connected to the sea via three breaches: one in the NW, and two in the SW. Two prominent NE-SW lineaments cut the caldera (Fig. 7):

- The Kameni Line cuts the caldera in two, and is defined by alignment of historical vents of Nea Kameni and by epicentres of microseisms during the 2011-12 period of caldera unrest. The Kameni Line is marked by a small fault in the caldera cliff of central Fira, and by a line of gas emission across Thera island (Barberi and Carapezza, 1994).
- The Kolumbo Line runs along the northern limit of the caldera, and is defined by alignments of ancient vents (Megalo Vouno cinder cone, Kokkino Vouno cinder cone, Cape Kolumbo tuff ring).

The two lines are interpreted as deep basement faults parallel to the trend of the Anhydros rift; they have played important roles in guiding magma to the surface and in controlling caldera collapse.

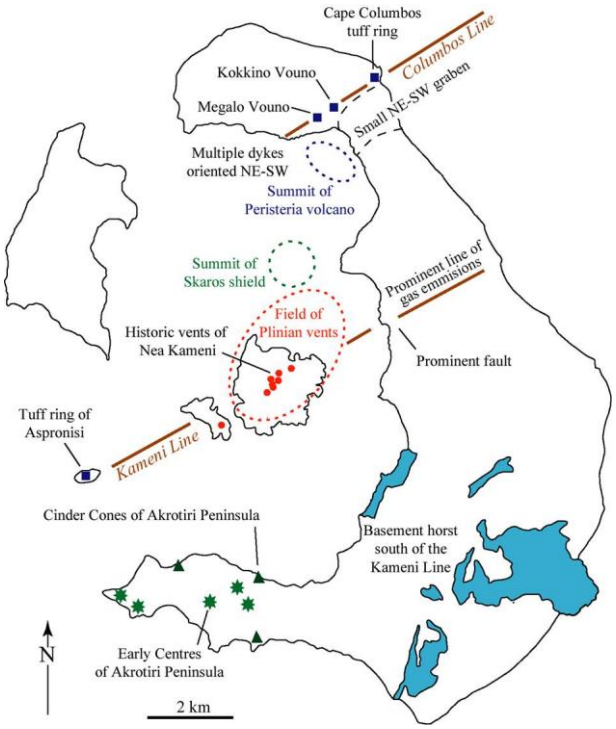

Figure 7. Vent distribution in the Santorini Islands, and the two main volcano-tectonic lineaments (Druitt et al. 1999).

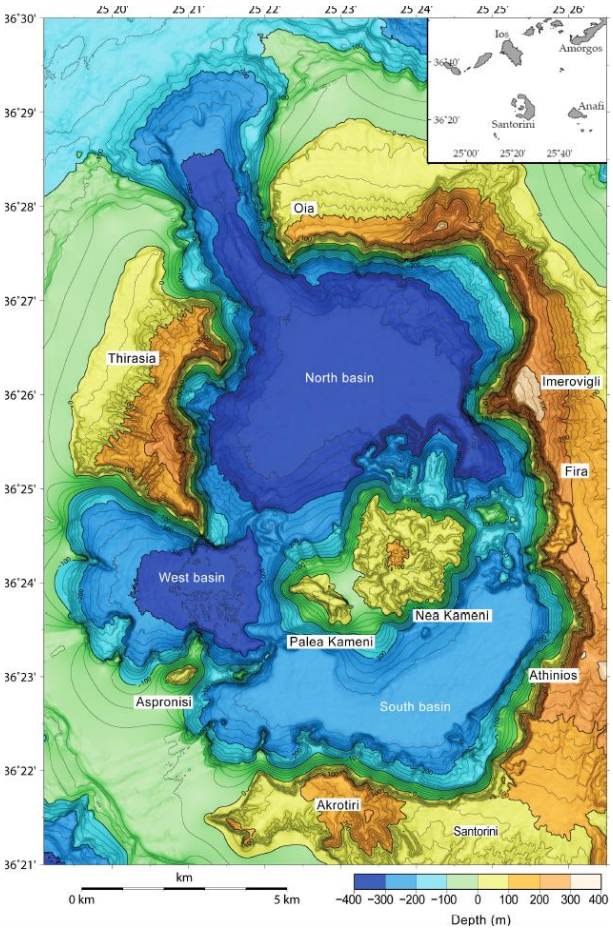

Figure 8: Caldera floor bathymetry (Nomikou et al. 2015).

The caldera is characterised by a negative gravity anomaly elongated parallel to the regional tectonic fabric and is filled with low-density material up to 1 km thick (Budetta et al. 1984) (Fig. 9). High-resolution seismic profiling has imaged the top ~200 m of this fill, revealing three main layers (Johnston et al. 2015) (Fig. 10):

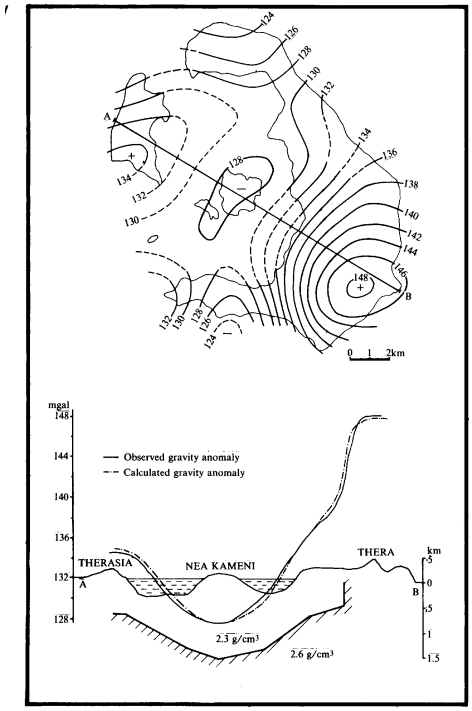

Figure 9. Filtered gravity anomaly map and interpretative section (Fytikas et al. 1990).

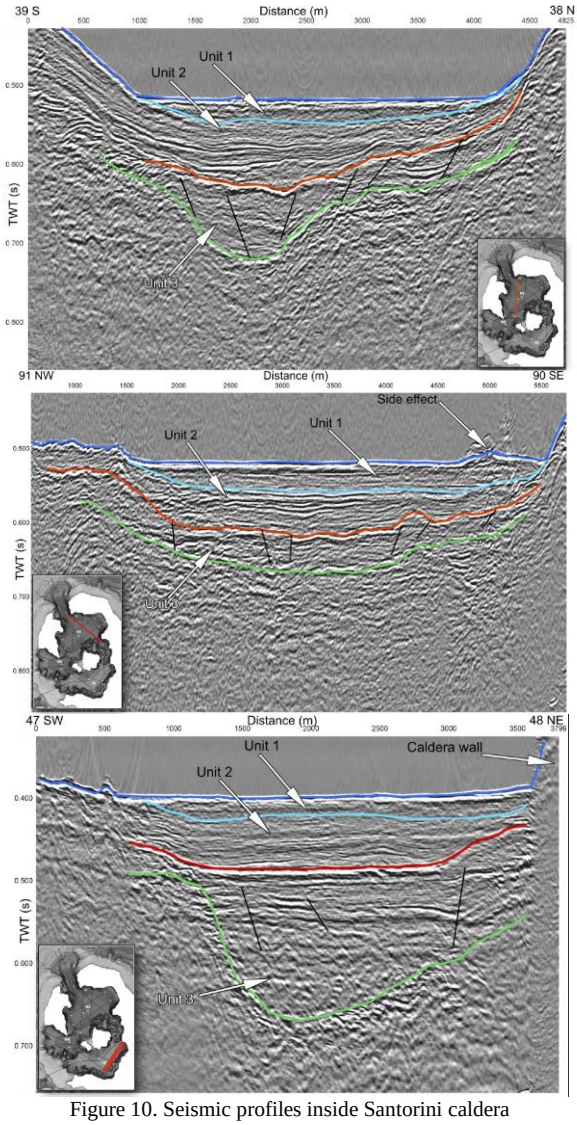

Figure 10. Seismic profiles inside Santorini caldera

- Unit 1: Flat-lying layers up to 25 m thick interpreted as modern sediments from mass wasting;
- Unit 2: Flat-lying sediments up to 80 m thick that merge into the clastic apron of the Kameni edifice and interpreted as debris from shallow-marine phreatomagmatic eruptions of the Kamenis;
- Unit 3: Down-faulted and down-sagged deposits at least 80 m thick, interpreted as the uppermost part of the intracaldera tuff fill from the Minoan eruption

VOLCANOLOGICAL SUMMARY

The geology of Santorini was described by Fouqué (1879), Reck (1936), Pichler & Kussmaul (1972, 1980), and Heiken & McCoy (1984). Pichler & Kussmaul (1980) published a 1:20000 geologic map of the islands. The pyroclastic deposits and their facies were described by Druitt et al. (1989). A geological map (simplified version on cover) and summary of field, volcanological, petrological and geochemical and isotopic work carried out by the Cambridge-Clermont group was published in a Geological Society of London Memoir by Druitt et al. (1999). The chronology is based on whole-rock K-Ar and $^{40}Ar/^{39}Ar$ age determinations carried out by M. Lanphere, and on $^{40}Ar/^{39}Ar$ age determinations carried out by S. Scaillet. Part of the map is shown in Fig. 11. Photos of the caldera cliffs are shown in Figs 12 and 13. The volcanic evolution and age data are summarized in Fig. 16.

In southern Thera, basement of the prevolcanic island makes up the massif of Profitis Ilias and crops out in the caldera cliffs near Athinios. The Akrotiri Peninsula is composed of a complex of submarine rhyodacites and dacites that are the earliest products of the volcanic field. The basement and early rhyodacites are then overlain and plastered by a sequence of pyroclastic deposits up to 200 m thick that dominates the cliffs of southern Thera and Aspronisi (Figs. 12 and 14).

The northern half of Thera, and the whole of Therasia, are composed principally of lavas (Figs. 11 and 13). These successions represent the products of at least three large shield complexes (Simandiri, Skaros, and Therasia shields) and a composite stratocone (Peristeria Volcano) truncated by caldera collapse.

White tuffs of the Bronze-Age Minoan eruption form an essentially continuous mantle over the islands of Thera, Therasia, and Aspronisi (Fig. 12).

The evolution of Santorini is divided into six stages:

- Early centres of the Akrotiri peninsula (predominantly dacites and rhyodacites),
- Cinder cones of the Akrotiri Peninsula,
- Peristeria Volcano (andesitic stratocone complex) (Fig. 11).

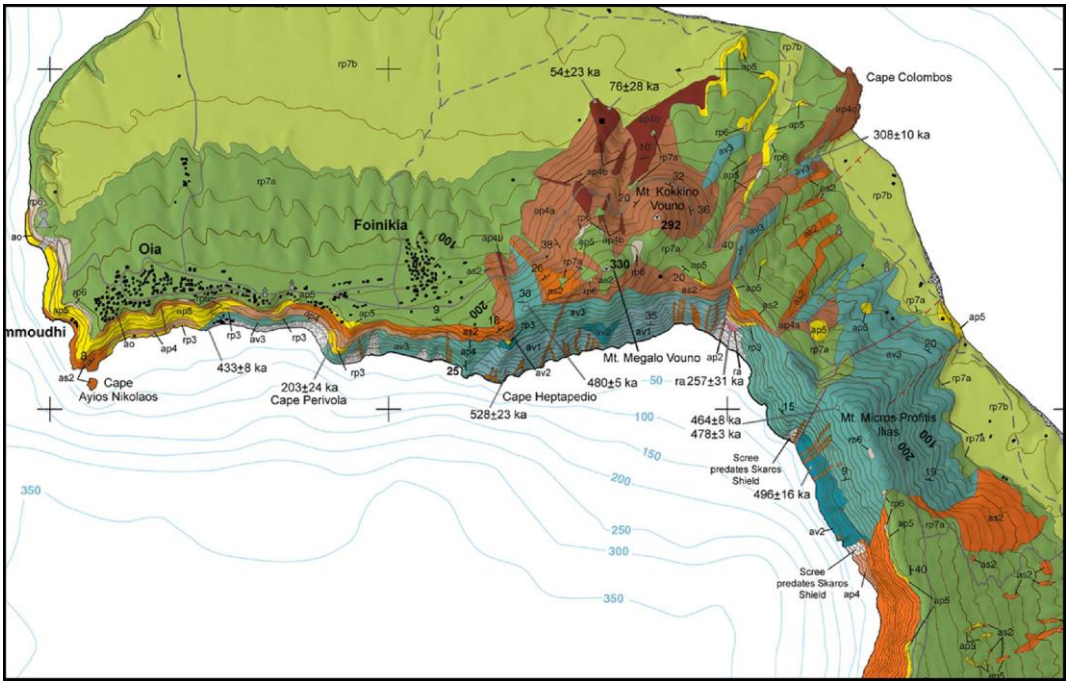

Figure 11. Part of the geological map for northern Thera (Druitt et al. 1999). The lavas of Peristeria Volcano are in blue-greens. The red is lava from Skaros. The browns are scoria from Kokkino and Megalo Vouno cinder cones. The greens are Minoan phase-3 and phase-4 deposits

Figure 12. Pyroclastic succession from the first (names in white) and second (names in black) explosive cycles, Cape Therma.

- Products of the first explosive cycle (pyroclastic eruptions and minor shield formation)
- Products of the second explosive cycle (pyroclastic eruptions and formation of the Simandiri, Skaros and Therasia shields)
- The Kameni shield (start of the third cycle?).

Of these six stages, the products of the two explosive cycles are volumetrically the most important (Fig. 14). They contain the deposits of ~12 major explosive eruptions, as well as remnants of at least three large lava shields (e.g., Fig. 13). Deposits of the twelve main eruptions are jointly referred to as the 'Thera Pyroclastics'. Each named tuff of the Thera Pyroclastics is the product of a single explosive eruption (Figs. 14 and 16). All began with a phase of Plinian or subplinian type and most generated pyroclastic flows. A prominent feature of the Thera Pyroclastics is the abundance of lithic breccias and spatter agglomerates laid down by

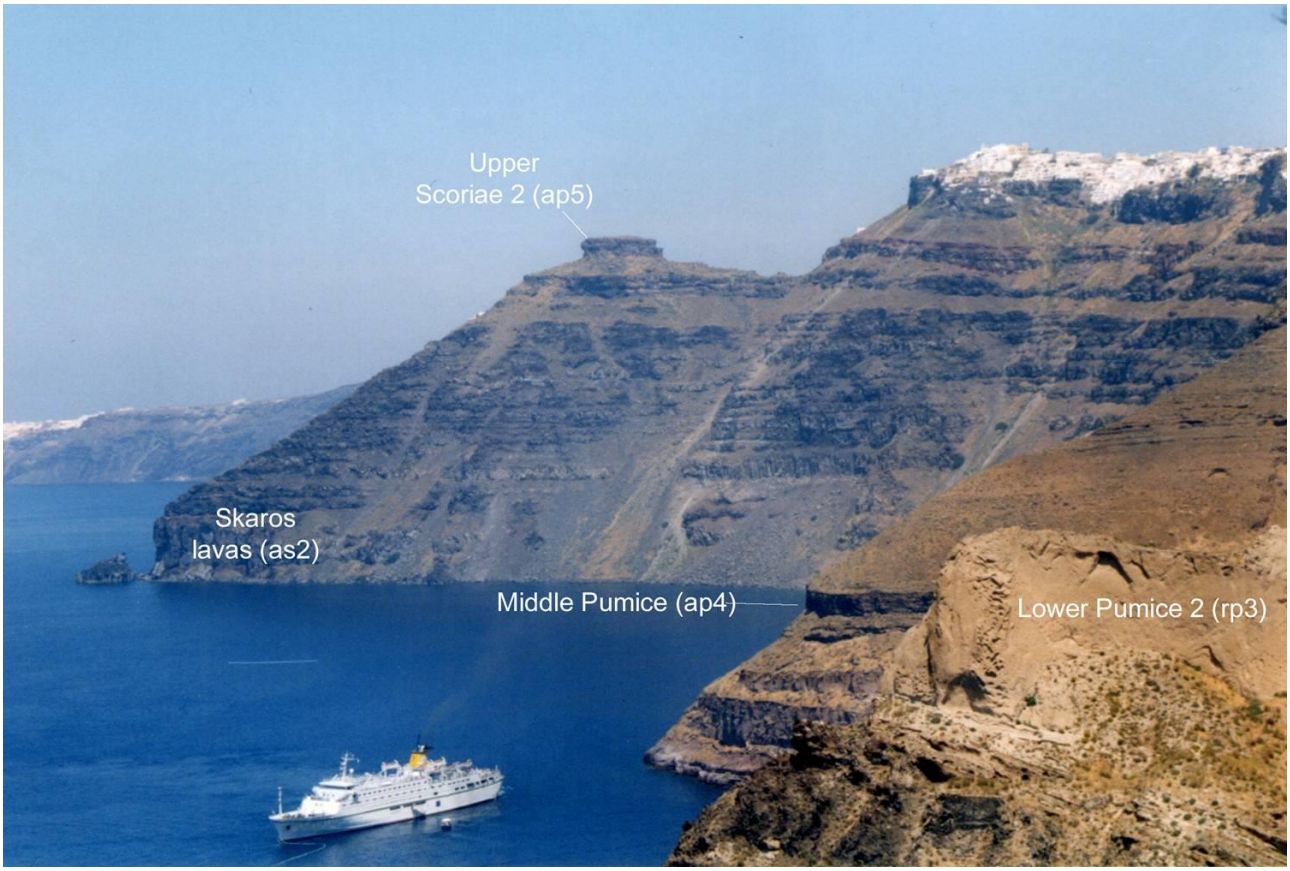

Figure 13. The caldera wall near Fira harbour. The Skaros lavas are 300 m thick here. The knoll on the headland is the welded spatter agglomerate of Upper Scoria 2. Also marked are the Plinian pumice fall deposits of Lower Pumice 2 (25 m thick), and Middle Pumice (here densely welded).

pyroclastic flows. These 'co-ignimbrite lag deposits' are referred to respectively as lithic-rich and spatter-rich lag deposits, and are described and explained later. Figure 15 shows the mapped distributions of the Thera Pyroclastics, and Fig. 17 shows isopach maps for pumice-fall deposits of six eruptions for which sufficient data are available. Volume estimate is possible only for the Minoan Tuff (30-60 km^3 DRE), but the considerable thicknesses, coarse grain sizes, and wide dispersals of the other 11 deposits suggest individual volumes in the range of km^3 to tens of km^3 (Druitt et al., 1989).

The two explosive cycles (Figs. 12 and 14) are recognised on the basis of long-term trends in magma composition. Each cycle commenced with the eruption of mafic to intermediate magmas and terminated with a pair of major silicic eruptions (Lower Pumice 1 - Lower Pumice 2; Cape Riva - Minoan) accompanied by caldera collapse. The existence of two long-term cycles is an important feature of the volcanic and geochemical evolution of Santorini.

The following section describes the evolution of Santorini in detail (Fig. 16). Reconstructions of the volcanic field at six stages in its development are shown in Fig. 18.

EVOLUTION OF SANTORINI

The prevolcanic island (Triassic to Eocene)

Santorini is founded on a 6 x 6 km cruciform island of late Mesozoic to early Tertiary basement (Fig. 18a). The basement lithologies crop out widely in SE Santorini. There are two principal components:

- A ~250 m-thick complex of low-grade phyllites and schists,
- Crystalline limestones.

The former are exposed widely along a 2-km-long stretch of the caldera wall near Athinios, but also occur around the base of Profitis Ilias and in the saddle between Profitis Ilias and Mesa Vouno. The limestones form the massifs of Profitis Ilias and Gavrillos (cover).

Reviews of the basement lithologies have been published by Davis & Bastas (1978) and Skarpelis and Liati (1990). The phyllites include metapelites and metasandstones with intercalations of metaconglomerates, limestones, metavolcanics, and metadolerites. The whole has been metamorphosed to blueschist grade, then overprinted under greenschist to

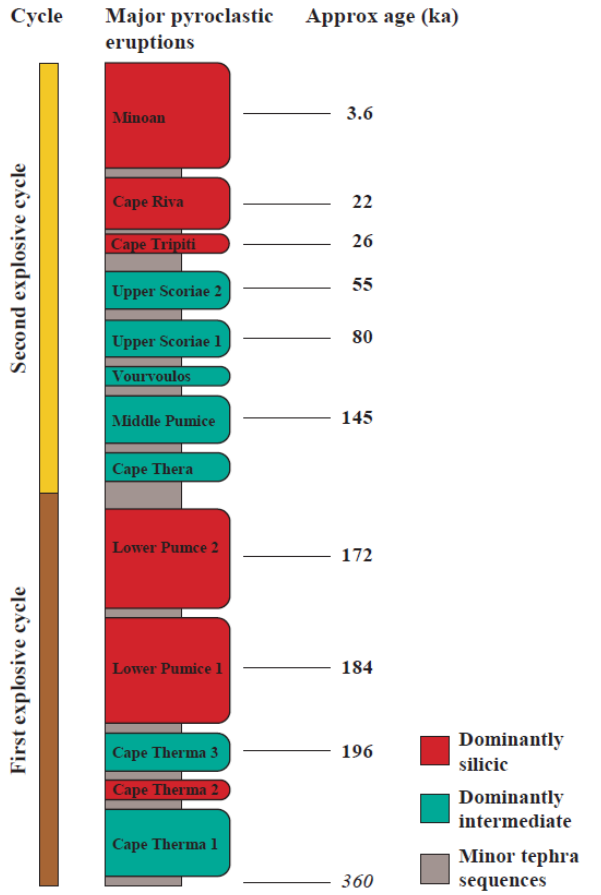

Figure 14. Stratigraphy of the pyroclastic succession, showing the two eruptive cycles based on magma composition and eruptive style. The grey bands are succession of minor tuffs and palaeosols.

amphibolite facies conditions, in a manner similar to other Cycladic islands.

The occurrence of *Miliolidae* in the upper parts of the phyllite succession suggests a Palaeocene-Eocene sedimentary age (Tartaris, 1964). Intrusions of granite porphyry occur locally in the phyllites, and an I-type, late-Miocene granite has been intersected in a geothermal borehole (Skarpelis et al., 1992).

The limestones of Profitis Ilias and Mesa Vouno contain *Megalodontidae*, and are of Triassic, probably Upper Triassic, age (Papastamatiou, 1958).

Early centres of the Akrotiri Peninsula (Late Pliocene – 580 ka)

The first known eruptions of Santorini discharged hornblende-bearing silcic lavas and tuffs which today form the hills of the Akrotiri Peninsula of southern Thera (cover). The presence of abundant hornblende distinguishes these rocks from younger Santorini volcanics, which generally lack hornblende.

Prolonged eruption on the sea floor generated a rhyodacitic complex with an original basal diameter exceeding 4 km and a height exceeding 200 m (Fig. 18a). The occurrence of similar rocks in drill holes located SW of Profitis Ilias (Fytikas et al. 1990) suggests that the original complex was larger than implied by present-day outcrops. In the central Akrotiri Peninsula, successions are dominated by submarine domes, coulées, and hyaloclastite aprons that interdigitate with water-lain vitric tuffs, pumice breccias, and conglomerates. Some lavas at higher elevations may have erupted subaerially. An altered andesite of unknown age crops out locally between Loumaravi and Archangelo summits. Intercalation of marine sediments bearing benthic and planktonic forams within vitric and pumice tuffs at heights up to 100 m or more above present-day sea level provide evidence for submarine eruption (Seidenkrantz, 1992).

A smaller fault-bounded rhyodacitic complex of similar age forms the cape at the end of the peninsula (Fig. 18a). Marine deposits rich in siliceous sponge spicules occur near the top of this mass at an altitude of ~100 m (Seidenkrantz, 1992). The complex lies in faulted contact to the SE with the dacitic hyaloclastite of Cape Mavros (cover).

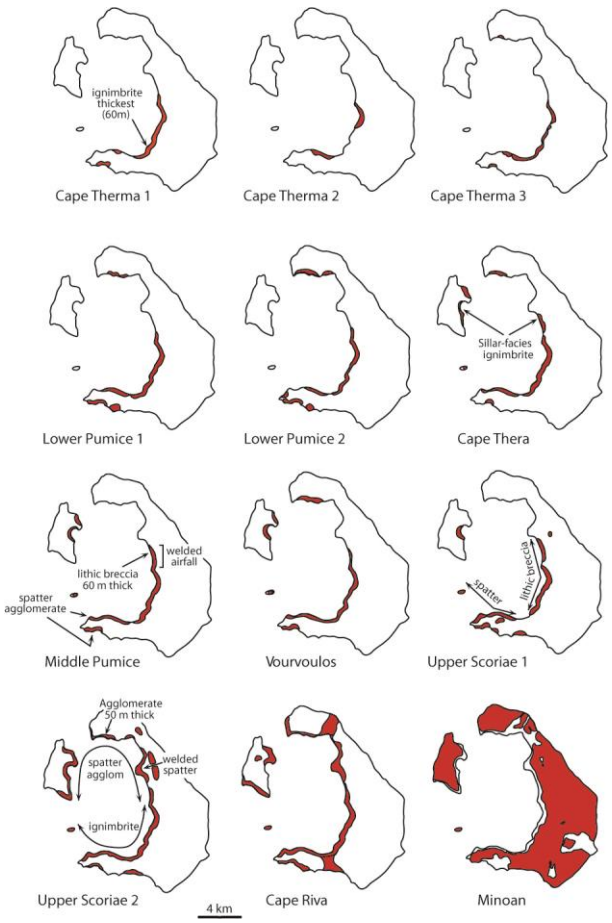

Figure 15. Distribution of the deposit of each major pyroclastic eruptions

Summary of the history of Santorini Volcanic Field

	Event	Magma [1]	Age (ka)
Kameni Volcano	Formation of Kameni Volcano	D	197 BCE to 1950 CE [2]
Second explosive cycle	*Caldera collapse*		
	Minoan eruption	R	3.6 - early 17th century BCE [3]
	Caldera collapse		
	Cape Riva eruption	R	21.8 ± 0.4 [4]
	Eruption of the Andesites of Oia	A	
	Construction of Therasia dome complex	R	48.2 ± 2.4; 39.4 ± 2.2; 33.2 ± 1.1; 24.6 ± 1.3 [6]
	Upper Scoriae 2 eruption	A	79 ± 8; 54 ± 3 [5]
	Construction of Skaros lava shield	B, A, D	67 ± 9 [5]
	Caldera collapse (incremental?)		
	Upper Scoriae 1 eruption	A	80]7]
	Vourvoulos eruption	A, D	
	Eruption of Megalo and Kokkino Vouno; Columbos tuff ring	A	76 ± 28; 54 ± 23 [5]
	Middle Pumice eruption	A, D	145 [7]
	Cape Thera eruption		
	Construction of Simandiri lava shield	A	172 ± 33; 172 ± 4 [5]
First explosive cycle	*Caldera collapse*		
	Lower Pumice 2 eruption	R	172 [7]
	Lower Pumice 1 eruption	R	203 ± 24 [5]; 184 [7]
	Cape Therma 3 eruption	A	196 [7]
	Extrusion of Rhyodacites of Cape Alonaki and NE Thera	R	257 ± 31; 224 ± 5 [5]
	Cape Therma 2 eruption	R	
	Cape Therma 1 eruption	A	
	Extrusion of the Andesites of Cape Alai	A	456 ± 138; 364 ± 62; 345 ± 88 [5]
Peristeria Volcano and Cinder Cones of Akrotiri Peninsula	Eruption of the Cinder Cones of Akrotiri Peninsula	B, A	522 ± 104; 451 ± 27; 344 ± 24 [5]
	Construction of Peristeria 3	B, A, D	480 ± 5; 478 ± 3; 464 ± 8; 433 ± 8; 308 ± 10 [5]
	Extrusion of lavas of Peristeria 2	A	496 ± 16 [5]
	Construction of Peristeria 1	A	528 ± 23 [5]
Early Centres of Akrotiri Peninsula	Eruption of the Early Centres of Akrotiri Peninsula	D, R	645 ± 92; 619 ± 35; 586 ± 15, 582 ± 24; 553 ± 10 [5]

[1] B basalt, A andesite, D dacite, R rhyodacite
[2] Historical ages
[3] Carbon-14 ages of various authors
[4] Mean of carbon-14 and tephrastratigraphy ages (Fabbro et al. 2013)
[5] K-Ar and Ar-Ar ages of Druitt et al. (1999)
[6] Ar-Ar ages of Fabbro et al. (2013)
[7] Tephrastratigraphy ages of Keller and colleagues, cited in Gertisser et al. (2009) and Vespa et al. (2006)

Figure 16. Summary of the evolution of Santorini Volcanic Field (Druitt et al. 1999).

The occurrence of water-lain vitric tuffs, foram- or sponge-bearing marine sediments, and hyaloclastite up to heights of 100 m or more above present-day sea level implies considerable post-formational volcanotectonic uplift of these early centres. Eustatic sea-level fall of 100 m or more since ~600 ka is inconsistent with current models. Widespread soft-sediment faulting, slumping and brecciation of the tuffs is compatible with major uplift, probably along NE-SW and NW-SE faults as suggested by outcrop patterns and terrain morphology.

K-Ar dating of the rhyodacites of Cape Akrotiri gave an age of 645±92 ka, and the Cape Mavros complex gave 619±35 ka. A prominent 600-m-long rhyodacite flow SE of Akrotiri village yielded 586±15 ka. Shallow-marine effusive volcanism at Santorini therefore began about 650 ky ago and continued until at least 580 ka. These ages are consistent with Huijsmans' (1985) observation that Santorini lavas are all normally magnetised and hence younger than the Brunhes-Matuyama reversal (730 ka). However, Seward et al. (1980) obtained zircon fission-track ages of 940-1950 ka on thin silicic ashes that drape the basement inlier at Athinios. Moreover, late-Pliocene marine sediments rich in ash and hornblende occur in the Akrotiri area. Evidently explosive magmatism in the area began in the late Pliocene, long before effusion of the oldest preserved lava.

In summary, late-Pliocene to 580 ka silicic volcanism constructed a complex of domes, hyaloclastite aprons, and pumice cones on the western submarine flank of the pre-volcanic island. Later stages in the development of the complex were probably subaerial, suggesting shoaling during construction. Subsequent uplift of the complex occurred as two fault blocks (Fig. 18a). Uplift was probably complete by the time the subaerial cinder cones of Mavrorachidi (522±104 ka) erupted.

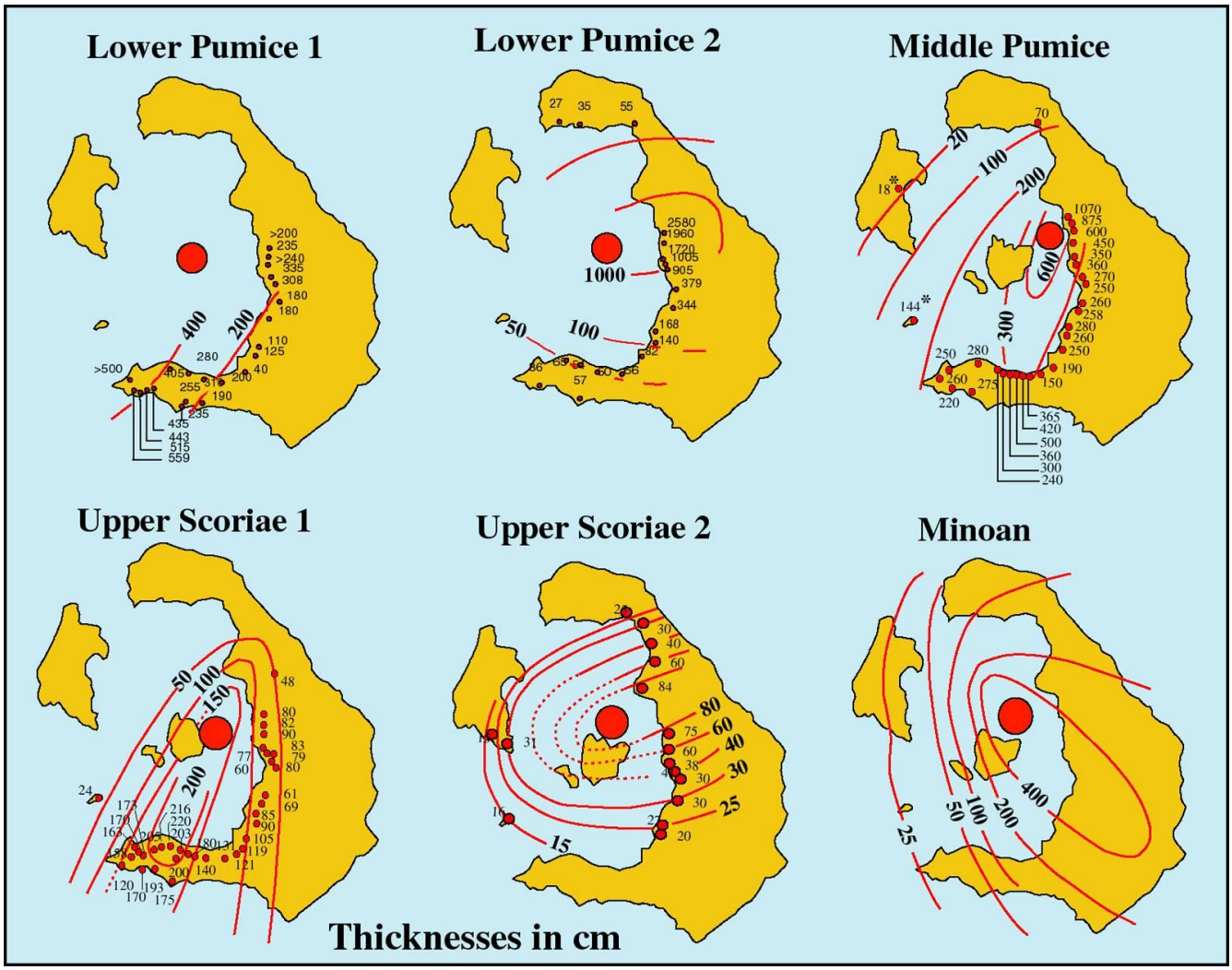

Figure 17. Isopachs of pumice-fall deposits of six pyroclastic eruptions (Druitt et al. 1989; 1999).

Peristeria Volcano (530-430 ka)

Between 530 and 430 ka a composite stratocone was constructed in the north of the volcanic field (Fig. 18a). Remnants of this Peristeria Volcano form most of the Megalo Vouno massif and all of Micros Profitis Ilias (Fig. 11; cover). We recognise three units of Peristeria:

- A core complex of andesitic lavas and tuffs (P1),
- Massive silicic andesite lava flows (P2),
- Thinly bedded basaltic to andesitic flows (P3).

The core complex (P1) forms the lower 120-180 m of the caldera cliffs below Megalo Vouno. It consists of andesitic lava flows, tuffs, breccias, and hyaloclastites, cut by ~50 dykes. Most dykes trend N to NE. Dating of one P1 andesite from the lowest stratigraphic level yielded 528±23 ka.

The P2 lavas occur sporadically as eroded remnants above the core complex, and as a massive silicic andesite flow up to 80 m thick at the base of the caldera wall of Micros Profitis Ilias.

The core complex of Megalo Vouno is capped by 120 m of well-bedded P3 lavas consisting of aphyric to plagioclase-phyric andesites and basalts, commonly fed by dykes. The stratigraphically highest P3 flow yielded a K-Ar age of 480±5 ka. On its western flank, the core complex is onlapped steeply by a 100-m-thick succession of P3 andesites with westerly or southwesterly dips. These extend as far west as Oia, where the youngest flow yielded an age of 433±8 ka.

In the cliffs of Micros Profitis Ilias, the P3 lavas and tuffs overlie the basal P2 silicic andesite and include

sparsely to strongly plagioclase-phyric andesites, and subordinate basalts. The topmost P3 flow on Micros Profitis Ilias has been dated 464±8 ka.

The core complex (P1) represents the dissected remains of an ancestral Peristeria stratocone, the construction of which had commenced by ~530 ka. Following probable

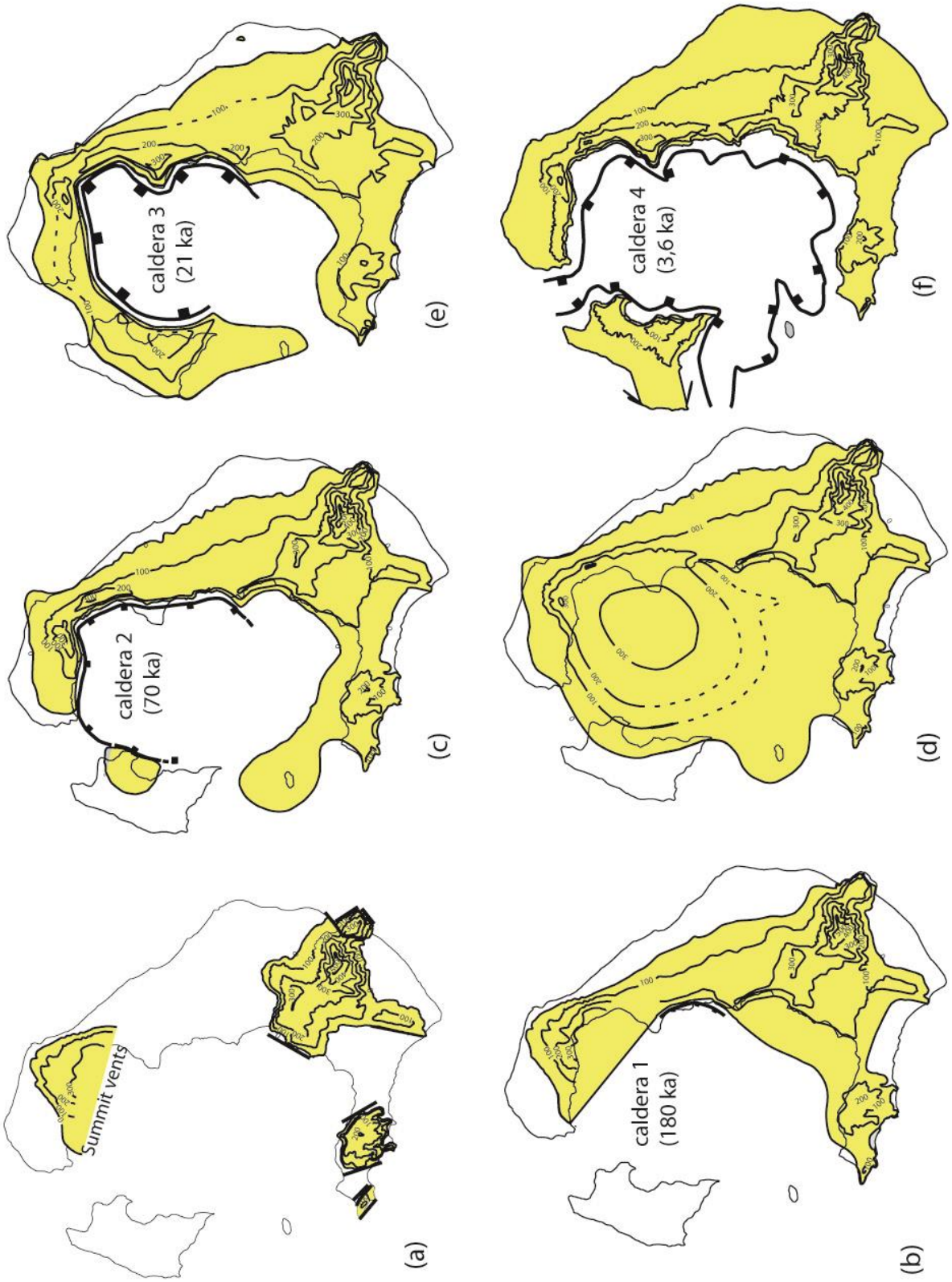

Figure 18. Reconstructions of Santorini Volcanic Field (relative to present-day sea level) at six moments in its evolution. (a) About 580 ka: the prevolcanic island, uplifted early centers of Akrotiri Peninsula, and Peristeria Volcano. (b) About 172 ka: caldera 1 formed by collapse during the Lower Pumice 2 eruption. (c) About 70 ka: caldera 2 formed by collapse during one or more of the Middle Tuff eruptions. (d) About 65 ka: the Skaros shield. (e) 22 ka: caldera 3 after the Cape Riva eruption. (f) 3.6 ka: Caldera 4 after the Minoan eruption (Druitt et al. 1987).

collapse of this volcano, silicic andesite magma (P2) was extruded. Later, the cone of Micros Profitis Ilias (P3) grew up against the steep, southern flank of the core complex. Dyke-fed P3 lavas covered the eroded remains of the core complex and enveloped it to the north and west. At its maximum development, Peristeria Volcano had a basal diameter of ~4 km (Fig. 18a). Extrapolation of bedding dips suggest that the summit lay in the NE corner of the present caldera (Fig. 7), and that its height may have reached 350 m above sea level. The main activity of Peristeria lasted 100 ky, although the existence of an andesite flow near Cape Kolombo (P3) dated 308±10 ka implies continued flank eruptions until that time.

Cinder cones of the Akrotiri Peninsula (~350 and ~520 ka)

Strombolian eruptions on the Akrotiri Peninsula between ~350 and ~520 ka formed cinder and spatter cones at Capes Balos, Kokkinopetra, and Mavrorachidi. All three cones overlie tuffs and lavas of the early rhyodacitic centres, but underlie the Thera pyroclastics.

Dating of the Balos cone gave a K-Ar age of 344±25 ka. Mavrorachidi andesite yielded a low amount of radiogenic argon and an imprecise age of 522±104 ka. Activity at these vents brackets that of Peristeria Volcano, suggesting that the cinder cones represent peripheral mafic magmatism around the central complex further north.

First explosive cycle (~360-172 ka)

The first of the two explosive cycles began about 360-460 ky ago. Activity thereafter appears to have been focused along the Kameni Line, suggesting that perhaps this fault system became active at that time. Pyroclastic deposits and lavas of the first cycle occur widely in the cliffs of southern Thera, but only intermittently in the north. They lie below sea level on Therasia and Aspronisi, both of which consist uniquely of second-cycle products.

Andesites of Cape Alai (360-460 ka).

Discharge of lava from vents on the Kameni Line some 360-460 ky ago constructed a low andesitic shield complex. Remnants of this complex crop out intermittently at sea level for 1 km south of Fira harbour, where they stack to a thickness of 60 m. The quality of K-Ar and $^{40}Ar/^{39}Ar$ ages from these lavas is poor. Dates range from 209±85 ka to 543±88 ka, but samples with the best yields of radiogenic argon give 360-460 ka.

Cape Therma 1 eruption.

The first major explosive eruption of Santorini generated a dacitic scoria-flow deposit that crops out widely in southern Thera. This deposit forms high vertical cliffs at the base of the caldera wall at Cape Therma where it is about 60 m thick (Fig. 12). The lowest flow units are buff to black and non-lithified; upper units are a pink sillar facies. Locally the scoria-flow deposits pass laterally or vertically into clast-supported lithic- or spatter-rich lag deposits. Near Athinios they can be traced laterally into a 5-cm-thick, stratified veneer or surge deposit draped over the basement inlier.

Cape Therma 2 and the Rhyodacites of Cape Alonkai (~225 ka).

After a long pause, activity recommenced with the discharge of rhyodacitic lavas, preceded by a pumice-fall eruption. The white pumice-fall deposit occurs up to 2.5 m thick in the cliffs of southern Thera, and is a useful stratigraphic marker. It is called Cape Therma 2 and is the smallest of the twelve named pyroclastic units. Immediately following CTh2, at least two rhyodacitic lavas were extruded from vents on or near the Kameni Line. The lowest one yielded a precise K-Ar age of 224±5 ka. A small remnant of 257±31 ka silicic lava compositionally and stratigraphically identical to the Alonaki rhyodacites occurs in the NE corner of the caldera at the base of a wedge of first-cycle pyroclastic deposits preserved at the contact between the older massifs of Megalo Vouno and Micros Profitis Ilias. These widely separated outcrops of rhyodacite are interpreted as remnants of a low, extensive shield which existed ~225 ka ago.

Cape Therma 3 eruption (196 ka).

This eruption generated andesitic deposits preserved extensively in southern Thera (Fig. 15). A basal pumice fall deposit is overlain by a bed of complexly interdigitated scoria-flow deposits, spatter-rich lag deposits and lithic-rich lag deposits up to 20 m thick. Grey scoria-flow deposit is the main facies on the Akrotiri peninsula, while pink sillar-facies ignimbrite and red spatter aggolmerate dominate as far north as Fira and locally in northern Thera. The Cape Therma 3 deposits contain abundant plutonic nodules. The 196 ka age was obtained by chemical correlation with deep sea ash layer 'Intra S7' (Keller et al. 2000, abstract).

Lower Pumice 1 eruption (184 ka).

The first eruptive cycle culminated with a pair of large rhyodacitic eruptions termed Lower Pumice 1 and Lower Pumice 2. Distributions of these two deposits are widespread and almost identical (Fig. 15).

The Lower Pumice 1 eruption began with a Plinian phase from a vent near the present Kameni Islands (Fig. 17). The deposit is up to 5 m thick and dispersed to the southwest. Locally, a fine vitric surge deposit is preserved at the base. Following the Plinian phase, the eruption generated a non-welded, rhyodacitic ignimbrite preserved locally up to 15 m thick on the Akrotiri Peninsula, then thick lithic-rich lag breccias. The lithic breccias are pink-brown in colour, up to 15 m thick, and contain lithic blocks as large as 2 m. Where the breccia lies directly on the pumice-fall deposit, deep impact sags containing bombs are found, which suggest a strong ballistic component during the initial phase of

pyroclastic flow emplacement (Fig. 19). These sags are particularly common near Cape Athinios, where they dip consistently eastwards as expected from the inferred vent position. Commonly the breccia contains wavy stratification and foreset bedding on an outcrop scale, suggesting the existence of bedforms tens of metres in wavelength.

The Plinian deposit and ignimbrite are uniformly rhyodacitic with small amounts of grey pumice. The lithic breccias are compositionally zoned, being rhyodacitic at the base but containing ~30% andesitic scoria and banded pumice at the top.

An age of 203±24 ka was obtained on fresh, glassy fragments of densely welded tuff in the lithic breccia. The more precise 184 ka age was obtained by chemical correlation with deep sea ash layer V3 (Keller and colleagues, in Gertisser et al., 2009).

Lower Pumice 2 eruption (172 ka).

The first cycle concluded with rhyodacitic eruption called Lower Pumice 2, the deposits from which directly overlie LP1, separated only by a palaeosol. Lower Pumice 2, which strongly resembles the Minoan Tuff, is prominent in the caldera walls of southern Thera, where it is an important marker horizon.

An initial Plinian phase occurred from a vent situated near present-day Nea Kameni (Fig. 13). The deposit, the thickness of which varies from > 25 m near Fira to < 1 m on the Akrotiri peninsula, was dispersed to the east by strong winds. Rhyodacitic pumice is the dominant juvenile clast type, but clasts of grey basaltic to andesitic scoria increase in abundance upwards, reaching ~ 25% of the top.

The eruption then generated up to 7m of surge or ignimbrite veneer deposit with parallel and low-angle cross stratification, followed by ignimbrite.

The third and most prominent unit is a yellowish, poorly sorted, pumiceous deposit of possible phreatomagmatic origin. This occurs up to 20 m thick with lithic blocks as large as 6 x 2 m that define a crude stratification. It is overlain widely by as much as 10m of stratified, clast-supported lithic breccia with local pumiceous lenses. The breccias are either coignimbritic in origin, or formed by violent hydrothermal explosions as caldera collapse took place.

Since only a single palaeosol separates the two Lower Pumice tuffs, the eruptions must have occurred closely spaced in time. The 172 ka age was obtained by chemical correlation with deep-sea ash layer V-1 (Keller and colleagues, in Gertisser et al., 2009).

Caldera collapse accompanied the Lower Pumice 2 eruption (see below).

Second explosive cycle (172 ka - 3.6 ka)

A protracted period of predominantly andesitic volcanism followed the two silicic Lower Pumice eruptions. This marked the onset of the second cycle.

Andesites of Cape Simandiri (172 ka).

Construction of a lava shield commenced in northern Santorini following the Lower Pumice 2 eruption. A remnant of this shield occurs at the base of the cliffs of Therasia. Founded on about 10 m of stratified tuffs and conglomerates, the lavas include thinly bedded basalts and thickly bedded andesite domes and coulées. The shield summit must have lain east of Cape Simandiri because the lavas dip westwards. A K-Ar age of 172±33 ka was obtained on an andesite near the base of the exposed succession; an $^{40}Ar/^{39}Ar$ plateau age was measured on the same sample (172±4 ka).

There followed a series of explosive eruptions, four of which discharged at least a few km^3 of andesite or dacite as fallout and ignimbrite and thus are considered as major eruptions (Cape Thera, Middle Pumice, Vourvoulos, Upper Scoriae 1). Deposits from numerous smaller eruptions occur between the major tuff layers. The entire succession forms a coherent, widely dispersed package known as the 'Middle Tuff sequence'.

Cape Thera eruption.

Deposits from this eruption overlie Lower Pumice 2, separated by several metres of palaeosols and thin tephra layers. The eruption began with deposition of a thin phreatomagmatic ash pitted by impact sags, followed by discharge of a pumice-fall deposit 85 cm thick near Fira. Thickness variations in the pumice fall do not allow the vent position to be accurately constrained. There then followed the eruption of a pink, vapour-phase-cemented scoria-flow deposit that occurs widely near the base of the cliff on Therasia, but is most conspicuous where ponded to 60 m immediately below Fira (Fig. 15). Laterally this ignimbrite passes into cross-stratified surge beds, up to 7m thick, which drape higher terrains.

Middle Pumice eruption (145 ka).

This eruption generated first a Plinian pumice fall deposit, then lithic-rich pyroclastic flows. The Plinian pumice is dispersed to the SSW (Fig. 17). It is non-welded over most of its outcrop, but is densely welded in the region of Fira close to its source vent on the Kameni Line (Figs. 15 and 20). It is compositionally zoned and was described in detail by Sparks & Wright (1979).

Figure 19. Above. Products of the two Lower Pumice eruptions. LP1 consists of a brown Plinian fallout bed overlain by stratified lithic-rich pyroclastic flow deposits. LP2 deposits are white. Below. Impact sag at the base of the LP1 lithic-lag breccia, near Balos. The underlying Plinian pumice is 2 m thick.

The pumice fall is overlain by lithic-rich lag breccias containing blocks up to 2 m across and subordinate andesitic scoria. The contact between the pumice and breccias is commonly wavy and erosive due to widespread impact sags and to the scouring action of pyroclastic flows. The breccias, which everywhere consist of two flow units, are typically less than 10m thick, but thicken to 80 m in the cliffs below Fira. Deep impact sags with bombs as large as 3 m in the top of the pumice fall record violent ballistic activity at the onset of breccia emplacement. Locally the breccias pass vertically and laterally into fines-poor ignimbrite.

The eruption ended with discharge, from the same vent as the first phase, of a thin andesitic pumice fall.

The eruption has been dated at 145 ka by chemical correlation with the W2 deep-sea ash layer (Keller and colleagues, cited in Vespa et al. 2006).

Vourvoulos eruption.

The widespread dacitic products of this (relatively) small eruption comprise a basal pumice-fall deposit overlain by wavy- to cross-stratified, lithic-rich pyroclastic surge deposits. Locally the unit is capped by non-welded ignimbrite and rarely by lithic-lag breccia.

Upper Scoriae 1 eruption (80 ka)

The Middle Tuff sequence of eruptions culminated with the large andesitic Upper Scoriae 1 eruption, which laid down a widespread spatter-rich lag deposit. Pichler and Kussmaul (1980) correlated layers of spatter agglomerate in northern Thera, southern Thera, and on Therasia, and named them the Upper Scoriae. Druitt et al. (1989) were able to show that in fact this spatter agglomerates formed from two very similar eruptions of different ages. Agglomerates of USc1 crop out mainly in southern Thera and USc2 in northern Thera and on Therasia, although the two units are occasionally superimposed.

Upper Scoriae 1 eruption began at a vent on the Kameni Line (Fig. 17), from which was discharged a black scoria fall containing a pair of distinctive base-surge beds (Fig. 20). This association, surge-fall-surge-fall is a distinctive marker horizon in southern Thera. The surge beds, both less than a metre thick, contain typical base-surge climbing-ripple cross stratification of fine sand-grade material and poorly sorted ash-fall layers rich in accretionary lapilli. They cover more than 60 km^2 and, near Cape Akrotiri, fill broad U-shaped erosional channels. Plastering onto steep slopes and the presence of accretionary lapilli suggest a phreatomagmatic origin. Flow directions from foreset laminae are consistent with eruption from the vent deduced from fallout isopachs (Fig. 21).

Figure 20. Above. Welded facies of the Plinian fall deposit from the Middle Pumice eruption. Fira harbour. Below. Base surge and fallout deposits of the Upper Scoria 1 eruption. Balos.

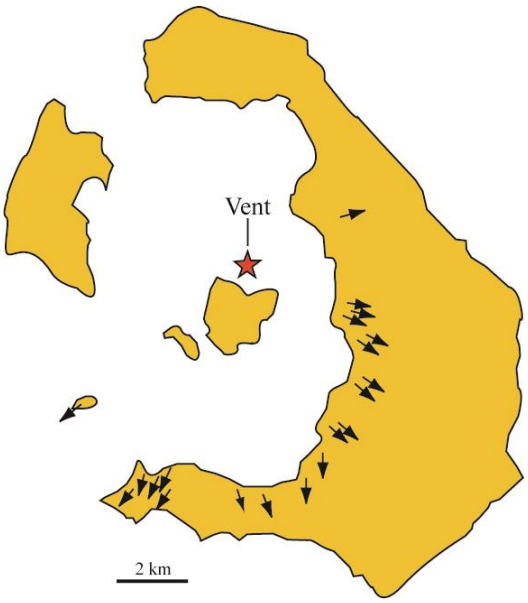

Figure 21. Flow directions of USc1 base surges inferred from dune foresets and channels. Star: vent inferred from fall isopachs (Mellors and Sparks 1991).

The eruption then generated voluminous scoria flows that poured over the southern part of the volcanic field, laying down a distinctive red to black spatter-rich lag deposit rich in contorted and imbricated spatter bombs as large as 3m. The deposit typically drapes topography, but thickens and coarsens into depressions. The eruption may have involved large-scale hydromagmatic explosions of andesitic magma or explosions through a lava lake (Mellors and Sparks 1991).

The eruption has been dated at 80 ka by chemical correlation with the X1 deep-sea ash layer (Keller and colleagues, cited in Vespa et al. 2006).

Cinder cones of NE Thera and Kolumbo tuff ring (approx. 125-80 ka)

Construction of the cinder cones of Megalo Vouno and Kokkino Vouno (northern Thera) occurred during the same period as the Middle Tuff eruptions. The Kolumbo tuff ring, in the extreme NE corner of Santorini, probably also dates to this period.

The two cinder cones and the tuff ring lie on the NE-SW Kolumbo Line. Eruption of the cinder cones generated a thick scoria-fall deposit of phenocryst-poor andesite that mantles the eroded remains of Peristeria Volcano. The two cones probably erupted simultaneously, since their products appear to form a single sheet.

The age of Megalo Vouno and Kokkino Vouno is constrained by field superposition to postdate Middle Pumice. K-Ar dating gave ages of 76±28 ka and 54±23 ka.

The ashes of Kolumbo tuff ring overlie a lava 308±10 ka old, and are themselves overlain by spatter agglomerate of Upper Scoria 2. The remnants of another tuff ring of broadly the same age occurs sandwiched between the Middle Pumice and Vourvourlos Tuff on Aspronisi. Evidently both tuff rings formed by interaction of andesitic magma with seawater at times when sea level was similar to the present day. Sea level between 125 ka and 80 ka lay only ≤25m below its present-day value (Shackleton, 1987), so the tuff rings probably formed during this period. This is consistent with an age of 145 ka for the Middle Pumice deposits that directly underlie the tuff ring on Aspronisi.

Skaros Shield (~70-54 ka)

The Skaros lava shield grew within, and overtopped, a caldera generated by eruptions of the Middle Tuff sequence. The dissected remnant of this shield at Cape Tourlos is composed of a basal complex of silicic andesite domes and coulées overlain by flat-lying, well-bedded mafic andesites and basalts (Fig. 13). The entire 300 m succession is banked up against an ancient caldera cliff line that trends roughly N-S from Fira to Micros Profitis Ilias. Isolated remnants of Skaros lavas also occur in northern Thera and extensively on Therasia, where the youngest lavas overspilled the old caldera rim.

Reconstruction of the shield (Fig. 18d) shows that its shape was essentially circular with a diameter at present sea level of 9 km and lava dips that were approximately radial. The profile was convex-up, as typical of shield volcanoes, with a maximum surface inclination of ~5º. The summit is estimated to have lain ~350 m above present sea level and situated 1-2 km west of Cape Tourlos. The volume is estimated at about 12 km^3. An $^{40}Ar/^{39}Ar$ age of 67±9 ka has been obtained on the lowest lava exposed at sea level..

Upper Scoria 2 eruption (54 ka)

Development of the Skaros shield culminated in a large andesitic eruption called Upper Scoriae 2. The dominant facies is thick spatter agglomerate that occurs widely in northern Thera and on Therasia (Fig. 15). Grey scoria-flow deposits dominate the eruption sequence on southern Thera and Aspronisi.

The eruption began with a fallout phase from a vent near present-day Nea Kameni (Fig. 17). Scoria flows then swept down the southern flanks of Skaros, filling drainages carved in the soft tuffs of the Middle Tuff sequence. Cross sections through these channels, which have approximately radial orientations, occur widely in the cliffs of southern Thera. In northern Santorini, the scoria flows transported lithic blocks and fluidal spatter rags up to 3 m in diameter, which settled rapidly from the flows to form lag deposits (Mellors and Sparks, 1991). These lag deposits typically are 10-20m thick, but reach 70 m at Oia where the spatter-rich facies forms a prominent horizon in the caldera cliffs (Fig. 22). The knoll that caps Cape Tourlos is composed of highly welded spatter laid down close to the summit of Skaros shield (Fig. 13). Isolated outcrops of Upper Scoriae 2 spatter-rich lag deposits occur all over northern Santorini.

Figure 22. The red spatter-rich agglomerate from the Upper Scoria 2 eruption dominates the cliff at Ammoudhi, in northern Thera. The lavas at sea level were erupted from the Skaros shield. The agglomerate is overlain by the white phase-3 deposits of the Minoan eruption.

Dating of the welded spatter yielded a K-Ar age of 79±8 ka and a more precise $^{40}Ar/^{39}Ar$ age of 54±3 ka. We infer an age of ~55 ka for the eruption, since this is consistent with the age of the underlying Skaros lavas (<70 ka).

Therasia dome complex (48 to 24 ka)

Following the Upper Scoriae 2 eruption, extrusion of ~2 km^3 of silicic magma from vents on and north of the Kameni Line built up a dome and coulee complex on the western flank of Skaros (Fig. 23). Remnants of this structure dominate the caldera cliffs of present-day Therasia, where the succession of domes and flows is over 200 m thick (Figs. 24 and 25). The lavas are predominantly dacitic, but thin flows of hybrid andesite (formed by the mixing of basalt and dacite) cap the succession (Druitt, 1985; Fabbro et al., 2013). Compositionally similar domes and flows occur near the top of the cliff at Fira (Fig. 25), showing that the Therasia complex extended across much of the northern basin of the present-day caldera.

Detailed mapping and $^{40}Ar/^{39}Ar$ dating of the lava succession was carried out by Fabbro et al. (2013) as part of a study to trace the build-up of the magmatic system towards the subsequent 22 ka Cape Riva explosive eruption. The Therasia lavas were discharged between 48 and 24 ka. A prominent dacitic pumice fall deposit intercalated within the succession of southern Therasia ('Cape Tripiti pumice'), correlates with the 26 ka Y4 deep sea ash.

Figure 26 summarises the compositional and age data from the start of construction of Skaros to the 22 ka Cape Riva explosive eruption that terminated the Therasia period.

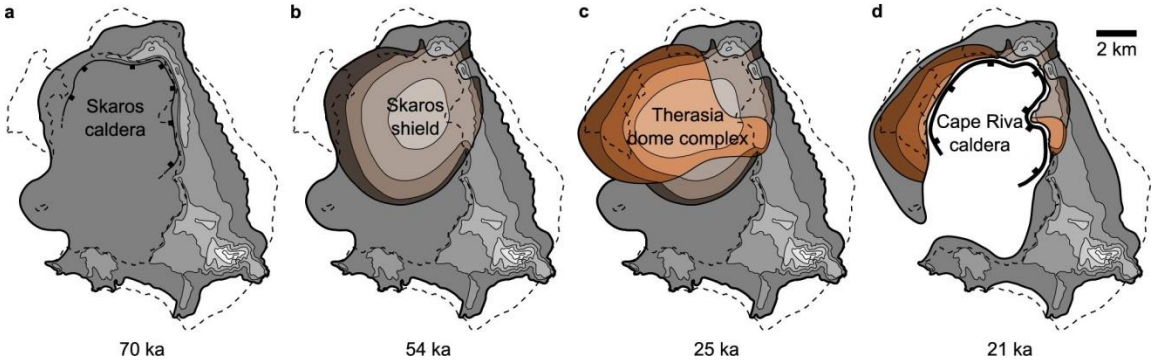

Figure 23. Extrusion of the silicic Therasia dome complex on the western flank of the Skaros shield.

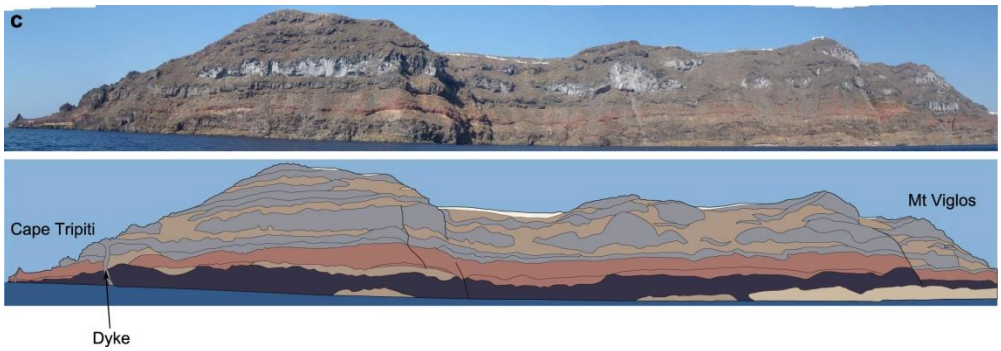

Figure 24. Lavas of the Therasia dome complex (grey) overlying those of the Skaros shield (in black). Upper Scoria 2 is in red.

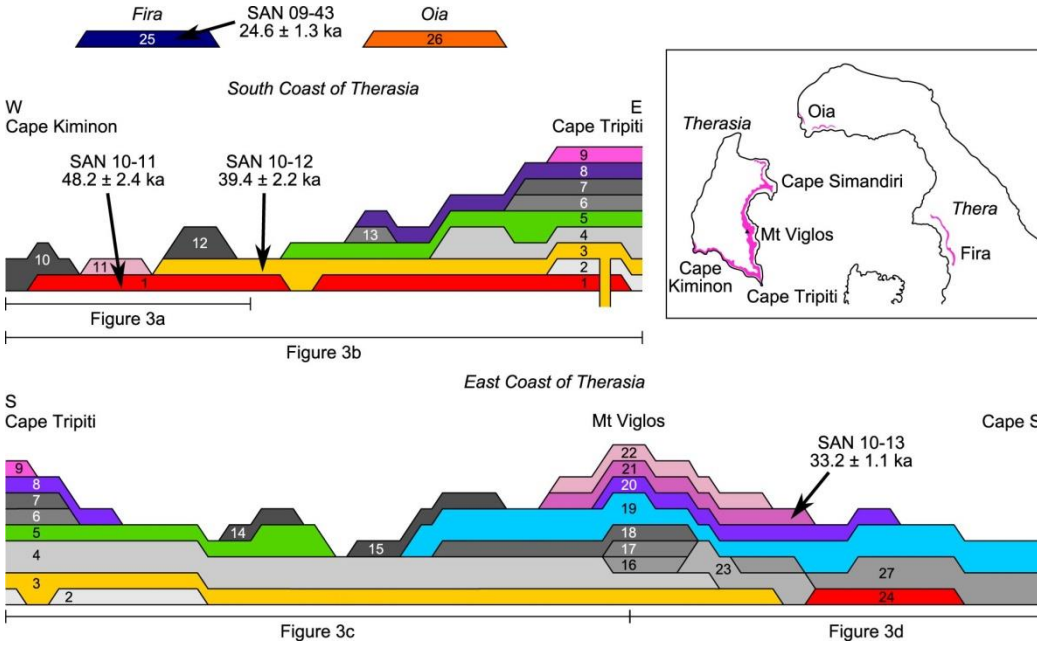

Figure 25. Architecture of the Therasia dome complex.

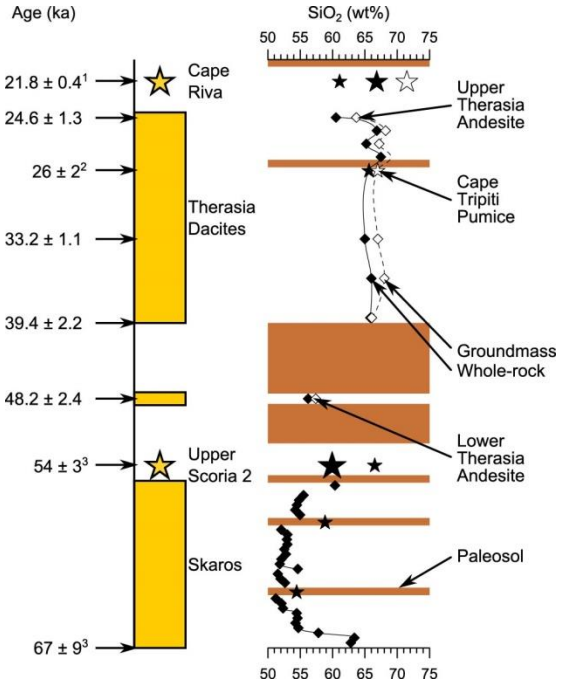

Figure 26. Chronology of the Skaros-Therasia-Cape Riva period.

Cape Riva eruption (22 ka)

Extrusion of the Therasia lavas culminated 22 ka ago with the Cape Riva eruption, which collapsed the Skaros-Therasia shield and laid down a prominent sequence of deposits all over the volcanic field (Fig. 27). The eruption began with a pumice-fall phase, the deposit from which is preserved only in northern Thera and is compositionally zoned. After the fallout phase, the eruption column collapsed and a distinctive welded ignimbrite was emplaced widely over the islands.

It was probably at this stage that the Skaros-Therasia shield began to founder. Pyroclastic flows poured out of multiple vents, laying down a succession of lithic-lag breccia and nonwelded ignimbrite up to 25m thick all over the islands (Druitt 1985). Evidence for multiple vents is provided by circumferential variations of lithic types in the pyroclastic flow deposits. The eruption terminated with a second welded ignimbrite across the peaks of northern Thera, followed by late-stage phreatomagmatic explosions.

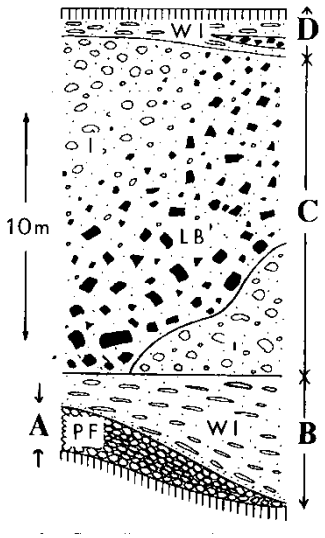

Figure 27. Generalized section through the Cape Riva products. PF: pumice fall; WI: welded ignimbrite; I: non-welded ignimbrite; LB: lithic-rich lag breccia.

The volume of magma discharged during the eruption is poorly constrained, as most of the ignimbrite lies under the sea. However distal tephra from the eruption, recognised as the Y-2 marine ash bed, is found over a very wide area of the eastern Mediterranean and as far north as the Island of Lesvos and the Sea of Marmara (Keller et al. 1978; Thunell et al. 1979; Federman and Carey 1980;Wulf et al. 2002; Margari et al. 2007; Asku et al. 2008) (Fig. 28). The dispersal area and thickness of the Y-2 ash are similar to those of the Z-2 ash from the Minoan eruption, suggesting that the Cape Riva and Minoan eruptions were of comparable magnitude (Narcisi and Vezzoli 1999; Asku et al. 2008). Fabbro et al. (2013) very approximately inferred a volume of >20 km^3 for the Cape Riva products, equivalent to >10 km^3 of magma.

The Cape Riva eruption has been dated previously by radiocarbon on charcoal from beneath the ignimbrite and via $\delta^{18}O$ wiggle matching in deep-sea sequences

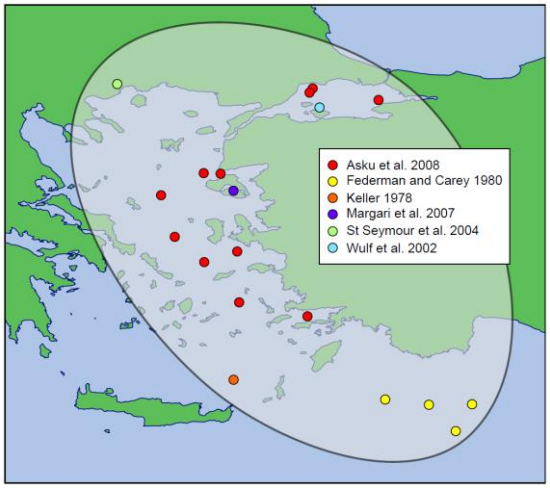

Figure 28: Distribution of the Cape Riva ash in marine and lake-bed sediment cores. Data from Asku et al. (2008), Federman and Carey (1980), Keller et al. (1978), Margar et al. (2007), St Seymour et al. (2004), Wulf et al. (2002).

hosting the distal equivalent Y-2 tephra layer. Calibration of the raw radiocarbon data against the curve of Fairbanks et al. (2005) returns a mean age of 21.8 ± 0.4 ka for Cape Riva. This yields an interval of 2,800 ± 1,400 (2σ) years between the youngest dated Therasia lava (flow 25) and the Cape Riva eruption.

The Minoan eruption (3.6 ka)

Tuffs from the Minoan eruption cover the entire outer islands (Thera, Therasia, Aspronisi), up to 55 m thick. The eruption, its products, and its effects on the Mediterranean Bronze-Age world are now summarized in detail.

Figure 29. Products of the Minoan eruption near Akrotiri.

THE MINOAN ERUPTION

The products

The Minoan eruption products (Fig. 29) have been described by Bond and Sparks (1976), Heiken and McCoy (1984), Sparks and Wilson (1990), Sigurdsson et al. (1990),Wilson and Houghton (1990), Cioni et al. (2000), Taddeucci and Wohletz (2001), Pfeiffer (2001), and Druitt (2014). Lithic thermal remnant magnetism (TRM) studies were carried out by McClelland and Thomas (1990) and Bardot (2000). Five eruption phases are recognized (phases 0 to 4, denoted P0 to P4).

Phase 0. The eruption began with precursory explosions that left two lapilli fallout layers and a phreatomagmatic ash totalling 10 cm in thickness. Cioni et al (2000) estimated that the two lapilli layers were laid down from a subplinian plume 7–10 km high. The plume was blown to the SSE, so that P0 is restricted to that sector of Thera.

Phase 1. The plinian pumice fall deposit from phase 1 is up to 5.5 m thick, with isopachs and a southeasterly dispersal axis indicative of a subaerial vent between present-day Nea Kameni and Fira (Fig. 17). The deposit has, from the base upwards, a reversely graded, crudely bedded unit overlain by a coarser, unbedded unit that is normally graded in its upper part and contains up to a few percent of andesitic scoria . An ash-rich pyroclastic surge layer separates the latter unit from a thin capping fallout unit. The fallout has a SSE dispersal similar to that of P0. The maximum eruption column height

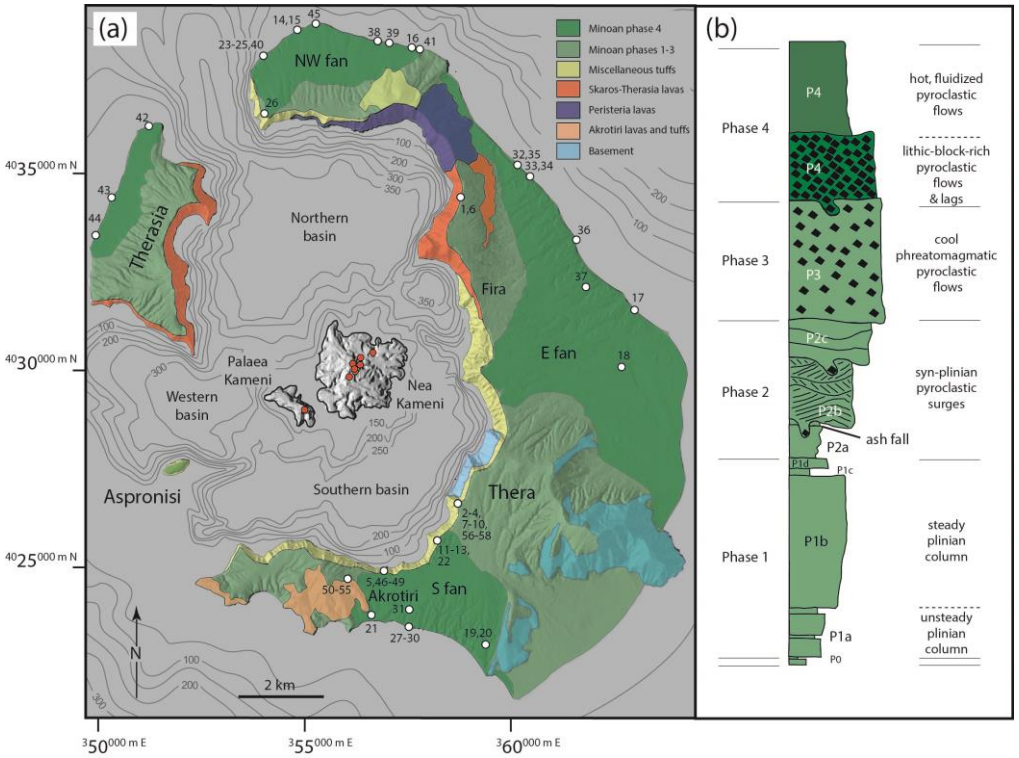

Figure 30. (a) Distribution of the Minoan products and the three ignimbrite fans. (b) Schematic profile through the products.

during phase 1 has been estimated as 36 ± 5 km (Sigurdsson et al. 1990; Sparks and Wilson 1990).

Phase 2. The phase 2 products are dominated by pyroclastic surge deposits with multiple bedsets, dune-like bedforms with wavelengths of several meters or more, bomb sag horizons, and TRM temperatures of 100–250 °C. The lowest bedset is fine-grained and contains accretionary lapilli. The overlying sequence of multiple bedsets is much coarser grained and contains lenticular layers of surge-reworked plinian fallout pumice, showing that the surges were synplinian.

Phase 3. P2 grades upwards though a series of massive, thick-bedded units into the low-grade ignimbrite of phase 3, the thickness of which reaches 55 m at the caldera wall. The P3 ignimbrite is massive to crudely bedded, with multiple flow units. Lithic blocks up to a meter or more in diameter are common. The evidence for an important component of water–magma interaction in the origin of P3 is (1) the commonly vesicular nature of the matrix, (2) the heterogeneity of the matrix vesicularity on an outcrop scale, (3) common breadcrusted pumices, and (4) emplacement on slopes of up to 30°, suggestive of significant particle cohesion. This is consistent with the low, and variable, emplacement temperatures obtained from TRM measurements (0–300 °C). Water–magma interaction occurred at a high crustal level, at or near the peak of magma vesiculation (Wilson and Houghton 1990). P3 has been interpreted as the deposit from low-temperature, three-phase (solid, gas, water) cohesive pyroclastic flows, with subordinate ballistic, surge, mudflow, and slump facies (Heiken and McCoy 1984; Wilson and Houghton 1990; Sparks and Wilson 1990).

Phase 4. The final phase of the eruption discharged hot, fluidized pyroclastic flows that constructed three

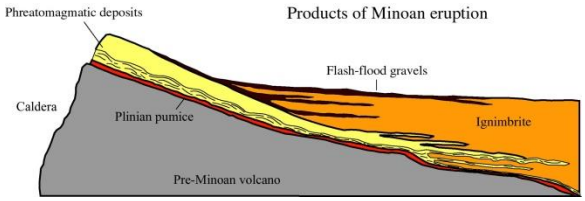

Figure 31. Schematic profile through the Minoan products (Bond and Sparks, 1976)

ignimbrite fans (NW, E and S) (Figs. 30, 31). The dominant facies is a tan coloured compound ignimbrite. The ignimbrite is mostly fine-grained (ash and lapilli grade), with a high abundance of comminuted lithic debris in the ash fraction (Bond and Sparks 1976). Lithic clasts in the ignimbrite give TRM temperatures of 200–400 °C (McClelland and Thomas 1990). Layers of intercalated lithic lag breccia give high TRM temperatures for lithic clasts (150– 350 °C; Bardot 2000), showing that the breccias were emplaced by hot pyroclastic flows. The S and E fans are composed mainly of ignimbrite, whereas coarse lithic lag breccias dominate much of the NW fan. Minoan ignimbrite up to 80m thick lies offshore (Sigurdsson et al. 2006).

The phase 4 deposits are capped in many places by fluvial gravels and sands (typically 1–3 m in thickness), overlain in turn by up to a meter of wind-reworked ignimbrite. The gravels cut the ignimbrite as broad, meandering channels, form multiple incisional terraces, and occur up to 40 m above sea level. They are best developed along the margins of high relief, as expected from an origin by rain runoff.

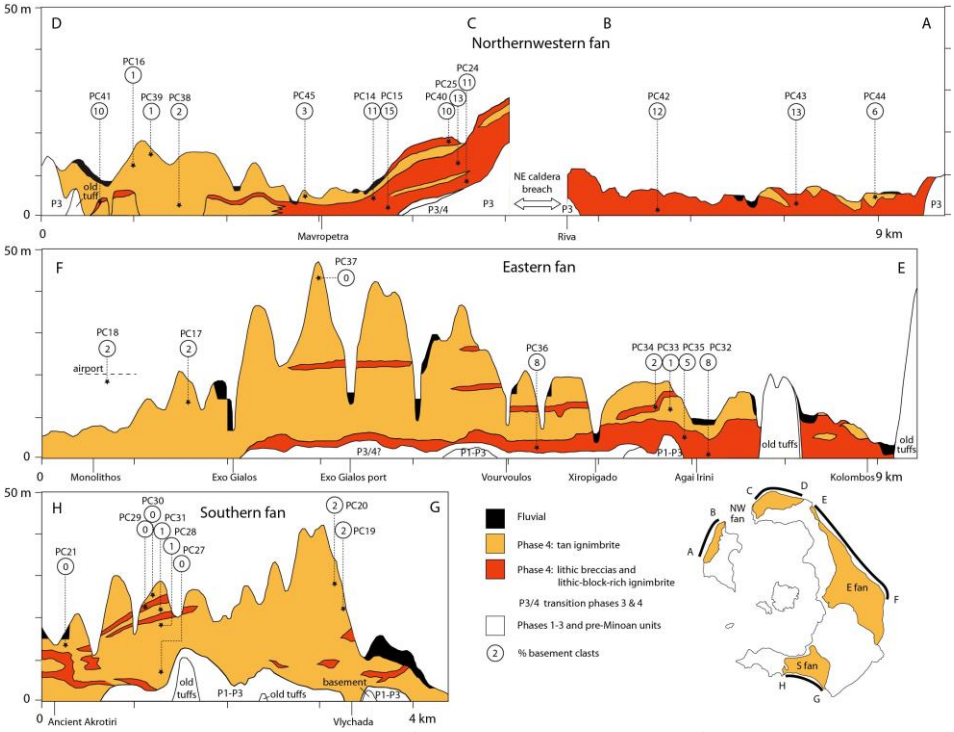

Figure 32. Coastal profiles through the three ignimbrite fans.

The discharged volume for the eruption was calculated by Pyle (1990) as 27–30 km^3 DRE, and Sigurdsson et al. (1990) estimated about 39 km^3 DRE. Sigurdsson et al (2006) revised these estimates upwards based on seismic imagery showing abundant young deposits on the seafloor surrounding Santorini. Interpreting these as Minoan ignimbrite, the authors concluded that the DRE volume of the eruption could be as high as 60 km^3. Most of the volume is accounted for by phase 4 ignimbrite. Downfaulted intracaldera fill could increase this estimate by 28–40 % (Johnston et al., 2015).

Eruption components

Three vesicular (magmatic) components occur in the Minoan products (Figs. 33, 34) (Druitt 2014).

- White rhyodacitic pumice is the dominant (>>99 %) type, and is compositionally uniform (70 wt% SiO_2, 10-15 vol% crystals) in all eruption phases.
- Microphenocryst-rich andesitic pumices occur in P0 and P1, and exceed the white pumice in abundance at the very base of P0. They are texturally and compositionally gradational into glass-bearing to holocrystalline dioritic nodules that are abundant towards the top of P1.
- Cauliform andesitic enclaves up to a dm in size occur in P1, especially towards the top. Many have adhering rinds of white pumice, showing that they were immersed in the rhyodacitic magma prior to eruption, and released from their host upon fragmentation.

The two andesitic components are a compositionally distinctive batch of andesitic magma that is rich in Ba and poor in Zr compared to other andesites of the last 550 ka at Santorini (see later). The enclaves represent quenched blobs of this magma that mingled with the

Figure 33. Components of the Minoan tuffs

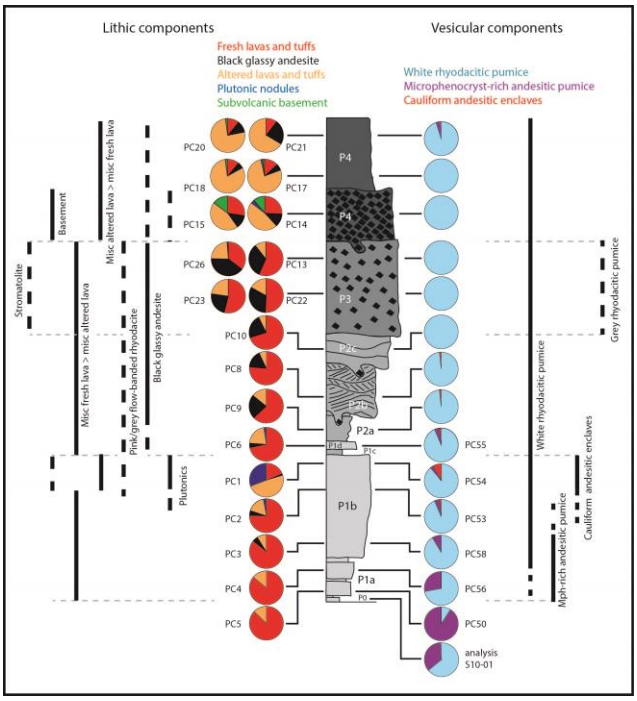

Figure 34. Distribution of some key components in the Minoan tuffs

rhyodacitic magma. The microphenocryst-rich pumices and granitoid nodules are interpreted as the contents of a shallow, variably crystallized andesitic-dioritic intrusion that was partially pushed out by the ascending rhyodacite during the eruption.

Some key lithic components are;

- Miscellaneous lavas and tuffs.
- Fragments of limestones and schists from the basement;
- Dioritic plutonic nodules, cogenetic with the microphenocryst-rich andesitic pumice.
- Blocks of stromatolite and travertine from within the partially flooded 22 ka (Cape Riva) caldera, which still existed prior to the Minoan eruption (see later);
- A distinctive black glassy andesite that is chemically similar (high-Ba, low-Zr) to the two magmatic andesitic components, and which is interpreted as fragments of an ancient edifice within the 22 ka caldera (Fig. 35).

The stromatolites and black glassy andesite are particularly abundant in P3.

Reconstruction of events

Vent development during the eruption has been reconstructed as follows (Fig. 35).

- Following initial phreatic and phreatomagmatic explosions, the rhyodacitic magma reaches the surface by exploiting a partially solidified shallow intrusion of high-Ba andesite.
- The subplinian (P0), then plinian (P1), phases take place at a subaerial vent near Nea Kameni.
- The vent migrates northwards into the partially flooded 22 ka caldera, causing production of synplinian surges (P2).
- The vent migrates fully into the 22 ka caldera, producing violent phreatomagmatic explosions and ejection of large quantities of the andesitic intracaldera edifice and stromatolite colonies (P3).
- Once the water supply is cut off, due either to exhaustion of the caldera water, or construction of a huge tuff cone (Johnston et al. 2015), the eruption reverts to dry mode, and large volumes of hot, fluidized pyroclastic flows are discharged, possibly from multiple vents (P4).
- The vents were still subaerial when the

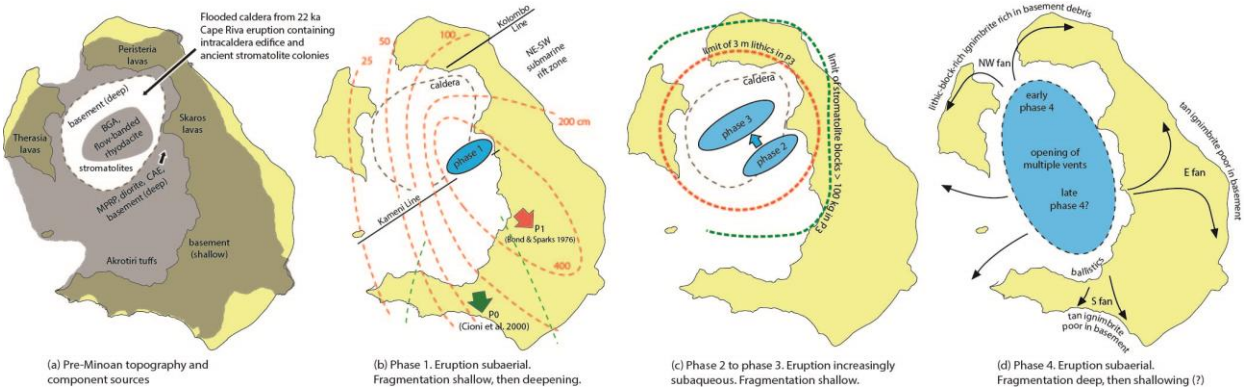

(a) Pre-Minoan topography and component sources

(b) Phase 1. Eruption subaerial. Fragmentation shallow, then deepening.

(c) Phase 2 to phase 3. Eruption increasingly subaqueous. Fragmentation shallow.

(d) Phase 4. Eruption subaerial. Fragmentation deep, then shallowing (?)

Figure 35. Vent evolution during the Minoan eruption

eruption ceased, implying that either (1) the caldera collapsed during the eruption but remained isolated from the sea, or (2) the caldera collapsed after the eruption.

Age of the eruption

The conventional archaeological age for the eruption (1500-1550 BCE) has recently been revised (Fig. 36). The eruption has been dated by the ^{14}C method on short-lived samples (seeds, twigs) preserved in the Bronze-Age town of Akrotiri (1660–1613 BCE; Manning et al. 2006; 95 % confidence limit) and by ^{14}C wiggle-match dating of an olive tree buried in the plinian fall deposit (1627–1600 BCE; Friedrich et al. 2006; 95 % confidence limit). Insect death assemblages constrain the eruption month to June or early July (Panagiotakopulu et al. 2013). Modelling of ash dispersal favours an eruption in the spring (Johnston et al. 2012).

Tree frost damage in high-altitude bristlecone pines from California (1627±2 BCE) (LaMarche and Hirschboeck 1984), and in Irish oaks (Baillie and Munro 1988), may or may not record the Minoan event.

Sulphuric acid peaks occur in Greenland ice cores at depths corresponding to the same time period (Hammer et al. 1987). However one of these (1645±4 BCE GRIP peak) is now known to be due to the Aniakchak eruption in Alaska (Eastward et al. 2004).

Effects of the eruption

At the time of the eruption, Santorini was a major commercial centre of the Aegean world. Events at the contemporary town of Akrotiri have been reconstructed thus: (1) orderly evacuation of the town, (2) earthquake destruction, (3) work teams return to demolish buildings, open up streets and clear rubble, (4) rapid and final abandonment, (5) burial.

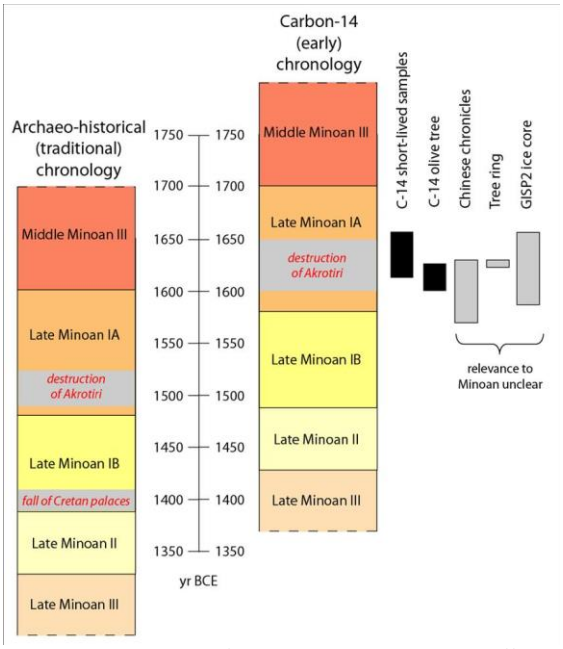

Figure 36 Age. estimates for the Minoan eruption using different methods.

The eruption has been proposed as a factor in the mid-16th century BCE collapse of the Minoan civilization on Crete (Marinatos 1939) due to ash fallout, tsunamis, climatic effects, or some combination of these.

Ash fallout did not in fact exceed a couple of cm on Crete (Fig. 37). Even the town at Trianda (Rhodes), which suffered ~30 cm of ash, subsequently recovered. So ash probably did not have a lasting effect on Minoan Crete.

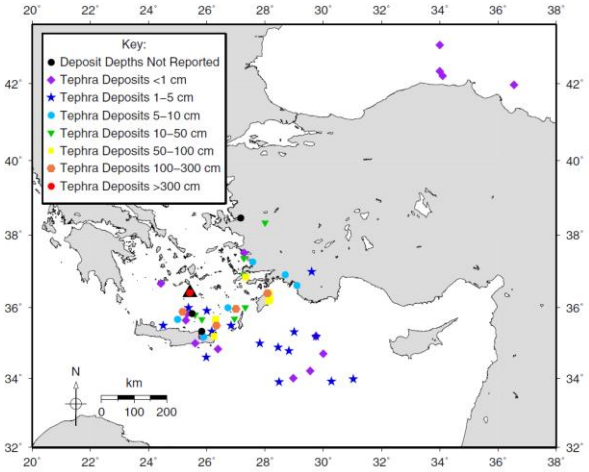

Figure 37. Occurrences of distal Minoan ash (Johnston et al. 2012).

Possible tsunami deposits from the eruption have been identified around the Aegean coastline. The most convincing case occurs at Paleokastro (E. Crete), where a thick debris layer rich in pot sherds, building debris, animal bones and marine organisms directly overlies the Minoan ash, at an elevation implying wave heights of >5 m (Bruins et al. 2008).

The Minoan magma is poor in S. Estimates give a SO_2 yield of only 5-8 Mt, less than that of Mount Pinatubo in 1991 (~18 Mt) (Pyle 1997). The resulting tropospheric cooling (<0.5 °C for 1-2 yrs) probably would not have had much impact on the late Bronze-Age world. On the other hand, the high dissolved Cl content of the melt, coupled with the probable existence of a magmatic hypersaline (brine) phase, could have released 50-675 Tg of Cl. Modelling has shown that, even if only 2% of the Cl reached the stratosphere, it could have reduced the thickness of the ozone column by 20 to >90 %, with recovery taking a decade (Cadoux et al. 2015).

The theory of Spyridon Marinatos (1939) that the eruption directly triggered collapse of the Minoan civilization does not appear to be supported by modern evidence. The eruption occurred up to a few generations before Minoan decline. Effects of ash fallout and climate modification were probably minor, although the effect of impact on the ozone column needs to be evaluated. Tsunamis could have weakened Minoan society through impact on shipping, ports and commerce prior to the known Mycenean invasions of the mid-to-late 16th century.

KAMENI VOLCANO (197 BCE – 1950)

Intracaldera volcanism since Minoan times has built the present-day islands of Palaea Kameni and Nea Kameni (Figs 38). These are the subaerial expression of a 4.3 ± 0.7 km^3 intracaldera shield, 3.5 km in basal diameter, the summit of which towers 470 m above the caldera floor. The shield was constructed by prolonged leakage of magma up the Kameni Line. Vents on Nea Kameni lie within a 600-m-wide NE-SW-trending zone which reflects fault control on magma ascent (Fig. 39).

Nine subaerial eruptions have been reported or deduced from historic records (Fytikas et al., 1990) Each discharged flows of highly viscous dacite at 1-4 m^3/s, typically accompanied by weak Vulcaniam explosions with plumes up to 3 km and ballistic showers (Figs. 40,

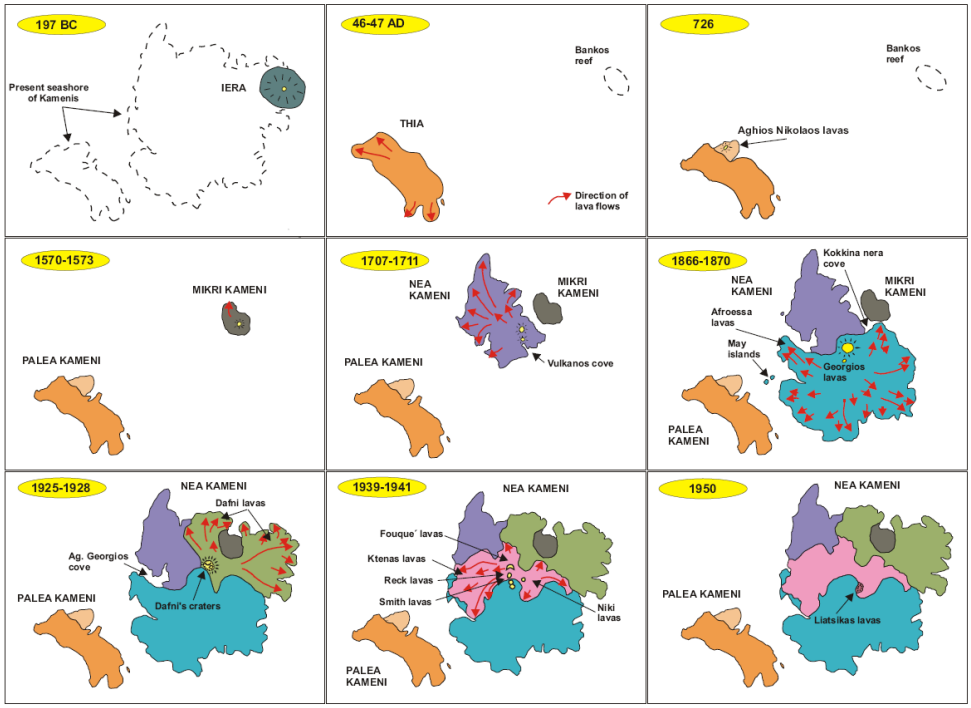

Figure 38. Evolution of the Kameni Islands (Fytikas et al. 1990).

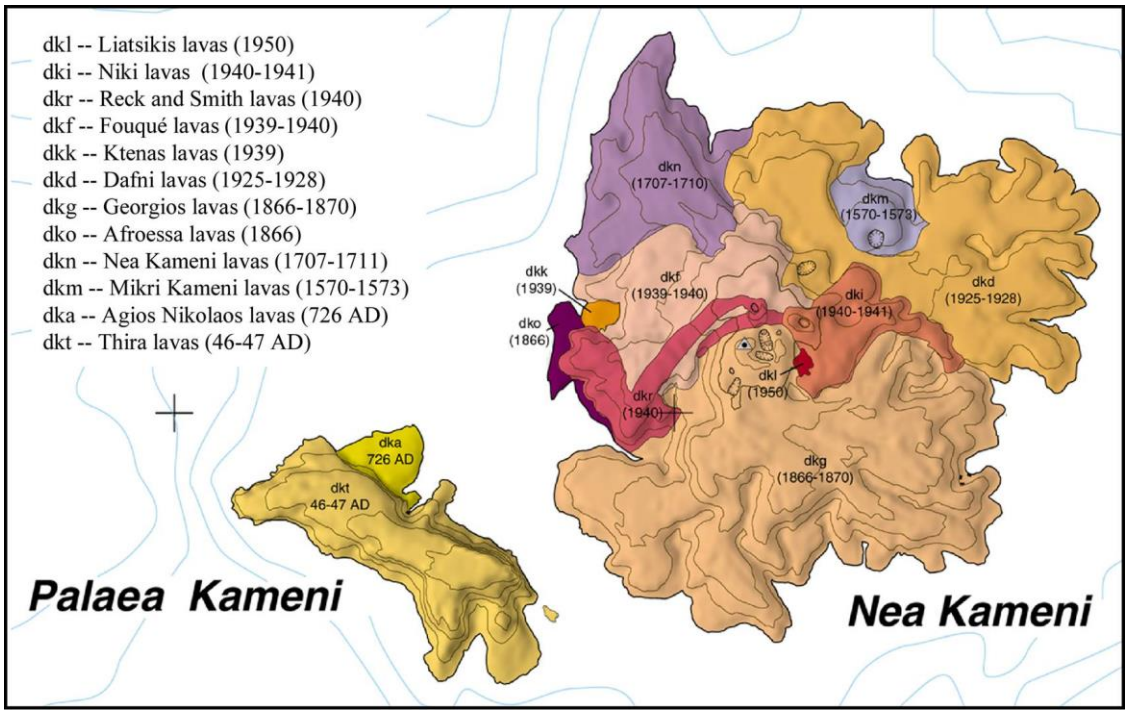

Figure 39. Geological map of the Kameni Islands (Druitt et al. 1999).

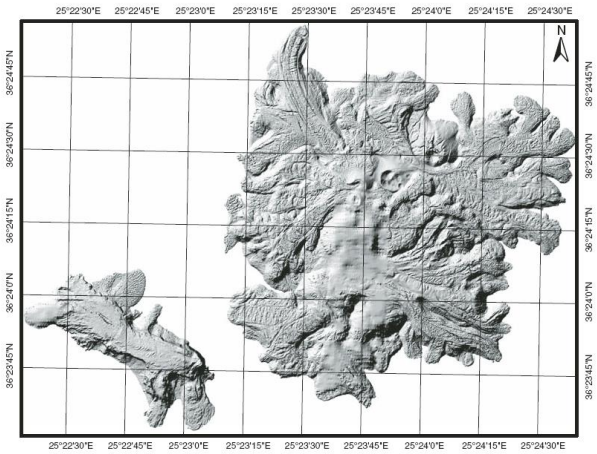

Figure 40. Viscous dacitic lavas of the Kameni Islands, showing channels and levees (Pyle and Elliot 2010).


Figure 41. A typical vulcanian explosion. Nea Kameni 1950.

41). The eruptions of 1866-70, 1925-28, and 1939-41 were preceded by increases in sea-water temperature and by coastal subsidence.

197 BCE. Explosive activity mentioned by Strabo built up a pyroclastic cone (Iera). The present-day Bankos Reef NE of Nea Kameni may be a remnant of Iera.

AD 46-47. Extrusive activity mentioned by Aurelius Victor in Historia Romana formed Thia island, which is believed to be present-day Palaea Kameni.

726. Following a repose of seven centuries, explosive activity occurred from a vent near Palaea Kameni, spreading pumice all over Asia Minor. This was probably followed by volcanotectonic collapse, forming the steep NE cliff of Palaea Kameni, then by extrusion of the Ayios Nikolaos lavas.

1570-1573. Activity shifted to the NE and formed the island of Mikri Kameni.

1707-1711. The eruption began on the west flank of Mikri Kameni with very slow lava extrusion.
Alternation of extrusive and explosive eruptions constructed the original island of 'Nea Kameni' over the next four years.

1866-1870. The eruption began with slow lava extrusion. Two days later the first explosions began and the eruption column height reached 2 km. In all there were three eruptive centres: Georgios, which was active continuously, Afroessa, characterised by slow, then rapid lava extrusion, and the centre of May's Islands, which emerged from the sea off the west coast of Nea Kameni.

1925-28. Activity began with jets of water from Kokkina Nera Bay, followed by the first lava and explosions. Soon the eruptions shifted to the NW to the centre of Dafni. Explosive activity dominated at Dafni, with clouds reaching 3 km. Some small pyroclastic flows were generated from this centre. A long repose period occurred between May 1926 and January 1928, before the extrusive activity which terminated the eruption.

1939-41. The eruption began with a submarine explosion. Activity then shifted to the centre of Nea Kameni, where lava extrusion built up the flows and domes of Ktenas, Fouqué, Smith-Reck, and Niki. In each case the appearance of lava was preceded by phreatic explosions. Only the 'twin-funnel' phreatic crater was not the site of later lava production.

1950. After some phreatic activity, extrusion of the Liatsikis lava occurred.

Recent bathymetric imagery of the Kameni edifice have revealed previously unknown lava flows and submarine extensions of historical ones (Fig. 42). The edifice is surrounded by a clastic apron that brings the total DRE volume of products from Kameni to 4.85 ± 0.7 km^3 (Nomikou et a. 2014). There appears to be a linear correlation between erupted volume and the length of the repose period preceding the eruption (Fig. 43). This can be used for predictive purposes (see later).

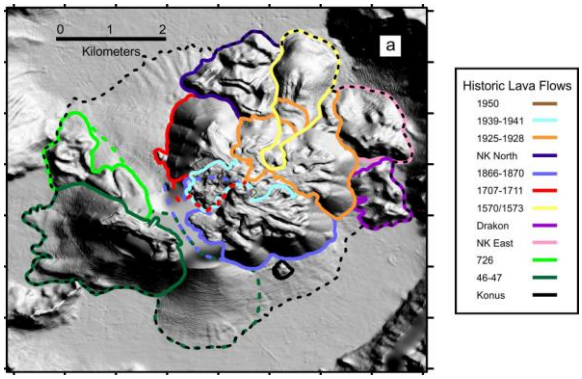

Figure 42. The Kameni edifice (Nomikou et al. 2014)

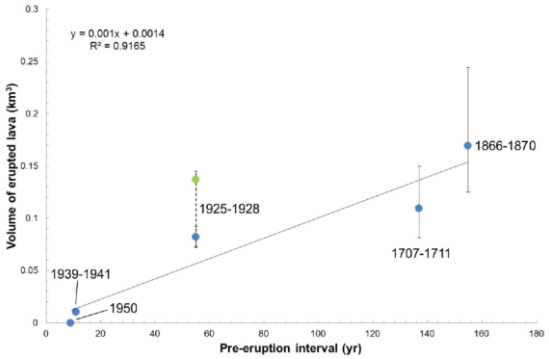

Figure 43. Volume-repose correlation at Kameni (Nomikou et al. 2014)

THE KOLOMBO ERUPTION (1650)

Following two years of intense seismic activity and submarine extrusion, an explosive eruption began on 27 September 1650 at the site of Kolombo Reef, 7 km NE of Thera. Initial calm extrusion was replaced by strong explosions, producing large quantities of ash. A large tsunami on 29 September caused widespread damage on Santorini and elsewhere within a 150 km radius. Abbé Pegues wrote: *'Monday 30 September, and the three following days, the inhabitants were suddenly seized with excruciating pain in their eyes. Few escaped this evil, and most remained blind three days. Many sank under the pain of this malady, and others were suffocated by the pestilential vapours thrown out of the volcano. In parts of the island nearest to it, the number of persons killed amounted to 50, and of animals upwards of 1000 of all kinds'.*

The eruption emitted about 2 km^3 of a H_2O-rich, biotite-bearing rhyolitic magma. The top of the subaerial cone was subsequently eroded to 18 m below sea level.

Kolombo is the largest of the line of 19 submarine centres extending up to 20 km NE of Santorini. It can be considered as part of the same magmatic system as Santorini. The cone is 3 km high with a 1.5-km-diameter, 500-m-deep summit crater (Fig. 44) containing a high-temperature hydrothermal field discharging acidic (ph 5), CO_2-rich fluids. Polymetallic spires and iron-microbial mats are present on the caldera floor (Cantner et al. 2013; Carey et al. 2013; Kilias et al. 2013).

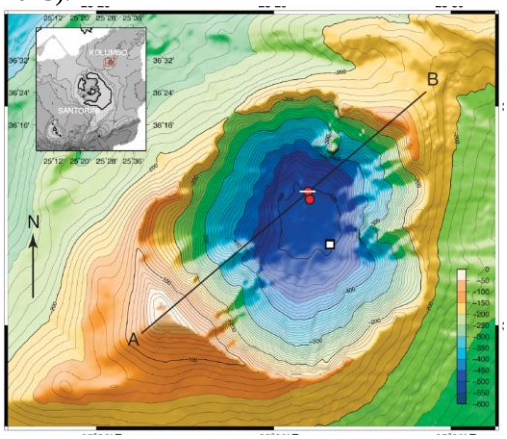

Figure 44. Kolombo summit crater (Carey et al. 2013).

THE EARTHQUAKE OF 1956

Santorini and neighbouring islands were struck on 9 July 1956 by a large earthquake, the epicentre of which lay to the NE, near the island of Amorgos. The magnitude is estimated to have been 7.8. The event caused extensive damage to the town of Oia and elsewhere on Santorini. It also generated a tsunami, the run-up of which was reported as 10-20 m on Amorgos and Astypalia. This tsunami is greatly in excess of what is expected from such an earthquake, and it has been attributed to (and modelled by) a submarine landslide generated by the event (Okal et al. 2009).

CALDERA UNREST OF 2011-12

In January 2011, the caldera entered a phase of unrest that lasted until March of 2012. The number of small-magnitude (M< 3.3) volcanotectonic earthquakes greatly increased at depths of 1-6 km on a near-vertical plane 6 km in length along the Kameni line (Newman et al. 2011) (Figs. 45 and 46a). The increased seismicity was accompanied by up to about 10 cm inflation of the islands measured by GPS networks and by radar interferometry and corresponding to a volume increase of about 10-20 million m^3 at a depth of 3-6 km beneath the caldera (Newman et al. 2011; Parks et al. 2012; Papoutsis et al; 2012; Foumelis et al 2013) (Fig. 46a). Small increases in the flux of H_2 and of mantle-derived CO_2 also occurred during the unrest (Parks et al. 2013; Tassi et al. 2013).

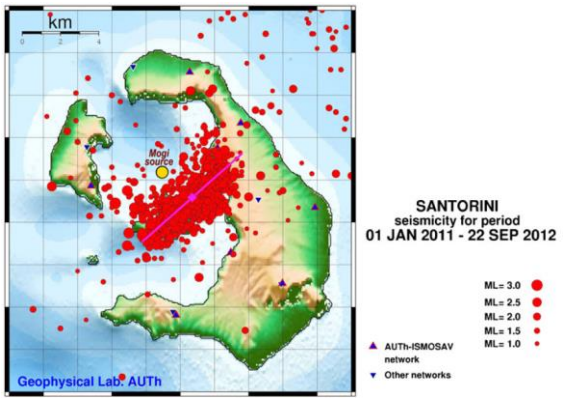

Figure 45. Seismicity distribution during the unrest period. Data from the University of Thessaloniki.

By combining measurements of $\delta^{13}C$ and ^{222}Rn, Parks et al. (2013) showed that the CO_2 liberated during the unrest was a mixture of deep, magmatic CO_2 and CO_2 liberated by thermo-metamorphic breakdown of basement limestones.

The volume increase has been attributed to intrusion of magma (Newman et al. 2011; Parks et al 2012). The inflation may have involved fluids in addition to magma. It may also have been in part tectonic in origin, stress accumulation on regional faults (Feullet 2013) causing flexuring of the caldera block and increasing rock permeability and hence gas emissions (Tassi et al. 2013).

Parks et al. (2015) used a 20 year record of GPS and Insar data to reveal a slow (~6 mm/y) subsidence of southern Nea Kameni between 1993 and 2010, followed by unrest-related inflation of 2011-2012. The subsidence is attributed to thermal contraction and ground loading due to the 1866-70 lavas (Fig. 46b). They modelled the unrest inflation as two intrusion pulses: one of 11.6 ± 0.1 million m^3, followed by another of 9.7 ± 0.1 million m^3, accompanied by a visco-elastic crustal response (Fig. 46c).

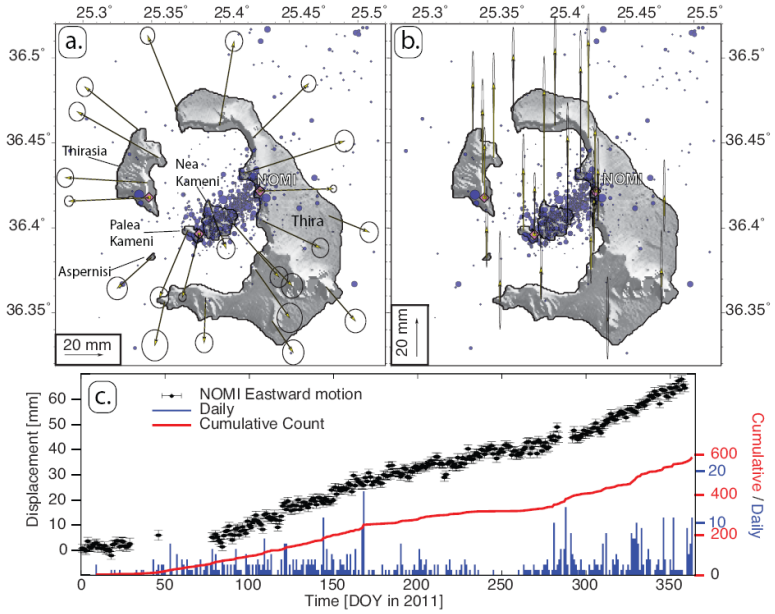

Figure 46a. Unrest GPS data of Newman et al. (2011)..

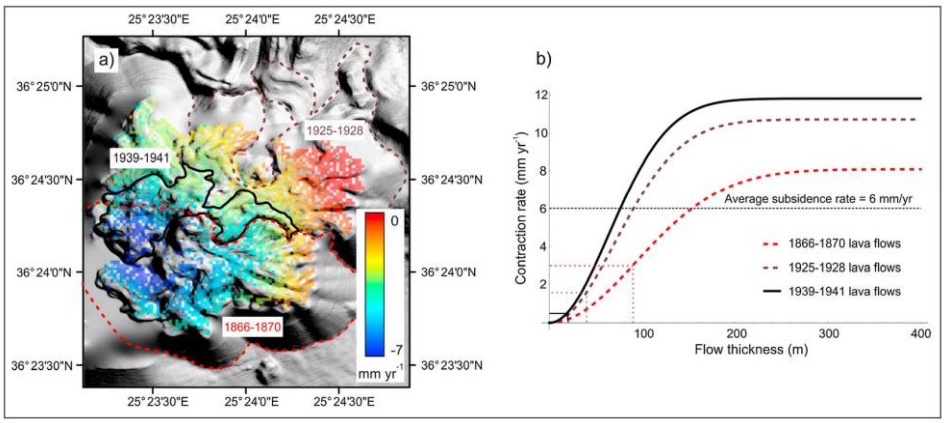

Figure 46b. (a) Merged bathymetry and LiDAR grid after Nomikou et al. [2014], overlain with mean LOS displacements (mm/yr) computed using ascending Envisat interferograms from track 329. LOS displacement is negative away from the satellite. The red dashed polygon represents the outline of the 1866–1870 lava flow. The brown dashed polygon represents the outline of the 1925–1928 lava flow, and the black polygon represents the outline of the 1939–1941 lava flow. The dashed lines represent the extrapolated boundaries of the 1866–1870 and 1925–1928 lava flows. The northwest part of the 1866–1870 flow is thought to reside beneath the 1939–1941 lava flows. (b) Modeled thermal contraction rate of historic lava flows (mm/yr), plotted as a function of lava flow thickness.

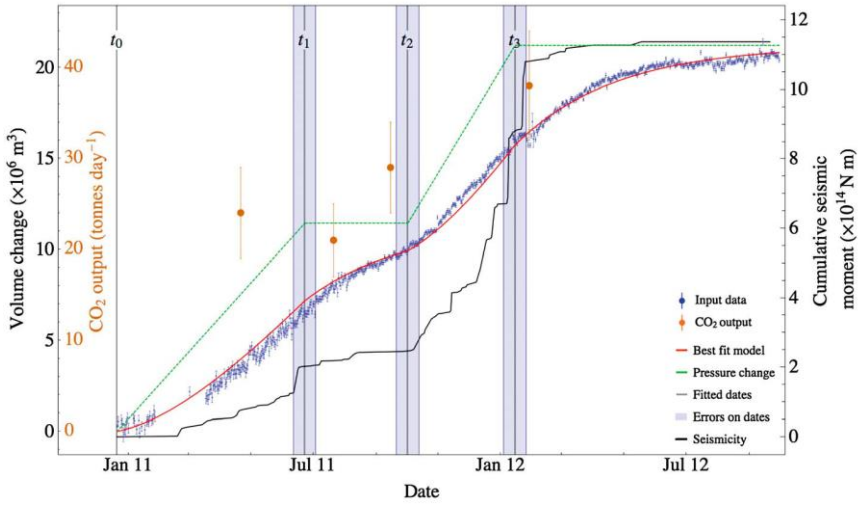

Figure 46c. Comparison between the viscoelastic relaxation model (red line), joint inversion result (blue dots), cumulative seismic moment released during VT earthquakes >ML 2.0 occurring within the caldera (black line) (derived using data from the Aristotle University of Thessaloniki [2005]—online catalog), and CO2 output from the summit of Nea Kameni (orange dots) (data from Parks et al. [2013], Figure 4). It should be noted that these CO2 values are derived from a small area on the summit of Nea Kameni and can only be seen as suggestive of trends in the broader flux of CO2 through the Santorini volcanic system. Temporal variation in the gas chemistry from fumaroles, reported by Tassi et al. [2013], is also consistent with a period of magma intrusion to the shallow system from early 2011 to early 2012. The green lines represent the normalized pressure model, displaying a linearly increasing pressure from t0 to t1 and from t2 to t3. In between t1 and t2 and after t3, the pressure within the shallow magma chamber is held constant

THE MINOR TUFF SUCCESSIONS

Deposits of the twelve main explosive eruptions of Santorini are separated by sequences of minor tephra, each of which is typically a few metres thick, but may exceed 15 m. These minor sequences contain four principal types of deposit: (1) scoria-fall deposits, predominantly of andesitic composition, generated by violent Strombolian or sub-Plinian eruptions; (2) ash fall layers generated by weak Strombolian or Vulcanian explosions; (3) thin, fine-grained base-surge layers; (4) deposits of yellowish wind-reworked ash and lapilli similar to deposits documented on Japanese stratovolcanoes such as Sakurajima, where they are related to long-lived Vulcanian or weak-Strombolian ash emissions over tens or hundreds of years; (5) yellow-brown palaeosols representing long periods of dormancy

The minor successions record prolonged periods of minor explosive activity, lava extrusion and shield construction between the main explosive eruptions.

ERUPTIVE CHRONOLOGY

Activity at Santorini began in the late Pliocene with the eruption of submarine ashes. The oldest preserved lava was extruded ~650 ka ago, and from then on volcanism continued without significant break until the present day (Fig. 47).

Owing to repeated caldera collapse and the probable existence of submerged flank vents and lavas, it is certain that our record of volcanism is incomplete. Nonetheless, the longest pause in volcanism allowed by the age data amounts at most to a few tens of thousands of years, and at the 1σ level is essentially zero.

Activity of the early rhyodacitic centres of Akrotiri Peninsula lasted until 580 ka. Formation of Peristeria Volcano, which consisted of at least two overlapping edifices, lasted from 530 to at least 430 ka. The onset of major explosive volcanism took place around 360-460 ka. During the subsequent period, 12 major explosive eruptions have each discharged considerable volumes (km^3 to tens of km^3) of intermediate to silicic magma, and lava extrusion has formed at least 7 lava shields of various sizes. The first mafic-to-silicic cycle persisted until 172 ka (Lower Pumice 2). The duration of cycle 2 was 168 ky (172 to 3.6 ka).

On the basis of available data, apparent intervals between major explosive eruptions varied between 20 and ~40 ky. Given that minor pyroclastic sequences between the major tuffs preserve evidence for some 100 or so minor explosive eruptions, the recurrence interval for an eruption large enough to lay down a deposit at least several cm thick on the caldera rim of Santorini is of the order of 3000-4000 y.

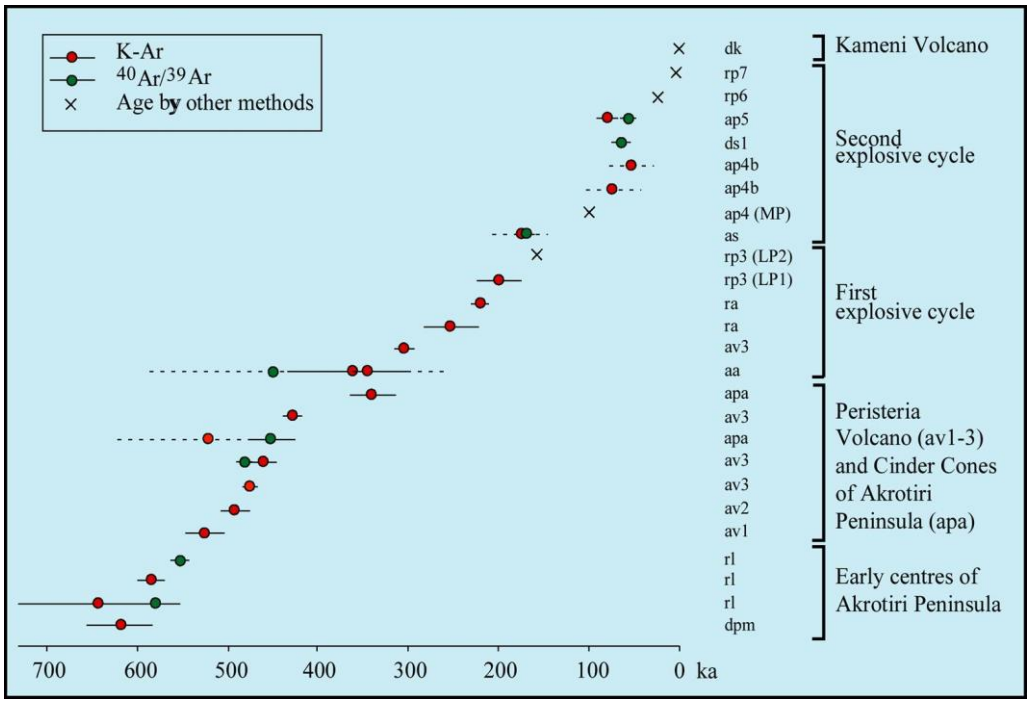

Figure 47. Summary of radiometric ages for Santorini (Druitt et al. 1999).

ERUPTIONS AND SEA LEVEL

Low sea level has been invoked as a possible mechanism for triggering eruptions at island volcanoes. Low sea level reduces the overload on a magma chamber, favouring tensile fracturing of the chamber roof and dyke injection (Wallman et al., 1988). The two Lower Pumice eruptions occurred during a period of strongly fluctuating sea level. Our best estimates of their

ages (184 ka for LP1 and 172 ka for LP2) correspond to glacial advances when sea level was low. It is therefore possible that these two eruptions were triggered by sea-level retreat. Another candidate is the 22 ka Cape Riva eruption, the age of which lies at the last glacial maximum when sea level was more than 100 m lower than present.

The Minoan eruption, on the other hand, was clearly not triggered by low sea level. The Aegean Sea 3600 years ago lay less than 0.5 m below its present level (Fleming and Webb 1986).

PROXIMAL IGNIMBRITE FACIES

Proximal facies of pyroclastic flow deposits abound in the caldera walls of Santorini, and consist of coarse-grained lithic breccias and spatter agglomerates (Druitt & Sparks, 1982; Mellors and Sparks 1991). Recognition of the primary nature of these deposits was crucial to unravelling the complex eruptive history of the islands.

Lithic-rich co-ignimbrite lag deposits.

These lithic breccias, which were first described and interpreted in detail by Druitt and Sparks (1982), form by proximal sedimentation of lithic blocks too large and too dense to be transported by the parent pyroclastic flows (Fig. 48). Efficient segregation and deposition of coarse, dense lithic debris occurs close to the vent due to complex sedimentation-fluidization processes at the base of the collapsing eruption column.

The breccias are thick (several metres or more), coarse-grained (lithics a metre or more in diameter), clast-supported, poorly sorted, and beds from individual eruptions are distributed widely over the islands (Fig. 49). As typical of deposits from pyroclastic flows, they thicken and coarsen into depressions and thin onto highs. Early workers interpreted the breccias as the deposits from debris flows, but a primary origin is favoured because (1) they grade laterally and vertically into ignimbrite, often in a coarse-tail manner, (2) they contain segregation pipes, pods and lenses indicative of gas fluidization, (3) they contain abundant pumice, (4) some examples have large basal impact sags, implying a strong ballistic component at the onset of breccia deposition (Fig. 19), and (5) lithic blocks in at least two examples were emplaced at temperatures greater than 300ºC, as shown by their thermal remnant magnetism (McClelland & Druitt, 1988) (Fig. 50). The breccias exhibit very complex and spatially rapid facies variations that seem also to be characteristic of proximal pyroclastic flow deposits elsewhere. At some locations, several stacked flow units are observed, each unit having a fine-grained basal layer analogous to an ignimbrite 2a layer (Fig. 51). Large volumes of ignimbrite generated by lag-breccia-forming eruptions are believed to lie buried on the coast and under the sea at Santorini.

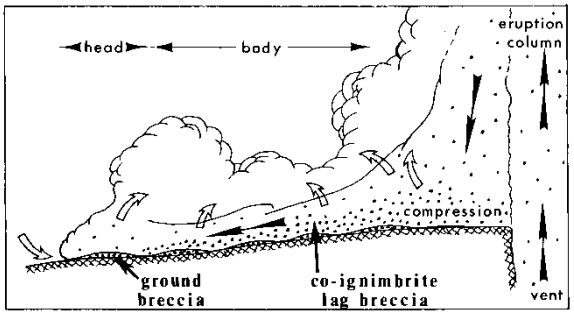

Figure 48. Cartoon showing segregation of lithics and sedimentation of lag breccias close to the base of a collapsing eruption column (Druitt and Sparks 1982).

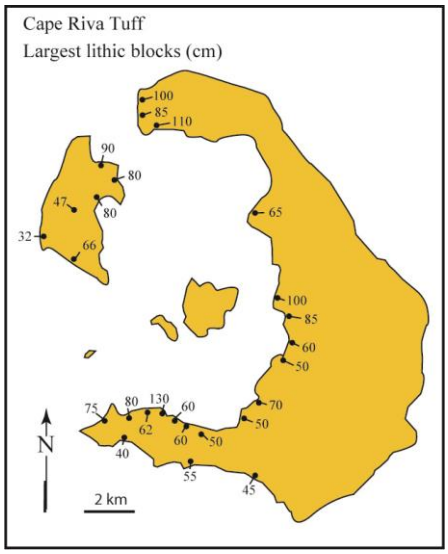

Figure 49. Average diameter (cm) of the largest three lithic clasts in the Cape Riva lag breccias (Druitt 1985)

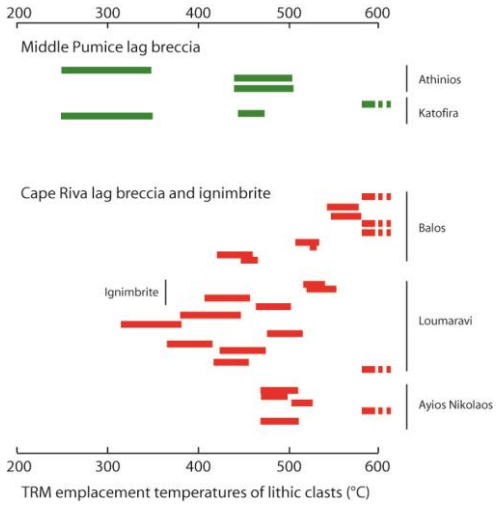

Figure 50. Estimates of emplacement temperatures of the Cape Riva and Middle Pumice lithic breccias using thermal demagnetization (McClelland and Druitt 1992).

Figure 51. The Cape Riva lithic-rich lag breccia overlying Plinian fallout from the first phase of the eruption. Oia. Two flow units of breccia are superposed here. Note erosion of the fallout at the contact.

Figure 52.Spatter-rich lag deposit of Upper Scoria 1 overlying fallout from the same eruption. Note the strong imbrication of spatter rags indicative of lateral transport from right to left. The deposit formed by proximal sedimentation of large and dense spatter rags suspended in a fast-moving pyroclastic flow. Hammer for scale.

Spatter-rich co-ignimbrite lag deposits

These coarse-grained and widespread spatter agglomerates are interpreted as a second type of proximal pyroclastic flow deposit. Type examples occur in Upper Scoriae 1 and Upper Scoriae 2, but the Middle Pumice lithic breccia grades laterally into a very similar facies at the end of the Akrotiri Peninsula. Scoria-flow deposits of Cape Therma 1 and Cape Therma 3 also develop local clast-supported lag facies.

Heiken & McCoy (1984) interpreted the agglomerates as airfall spatter. However, several features favour a significant component of lateral transport. (1) Unlike typical airfall deposits, the agglomerates exhibit no systematic variations in either thickness or grain size, despite wide distributions around the caldera (Figs. 15). One possibility is that they were erupted from vents close to the caldera wall, but there is no evidence for ring vents on Santorini. Unequivocal fallout deposits of the MP, USc1, and USc2 eruptions came from central vents on the Kameni Line (Fig. 17), so it is possible that the associated agglomerates were also erupted from near the caldera centre. In the NW corner of the caldera, the USc2 agglomerate can be traced radially outwards for a kilometre without significant fining, and the internal stratification dips outwards at only a few degrees. These are features not expected of airfall spatter. (2) The agglomerates locally drape topography but thicken and coarsen into depressions, unlike typical fall deposits. (3) They have abundant interstitial ash and are more poorly sorted than typical airfall spatter (although fines-poor

Figure 53. Highly fluidal spatter rag in the Upper Scoria 1 spatter-rich lag deposit.

facies also occur). (4) Basal inverse grading and imbrication of spatter rags imply emplacement by flowage (Figs. 52 and 53). (5) Intimate interstratification of spatter agglomerate, lithic breccia and scoria-flow deposits is ubiquitous. On the south coast of Therasia, spatter agglomerates pass radially outwards into scoria-flow deposits.

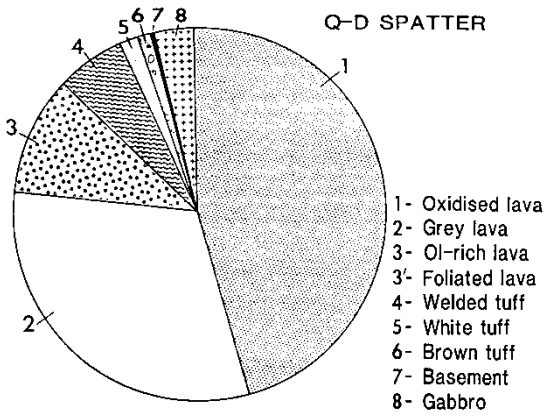

Figure 54. Lithic types in Upper Scoriae 2 spatter-rich lag deposit.

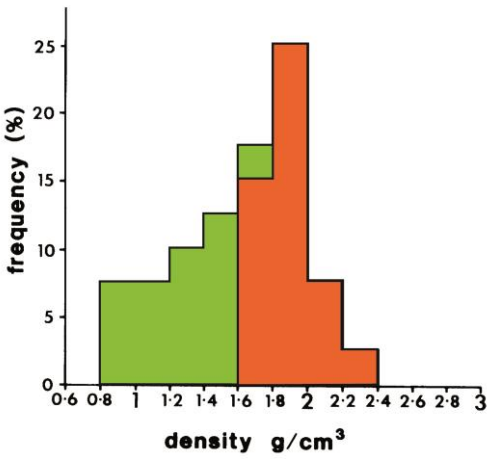

Figure 55. Densites of scoria clasts in the two Upper Scoria spatter-rich lag deposits (orange). The more vesicular scoria of associated fallout phases are shown in green.

The agglomerates are lag deposits formed by proximal sedimentation from scoria flows rich in contorted rags of andesite (Fig. 53). As the rags settled from the flows, they built up successions of clast-supported agglomerate which, close to source (as in the USc2 at Cape Tourlos), became densely welded. Complex interstratification of agglomerate and lithic breccia in Upper Scoriae I and Upper Scoriae 2 probably records alternations of spatter-rich and lithic-rich explosions. Eruption of the spatter-rich layers may have involved explosions through lava lakes.

A puzzling question is the source of energy for these eruptions. Since most of the juvenile fragments are dense (Fig. 55), it is not clear that magmatic vesiculation/fragmentation would have been very efficient. One possibility is that the high density of the spatter bombs is due to late-stage bubble collapse and densification of andesitic foam during and after eruption. Scoria in deposits from earlier phases of the same eruptions are indeed more vesicular, lending credence to this possibility. Another idea is that large volumes of more vesicular material were carried away by the parent scoria flows, the deposits from which are now under the sea. A third possibility is suggested by the abundance of hydrothermally altered lithics and plutonic nodules in the spatter deposits (Fig. 54). Stoping of the hydrothermal system into the magma chamber during eruption may have provided some of the necessary energy for magma fragmentation and explosive discharge.

CALDERA FORMATION

At least four explosive eruptions generated calderas (caldera 1-4) for which direct evidence has been found. The existence of multiple calderas at Santorini has given rise to a complex assemblage of present-day cliff surfaces (Fig. 56).

Caldera 1.

One kilometre south of Fira, a steep, 150-m-high unconformity truncates Lower Pumice 2 and underlying units. Overlying pyroclastic deposits drape the unconformity. This ancient cliff probably relates to collapse during the 172 ka Lower Pumice 2 eruption.

Caldera 2.

The Skaros lava shield infilled and, in places, overspilled a large caldera formed by the Middle Tuff eruption series. The lavas onlap an ancient, strongly eroded cliff surface, which disappears under the succession north of Fira and re-emerges at Micros Profitis Ilias, where ancient, cemented talus aprons are preserved at the contact (Fig. 57). Further north, subsequent collapse of the shield 22 ka ago has perfectly exhumed the old wall of caldera 2, such that its brown, weathered surface makes up most of the present cliffs of Micros Profitis Ilias and Megalo Vouno. Isolated occurrences of Skaros lavas in northern Thera occur where the shield overtopped the rim of caldera 2 (Fig. 57).

Caldera 3.

This caldera was formed 22 ka ago during the Cape Riva eruption. Evidence is provided by the occurrence of Minoan pumice plastered, apparently *in situ*, on the present-day caldera wall at six locations in northern Thera (Druitt and Francaviglia 1992). The best example is at Fira, where the pumice lies 140 m above sea level on an ancient, rounded cliff surface which extends to present sea level (locality 1; Fig. 56). Chemistry confirms that the pumice is Minoan in origin. Reworking from higher on the cliff is ruled out by the presence of an underlying palaesol.

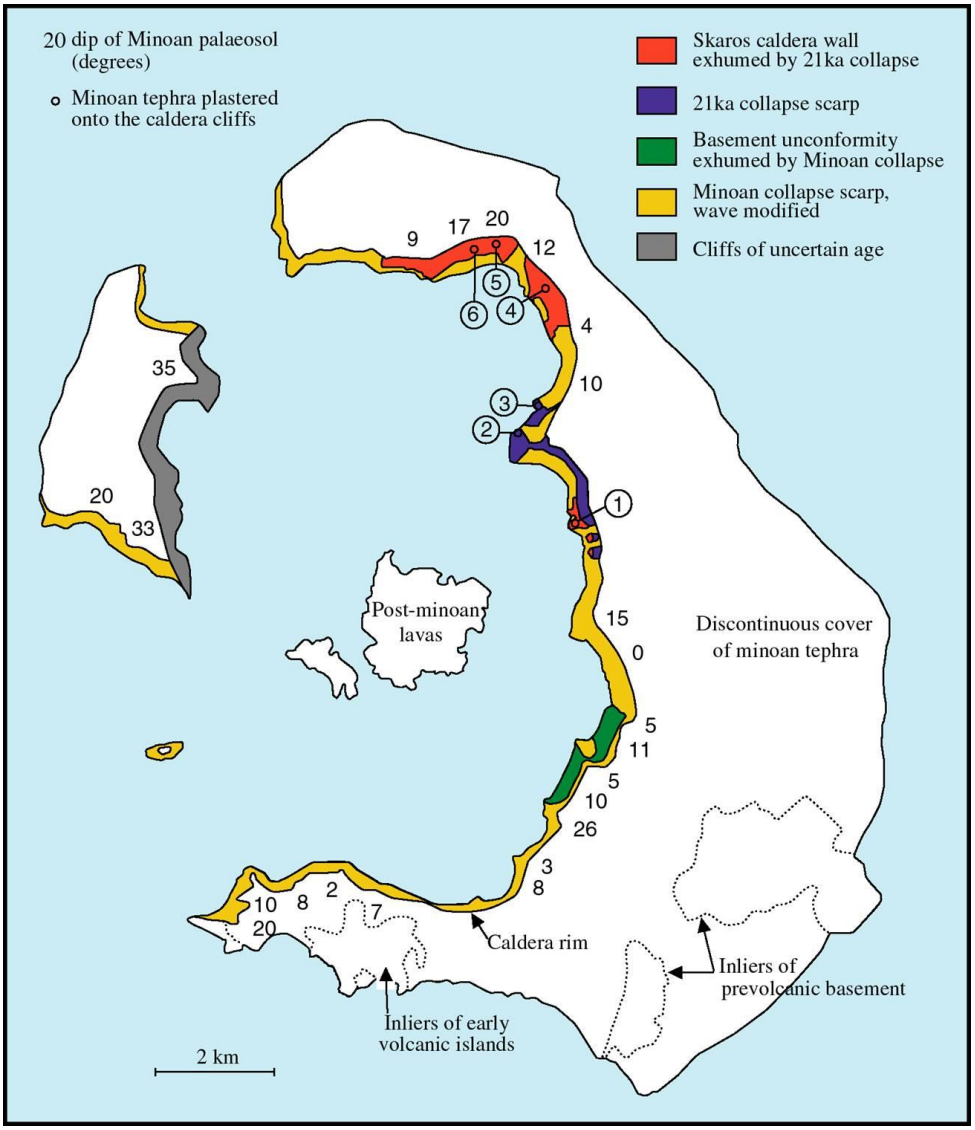

Figure 56. Geomorphological map of the caldera wall showing four generations of cliff surface.

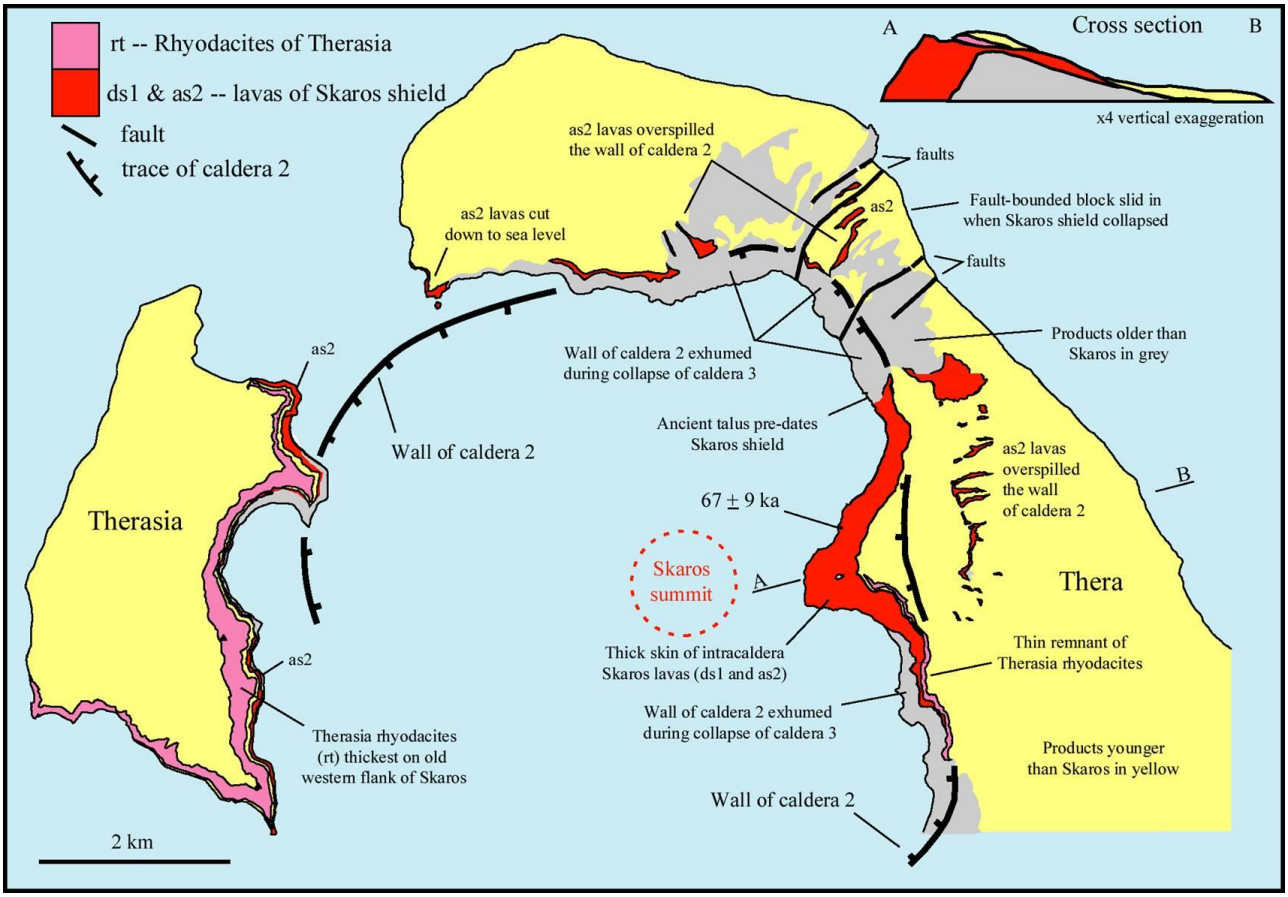

Figure 57. Present-day distribution of lavas of the Skaros and Therasia shields, and outline of the former caldera 2.

Existence of a large caldera prior to the Minoan eruption is also required by volume constraints. The total volume of the present caldera is ~60 km^3, about double the ~30 km^3 of Minoan magma discharged. Minoan collapse can only account for all of the 22 km^3 of the present caldera underwater, and a few km^3 of the subaerial part, so the prior existence of a large and deep depression is required (Druitt and Francaviglia 1992).

Evidence for caldera 3 is also provided by the presence, in the Minoan phase-3 deposits, of abundant fragments of stromatolites and travertines containing gastropods and forams characteristic of shallow brackish to saline water (Eriksen et al. 1990). Such conditions are consistent with the existence of a shallow, flooded pre-Minoan caldera with poor circulation similar to the reconstruction of Fig. 58.

Abundant fragments of a high-Ba, black glassy dacite in the Minoan Tuff are believed to be fragments of a ~2.5 km^3 intracaldera shield that grew on the floor of caldera 3 between 22 and 3.6 ka, but which was destroyed during the Minoan eruption (Fig. 58).

Subsidence during the 22 ka Cape Riva eruption collapsed the Skaros and Therasia shields. Landslips ate back until they hit, and partially exhumed, the ancient wall of caldera 2, which today form much of the cliffs of NE Thera (Fig. 56). Collapse of the Skaros shield removed support from the thin, NE corner of the volcanic field, causing the slumping in, and down, (each

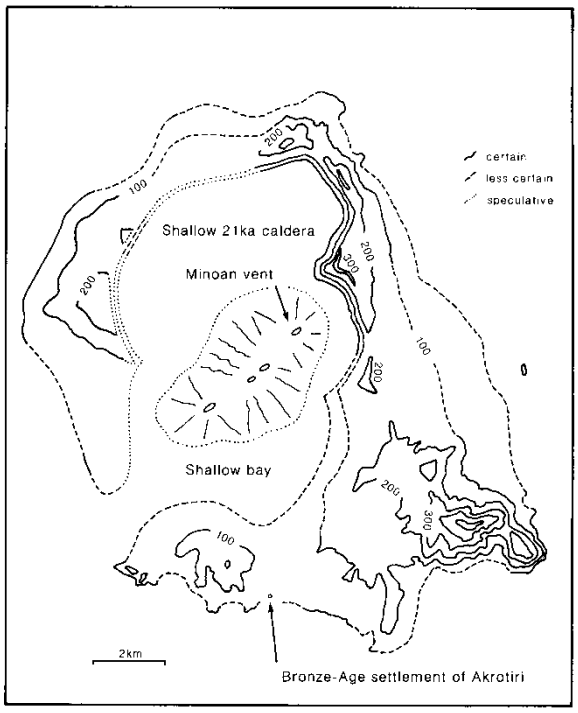

Figure 58. Reconstruction of Bronze-Age Santorini immediately before the Minoan eruption (Druitt and Francaviglia 1992).

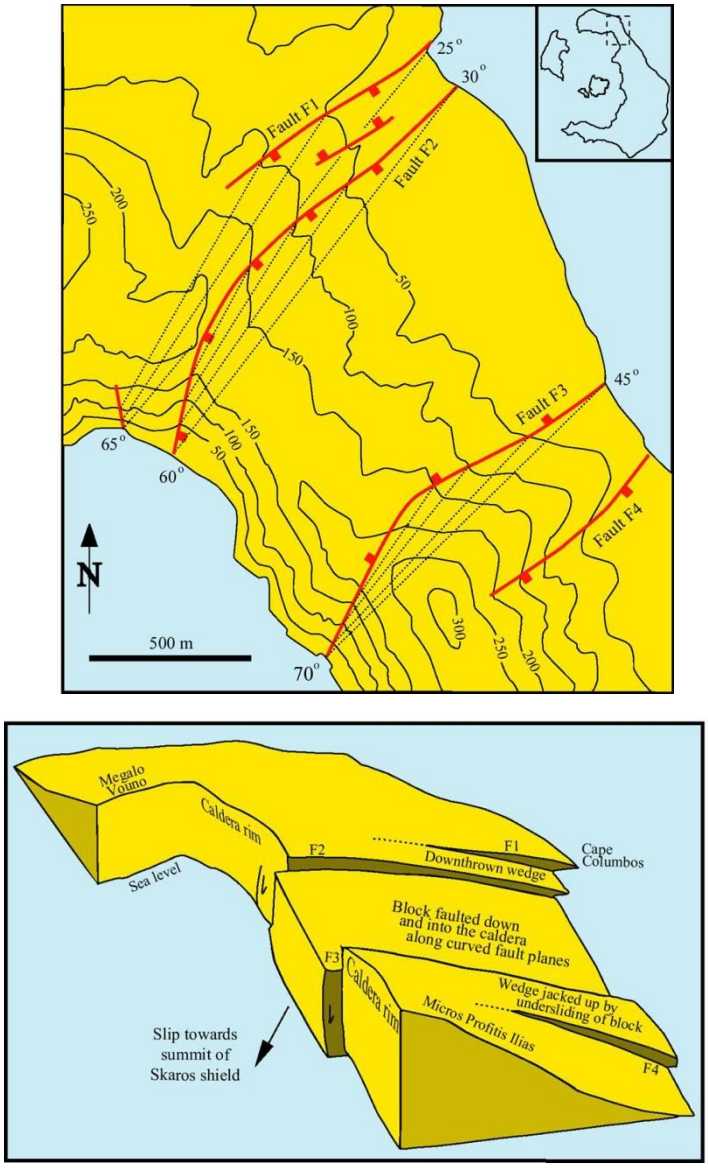

Figure 59. Collapse of the Skaros shield 22 ky ago caused insliding of the NE corner of Santorini.

by several tens of metres) of an 800-m-wide block along two major, curved faults (F2 and F3; Fig. 59). Movement of the block to the SSE caused downthrow of a wedge of rock to the north and upjacking of another to the south along two accommodation faults (F1 and F4).

Caldera 4.

Collapse during the Minoan eruption deepened and enlarged the extant caldera 3 (Fig. 58), forming the complex present-day assemblage of three basins (Fig. 8). In southern Thera, collapse truncated the wedge of older tuffs draped over and plastered up against the prevolcanic island and early centres of the Akrotiri Peninsula. At Athinios, Minoan collapse exhumed the northwest cliff and shore of the prevolcanic island.

Minoan collapse took place mainly north of the Kameni Line, forming the present-day northern basin. Opening of the northwestern breach by insliding may have occurred during Minoan collapse, or may be an earlier feature. Judging from its morphology, the western basin formed by large-scale rotational slip into the subsiding caldera.

Collapse mechanisms

At least three of these calderas have broadly similar locations and sizes, suggesting that subsidence repeatedly used the same collapse faults (such as the Kameni and Kolumbo Lines). Moreover, landslides during and following collapses commonly ate back until they exhumed ancient caldera cliffs and unconformities. Repeated caldera collapse at Santorini has occurred in such a way that the long-lived Plinian conduit system near present-day Nea Kameni has survived each time to feed subsequent eruptions (Fig. 17), so collapse can never have been totally chaotic.

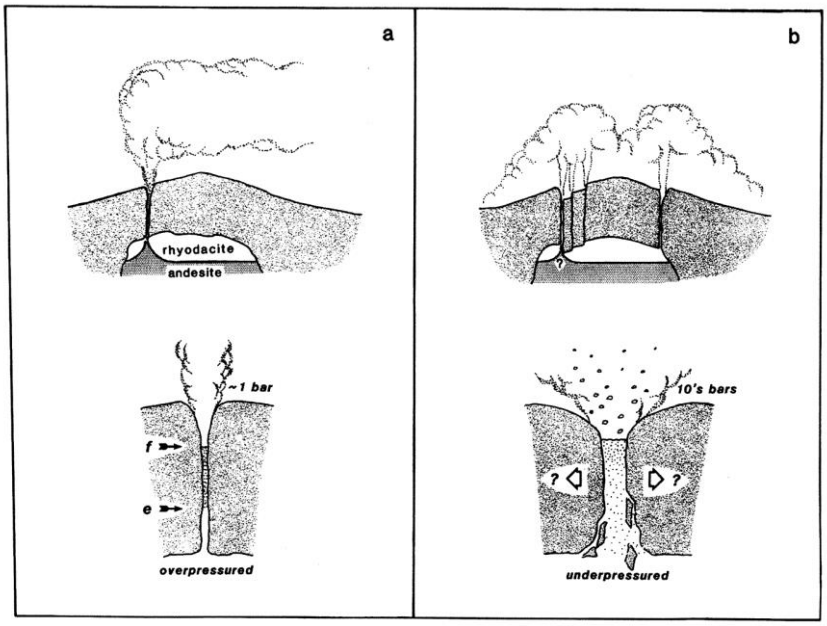

Figure 60. Cartoon showing evolution of the Cape Riva eruption. (a) Initial stage in which the magma chamber is overpressured and discharge is steady, permitting decompression of the erupting mixture to ~1 atm. This is the Plinian stage. (b) Underpressuring the chamber causes caldera collapse, escalation of magma discharge rate, and outpouring of pyroclastic flows. Vent erosion and elevated surface pressures result in eruption of coarse lithic debris to form lag breccias (Druitt 1985).

IMPORTANCE OF THE REGIONAL STRESS FIELD

These observations highlight the important role played by regional faults in the evolution of Santorini (Fig. 7).

- The volcanic field is situated at the intersection of NE-SW and NW-SE faults which border the southern margin of the Central Aseismic Plateau.
- Volcanism has been concentrated in a graben on the faulted NW flank of the Santorini-Amorgos basement ridge.
- Vent locations and sites of gas emission are concentrated along two lines parallel to the NE-SW regional fault trend. At least six large explosive eruptions began at vents on the Kameni Line (Fig. 17), which is also the focus of historical intracaldera activity.
- Dykes of northern Thera are preferentially oriented NE-SW (Heiken and McCoy 1984).
- Crater rows and spatter ramparts on the Kameni islands are preferentially aligned NW-SE.
- Orientations of caldera breaches and the NE fault block reflect the regional NE-SW and (lesser) NW-SE tectonic fabrics. Historical lava production has been highest in the caldera centre at the intersection of the two fault sets.
- The Kameni Line splits the present-day caldera basin into two main halves of different depths and morphologies.
- Seismic epicentres during the 2011-12 unrest lay along the Kameni Line (Fig. 45).

Only smaller-scale, second-order features reflect the local stress field of the volcanic plumbing system. These include a subradial orientation of some dykes in northern Thera and of some historical fissures on the Kameni Islands.

ERUPTIVE MECHANISMS

Several explosive eruptions on Santorini show evidence for very violent climatic phases that generated pyroclastic flows and laid down widespread and very coarse-grained lithic breccias and agglomerates. Examples include the Lower Pumice 1, Middle Pumice, Upper Scoriae 1, Upper Scoriae 2, and Cape Riva eruptions. The marked contrast in grain size between these deposits and their preceding fallout phases suggests abrupt changes in eruptive conditions at the onset of flow generation (Fig. 60). Druitt & Sparks (1984) and Roche and Druitt (2001) showed that a stage is reached during large explosive eruptions when the pressure at the top of a magma chamber drops below lithostatic. The volume of magma that can be discharged before this occurs can account for as little as a few percent of the chamber. Subsequent caldera collapse could then cause a large increase in magma discharge rate by opening new conduits and widening existing ones. Unsteady flow of magma up enlarging conduits would result in violent reaming of surface vents and, together with hydrothermal explosions from the newly exposed caldera walls, discharge of the coarse lithic debris observed in the breccias and spatter agglomerates. Direct field evidence for at least four episodes of caldera collapse on Santorini lends support to this model.

MAGMA ERUPTION RATES

The magma eruption rate at Santorini can be constrained by three cases. The Skaros lava shield had a volume of about 10 km^3 and was built up over about 12 ky, from 67 to 54 ka, giving about 0.8 km^3/1000 y. The 30-60 km^3 DRE Minoan eruption terminated a period of low magma eruption between 21.8 and 3.6 ky, giving 1.6-3.2 km^3/1000 y. The best constrained is the present-day Kameni volcanism (Johnston et al. 2015). Including the clastic apron of the edifice (seismic unit 2), Kameni has a DRE volume of 4.85 km^3. Assuming that this was discharged since the Minoan eruption, the magma production rate is 1.3 km^3/1000 y. This is similar to the rate since the 1707 A.D. of 1.2 km^3/1000 y based on historic lava volume estimates. These rates bracket those typical of island-arc volcanoes (Crisp, 1984).

HAZARDS AND MONITORING

Santorini has been dormant since the last eruption of Nea Kameni in 1950. Until January of 2011, there was little detectable bradyseismic activity, apart from a very small inflationary period between 1994 and 1999 (Stiros et al. 2010). Then the unrest period between January 2011 and March 2012 resulted from the injection of about 14 million m^3 of magma and/or fluids at a depth of 3-6 km beneath the northern caldera basin. Although the episode ended without eruption, it focussed the scientific and civil defence communities on hazards issues at Santorini.

If an eruption took place today, about 65 years after the last one (1950), then the observed volume-time relationship at Kameni (Fig. 43) would predict an event similar to that of 1925-28, which lasted three years and was mainly effusive (Pyle and Elliot 2007). However small ash plumes would threaten aviation traffic, ballistic showers would threaten shipping, and small tsunamis from submarine explosions could threaten the caldera coastline. A worse-case Kameni scenario might involve a subplinian eruption similar to that of past interplinian periods or to the Kameni eruption of AD 726. An eruption of Kolombo Volcano also remains a serious threat. The hazard map for Santorini-Kolombo published by Georges Vougioukalakis prior to the unrest period remains more or less valid (Fig. 61).

The Santorini volcano monitoring network is managed by the Institute for the Study and Monitoring of the Santorini Volcano (ISMOSAV), an organization founded in 1995 and supported by the Aristotle University of Thessaloniki, the Geodynamic Institute of the National Observatory of Athens, and IGME. The monitoring programme includes.

- Seismic monitoring by a local network of stations. The data are digitized and transmitted in real-time via a digital antenna to the ISMOSAV building in Fira, then to the Central Seismological Station of the Geophysical Laboratory of Aristotle University of Thessaloniki.
- Geodetic measurements made using multiple GPS networks as well as by Insar; several Greek and overseas groups are involved in geodetic measurements.
- Chemical sampling of gases, including continuous monitoring of CO_2 and periodic measurement of Radon output.
- Thermal monitoring of fumaroles and hot springs on Nea Kameni and of a borehole in southern Thera.
- Sea level measurement, using a network of electronic tide gauges.

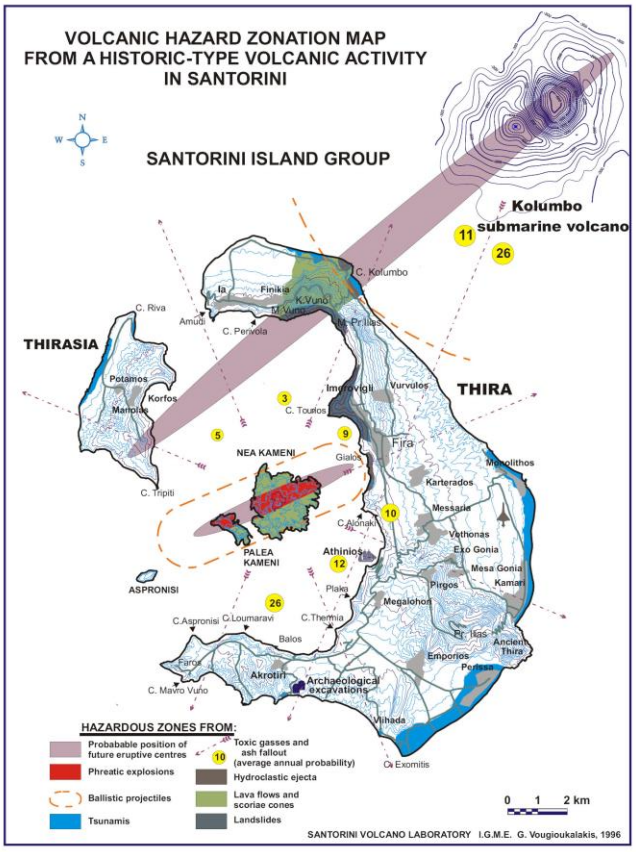

Figure 61. Hazard zonation map of Santorini (Vougioukalakis 1996).

CHEMISTRY AND PETROLOGY

General features

Santorini magmas range from low-K, high-Al basalt, through medium-K basaltic andesites, to medium and high-K dacites and rhyodacites (Fig. 62). Rhyolitic compositions occur in the early centres of Akrotiri Peninsula and as interstitial glasses in the rhyodacites.

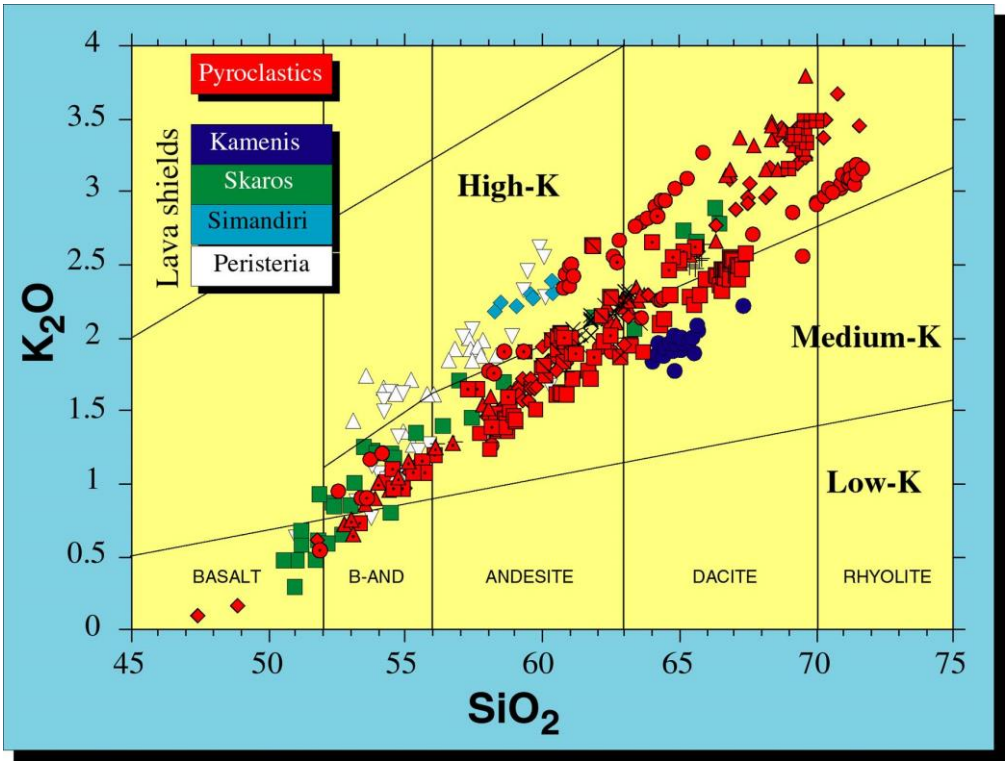

Figure. 62. K_2O vs SiO_2 diagram for Santorini rocks (Druitt et al. 1999).

Basalts occur uncommonly on the islands. The cinder cones of Balos, Megalo Vouno and Kokkino Vouno are basaltic. Some basalts also occur in the lavas of Persiteria and Skaros. They contain phenocryst assemblages of olivine, plagioclase, cpx and minor magnetite. The most primitive basalts have ~50 % SiO_2, 7 % MgO, Mg# 0.67, 100 ppm Ni and 250 ppm Cr.

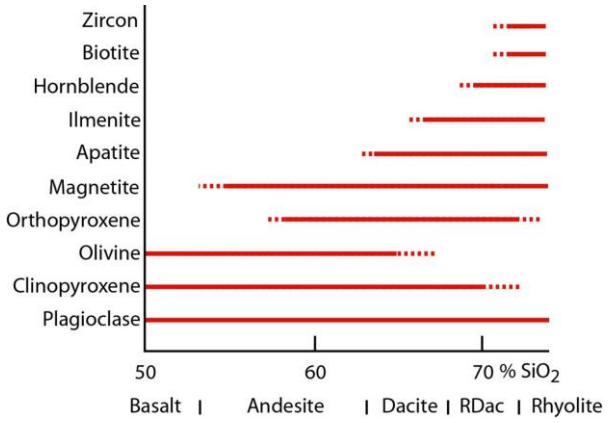

Figure 63. Mineralogy of Santorini magmas (Druitt et al. 1999).

They contain olivine as magnesian as Fo_{85} and plagioclase as calcic as An_{95}.

Basaltic andesites and andesites have plagioclase, cpx, olivine and magnetite ± opx (Fig. 63). Some highly phyric hybrid andesites formed by mixing of silicic and mafic magmas have disequilibrium mineral assemblages and textures. Dacites and rhyodacites have 5-20 % plagioclase, cpx, opx, magnetite, ilmenite, apatite and pyrrhotite; some dacites of more tholeiitic affinity contain fayalitic olivine. The early rhyodacites of Akrotiri Peninsula are distinctive in their abundance of phenocrystic hornblende, rare microphenocrysts of biotite, and accessory zircon. An ancient cummingtonite-bearing ignimbrite on Santorini was erupted from the Christiana Volcano, southwest of Santorini (Keller et al. 2015).

Santorini magmas span the tholeiitic-calcalkaline divide (Fig. 64). Andesitic components of the large silicic eruptions have greater calcalkaline affinities than those from earlier stages of each explosive cycle. The silicic compositions also span the calcalkaine-tholeiitic divide.

Trace elements and isotopes

Trace element abundances show significant variations in Santorini magmas. Like other primitive arc magmas, the basalts are enriched in large-ion lithophile elements (LILE) relative to MORB, probably due to slab components (Fig. 65). Rare-earth patterns for all Santorini magmas are LREE-enriched with variable Eu anomalies due to plagioclase fractionation (Fig. 66).

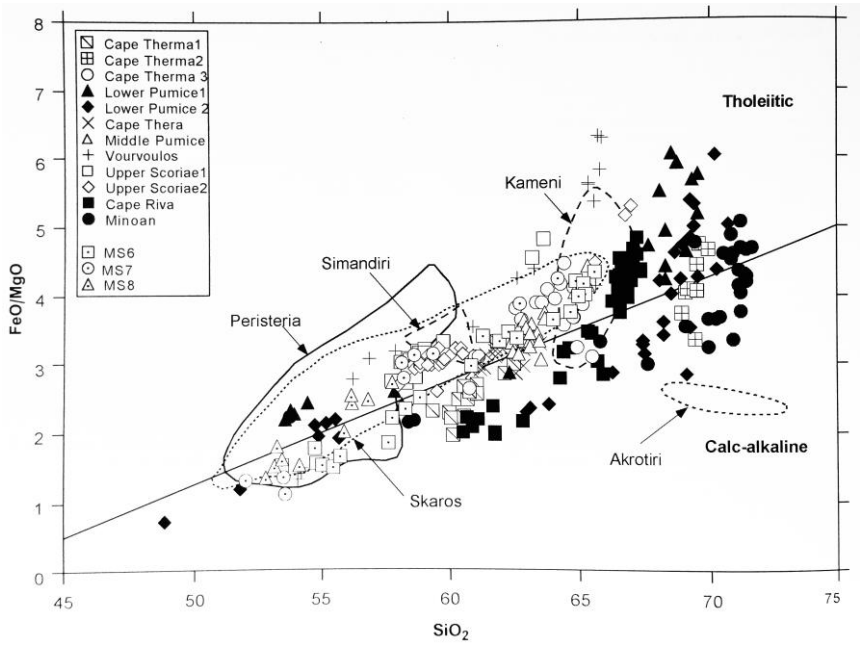

Figure. 64. FeO/MgO versus SiO2, showing calcalkaline and tholeiitic fields

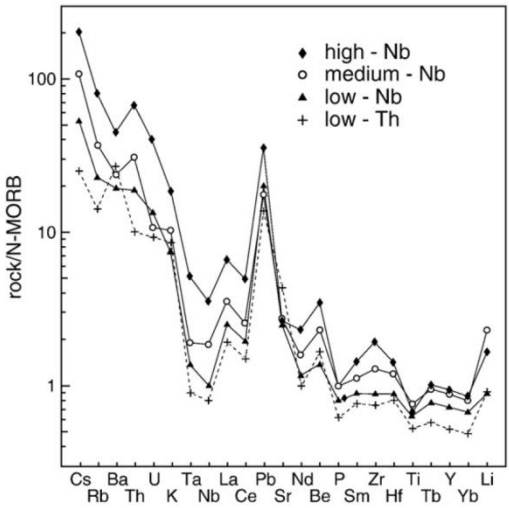

Figure 65. N-MORB trace element spectra for Santorini basalts (Bailey et al. 2009).

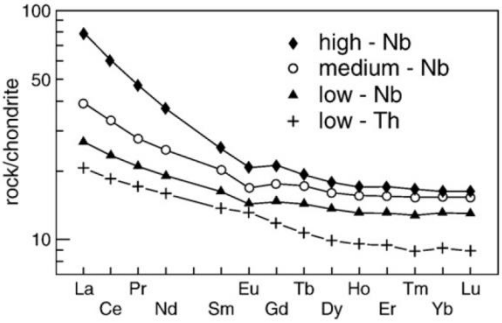

Figure 66. Chondrite-normalized REE spectra for Santorini basalts (Bailey et al. 2009).

$^{87}Sr/^{86}Sr$ ratios of Santorini magmas range from 0.7038 to 0.7070 and $^{143}Nd/^{144}Nd$ from 0.5125 to 0.5129 (Fig. 67). $\delta^{18}O$ values of plagioclase separates range from +6 to +7.5 per mil.

The basaltic magmas exhibit a range of trace element and isotopic characteristics. Bailey et al. (2009) recognized four groups based on plots of incompatible-

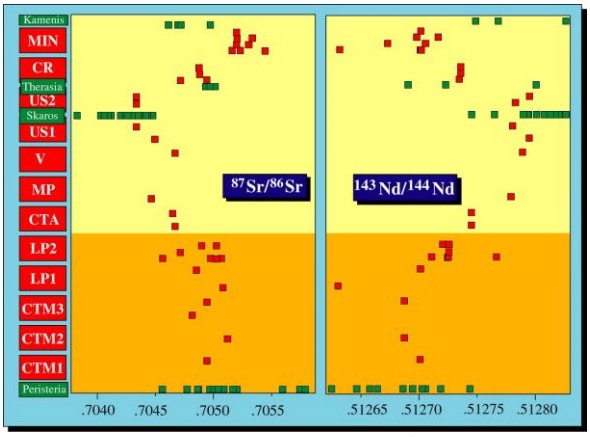

Figure 67. Sr and Nd isotopic compositions of Santorini magmas (Druitt et al. 1999)

element ratios, N-MORB normalized trace elements, and Sr–Nd–Pb isotopic ratios. The groups differ notably in their contents of incompatible elements (Rb, Ba, Th, U, K, Nb, Th) and in incompatible element ratios (La/Y, Zr/Th) (Fig. 65). Bailey et al. (2009) distinguished high-Nb, medium-Nb, low-Nb and (rare) low-Th basalts. High-Nb basalts have higher $^{87}Sr/^{86}Sr$ and lower $^{143}Nd/^{144}Nd$ than medium-Nb or low-Nb basalts.

The different basalt trace element patterns are believed to record variable metasomatism of the sub-arc mantle by terrigenous-rich sediments. Sediments were introduced mostly as bulk sediment or as sediment partial melts, rather than fluids (Bailey et al. 2009; Vagelli et al. 2009) (Fig. 68).

When plotted with andesites, dacites and rhyodacites, the four basalt groups form the parents of subparallel lineages that can be modelled by AFC processes (Druitt et al. 1999; Bailey et al. 2009).

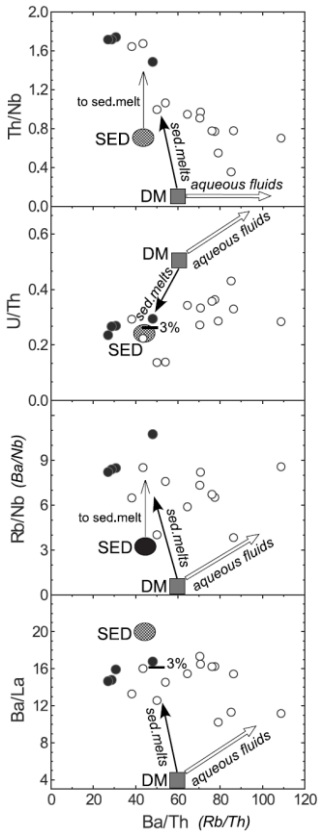

Figure 68. Trace element compositions of melt inclusions in basaltic andesite scoria from a M12 interplinian strombolian eruption, showing the modification of source composition by sediment input (Vaggelli et al. 2009).

TEMPORAL VARIATIONS

In general, incompatible elements in Santorini magmas have decreased with time, and are lowest in the historical Kameni magmas (Huijsmans 1985) (Fig. 69). This change is evident in both the parental basalts, as well as in their derivative magmas (Bailey et al. 2009). The liquid lines of descent form subparallel trends that lower and shallow with time. Changing proportions of different parental basalts that ascend into the crust, where they mix and differentiate to intermediate and silicic compositions (Andújar et al. 2010; Cadoux et al. 2013), may account for the observed temporal variations of trace element chemistry. However this progression is far from perfect (e.g., Vaggelli et al. 2009), and requires further study.

Recent jumps to incompatible-poorer magmas occurred following the Therasia eruptions (and prior to Cape Riva) and following the Minoan eruption (and prior to Kameni). Progressive depletion in K and other incompatible elements with time has also occurred at other centres in the Aegean region (Francalanci et al. 2005).

PHASE RELATIONSHIPS

Experimental studies of phase relationships of a Santorini basalt (Balos basalt) (Andujar et al. 2015) and of four silicic magmas from plinian eruptions (Cadoux et al. 2014) have been published.

The basalt experiments were carried out at 975-1040 °C, 100-400 MPa, and fO_2 from QFM to NNO+3.5.

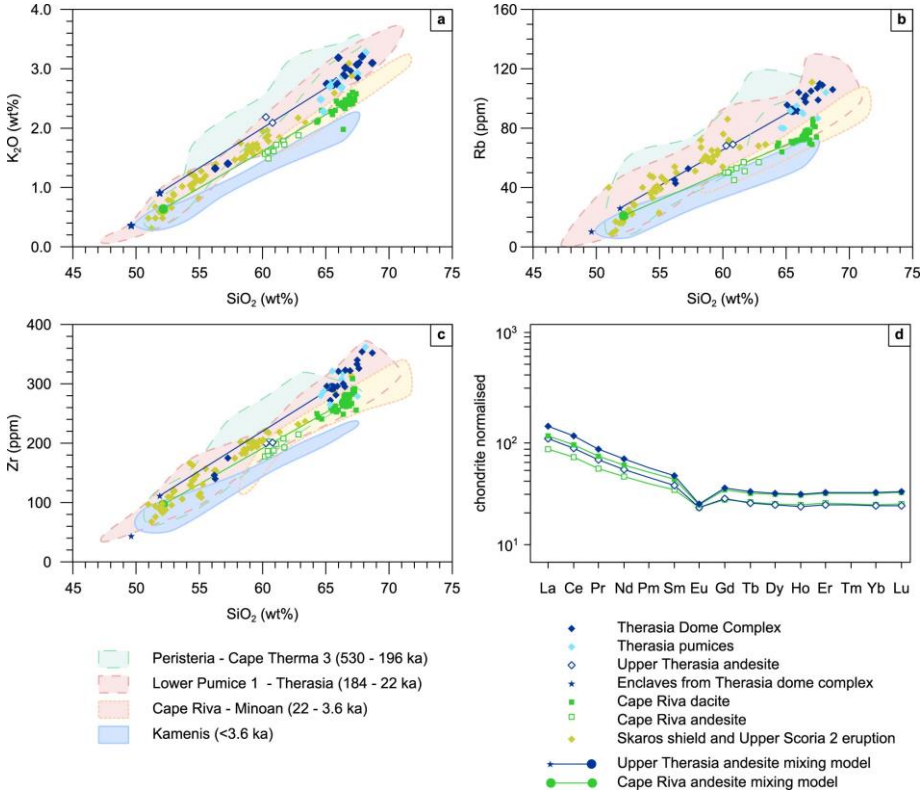

Figure 69. Evolution of composition with time of Santorini magmas (Fabbro et al. 2013).

Amphibole is stable in the basaltic melt at <975 °C and at >3.5 wt% H_2O (NNO) to >5.0 wt% H_2O (QFM) (Fig. 70). The amphibole-bearing basalts of the 650-550 ka Akrotiri centres probably evolved under conditions slightly cooler, and possibly slightly wetter, than those of the younger (<530 ka) basaltic magmas.

The experiments on silicic magmas were carried out at 850-900 °C, 100-400 MPa, and fO_2 from QFM to NNO+1. One important finding was that the phase diagrams for these magmas were very sensitive to small changes in bulk (starting) composition. Small differences in Fe, Mg or Ca content moved the phase boundaries considerably.

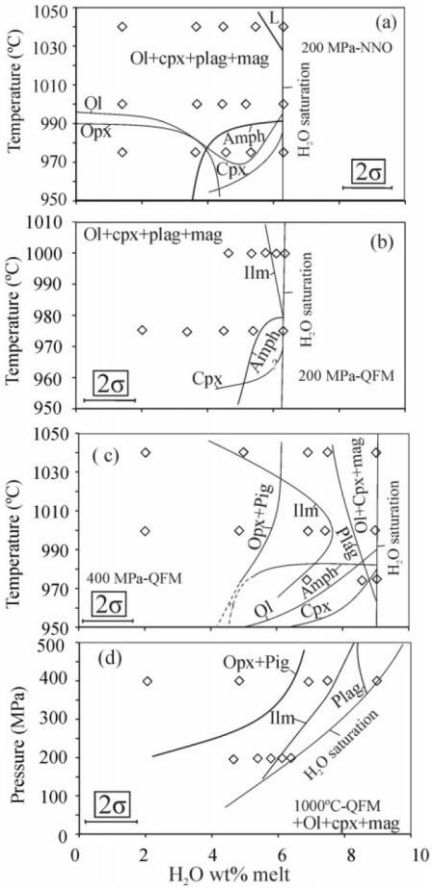

Figure 70. Equilibrium phase diagrams for the Balos basalt under different experimental conditions (Andujar et al. 2015).

MAGMA EVOLUTION

Four main processes have controlled magma composition at Santorini.

Source processes. Melting of a mantle wedge variably metasomatised by sediment-derived melts and aqueous fluids (Fig. 68). Temporal variations of incompatible elements in Santorini magmas probably record changes in these processes with time.

Fractional crystallization. The liquid lines of descent can be modelled, to a first approximation, by fractional crystallization of basaltic parent like the Balos basalt (Nichols 1971; Mann 1983; Druitt et al. 1999; Bailey et al. 2009). To derive andesite in such models requires ~60 % fractionation, and to generate rhyodacite requires ~75 %. Andesitic liquids with ~58 wt% SiO_2 are produced experimentally by 60–80 wt % crystallization of ol, cpx, plag, Ti-mag, opx, pig and ilm from a Balos-like basalt with melt water contents of 3-5 wt% (Andujar et al. 2015).

The primary liquid at Santorini has been estimated by back-calculation to have 9-12 wt% MgO (Nichols 1978). This would fractionate 6-13 wt% of olivine and small amounts of Cr-spinel and clinopyroxene to generate the most primitive (Balos-like) basalt erupted (7 wt% MgO).

The many tens of km^3 of differentiated magma erupted from Santorini over 650,000 years requires the presence at depth of proportionally larger volumes of cumulate residue. Abundant nodules of cumulate gabbro and diorite occur in scoria flows, spatter agglomerates and lavas. Cumulate gabbros contain primocrysts of plagioclase, clinopyroxene, orthopyroxene, oxides and rare olivine with intercumulus quartz, alkali feldspar, hornblende and biotite. Major element modelling reproduces observed phase assemblages and proportions of the gabbros if they are assumed to be cumulates from andesites with 56-66 % SiO_2 (Druitt et al. 1999).

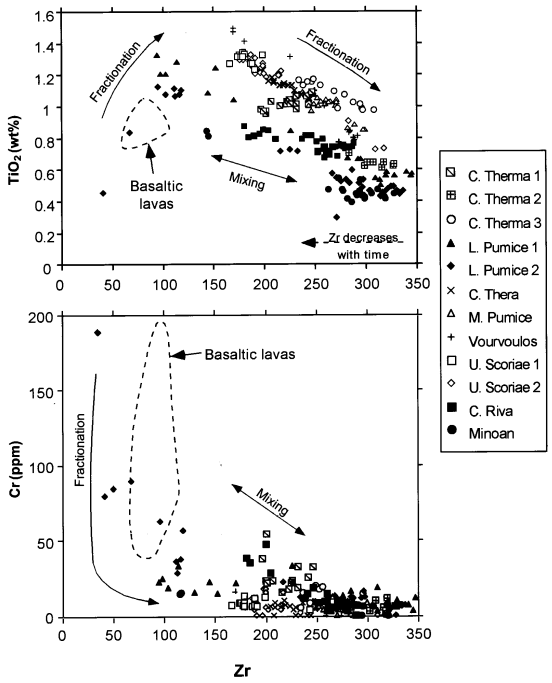

Figure. 71. Plots showing interpretations of chemical variations in Santorini volcanic rocks (Druitt et al. 1999).

Crustal assimilation. Fractional crystallization modelling fails in detail to reproduce the contents of the most incompatible elements in the liquid lines of descent. Moreover, there is a positive correlation between $^{87}Sr/^{86}Sr$ and SiO_2 content indicative of AFC processes in some series (Druitt et al. 1999; Bailey et al. 2009). Full modelling requires combined fractional crystallization and assimilation of continental crust known to exist beneath the arc (Barton et al. 1983;

Druitt et al. 1999; Bailey et al. 2009). Reasonable fits to trace element patterns and Sr, Nd and O isotopic data are obtained from AFC models using an assimilation-fractionation ratio of 0.1-0.2.

Magma mixing. Mingling and mixing of magmas is common at Santorini. Some andesitic magmas are demonstrably hybrids produced by the mixing of basaltic and silicic endmembers (Nichols 1971; Fabbro et al. 2013) (Fig. 71).

VOLATILE CONTENTS

Pre-eruptive volatile contents of <530 ka Santorini magmas have been well constrained by phase equilibria studies (Cadoux et al. 2014; Andujar et al. 2015) and by melt inclusion (MI) analyses (Cadoux et al. 2014; Druitt et al. submitted). Similar work has not yet been done for the early Akrotiri magmas.

MIs of basaltic to mafic andesitic composition contain up to 4 wt% H_2O and 1200 ppm CO_2 (Fig. 72); this agrees with the conclusion from phase equilibria that Santorini basaltic melts contain up to 3-5 wt% H_2O. MIs of dacitic to rhyodacitic composition contain up to 7 wt% H_2O and 200 ppm CO_2. Cl contents (<6000 ppm) are high, and S contents (<1500 ppm) are moderate to low, relative to arc magmas elsewhere.

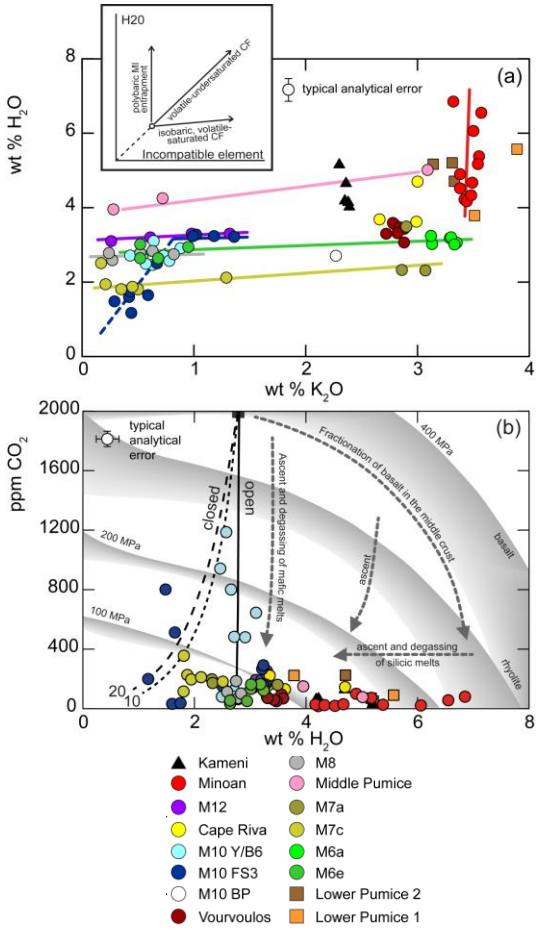

Figure 72. H2O and CO2 contents of Santorini melt inclusions. The lines on the H2O plot are trends within melt inclusions from the same eruption series (Druitt et al. submitted).

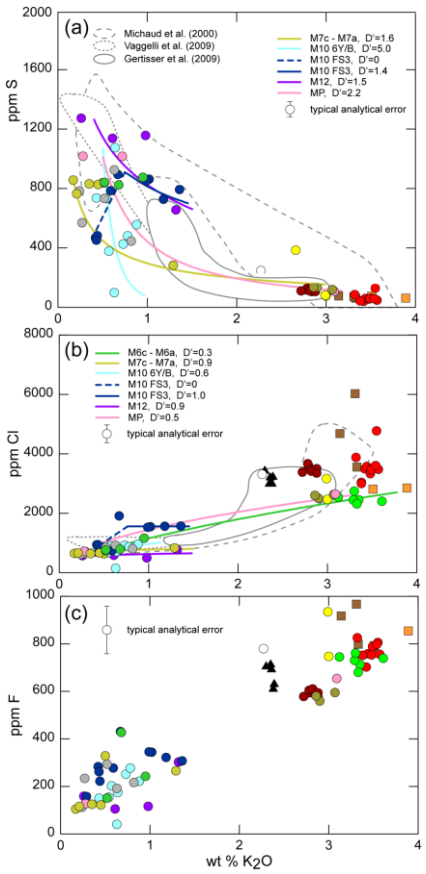

Figure 73. S and halogen contents of Santorini melt inclusions. See previous figure for legend. The lines are models of vapour-saturated fractional crystallization. (Druitt et al. submitted).

Most Santorini melts, from mafic to silicic, are saturated with a free COHSCl- vapour phase in the upper crust, as shown by the compatible behaviours of H_2O, S and Cl in fractional crystallization series (Figs. 72, 73). The parental basalts are inferred to contain up to 4 wt% H_2O, ~2000 ppm CO_2, 1200, ppm S, 500 ppm Cl and 100 ppm F. However some basalts may have less initial H_2O (1-2 wt%) and be volatile-undersaturated. Most Santorini magmas probably contain a free vapour phase at upper crustal pressures.

The Minoan rhyodacitic magma may have contained a free Cl-rich hypersaline liquid (brine) phase (Cadoux et al. 2014).

MAGMA OXIDATION STATES

Coexisting Fe-Ti oxides in Santorini silicic magmas give fO_2 from QFM-0.5 to NNO, with a suggestion in the data of increasing fO_2 with time (Lower Pumice 1 giving the lowest values, and the Minoan (also the Kamenis) the highest values (Cadoux et al. 2014; Druitt 2014) (Fig. 74)

Phase equilibria study of the Balos basalt indicated pre-eruptive storage at fO_2 ~QFM (Andujar et al. 2015).

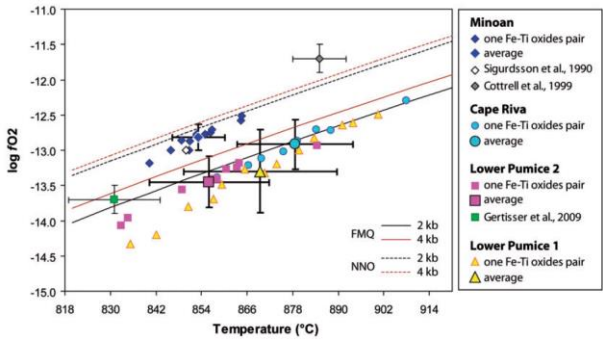

Figure 74. T-fO2 data for Santorini magmas, from analysis of touching Fe-Ti oxide pairs (Cadoux et al. 2014).

PRE-ERUPTIVE MAGMA STORAGE

Estimates of pre-eruptive storage pressures of <550 ka Santorini magmas have been made using (1) mineral equilibria, (2) phase equilibria experimentation, (3) melt inclusion $H_2O + CO_2$ saturation pressures using suitably calibrated solubility models, and (4) geodetic modelling of deformation during the 2011-12 period of unrest.

Pressures estimated by mineral barometry by a number of authors range from <100 to 400 MPa, equivalent to depths of <4 to 16 km based on geophysical estimates of the mean upper crustal density.

The phase equilibria studies of natural products have constrained pre-eruptive storage depths for silicic pumices from the four main plinian eruptions (≥ 8 km; Cadoux et al. 2014), for a basalt from the ~340 ka Balos cinder cone (~15 km; Andujar et al., 2015), and for an andesite from a plinian eruption (~8 km; Andujar et al., submitted).

Melt inclusion barometry has refined these results (Cadoux et al. 2014; Druitt et al. submitted). Demonstrable volatile saturation in most Santorini melts allows conversion of $H_2O + CO_2$ saturation pressures to total pressures (Fig. 75). The silicic reservoirs that fed large plinian eruptions were situated at >4 km and extended over depth ranges of several km or more: much greater than expected from sill-shaped reservoirs underlying the caldera. Plagioclase phenocrysts from the Minoan eruption have cores containing MIs trapped at depths up to 10-12 km, and rims with MIs trapped at 4-6 km. The large pressure range records the late-stage transfer of silicic melt (+ plagioclase cores) from the middle crust to the upper-crustal storage level where the

Table 1. Previous estimates of pre-eruptive storage depths of Santorini magmas

Unit	Comp	P (MPa)	D (km)	Method	Ref
Kameni	s	80 to 150	3.1-5.8*	cpx-plag equilibria	1
Skaros, Peristeria	m, i	170 to 340	6.6-13.1*	cpx-plag and ol-cpx equilibria	2
Lower Pumice 2	s	430 ± 10	16.6 ± 0.4*	Al in hb; equilibrium with qz	4
Minoan	s	≥200 to 50	>7.7 to ~1.9*	phase equilibria; melt inclusions	3,5
Min, CR, LP2, LP1	s	≥200	>7.7*	phase equilibria	5
Minoan	s	190 ± 50	7.3 ± 1.9*	hb composition (mph-rich pumice)	5
Balos basalt	m	~400	~15.4*	phase equilibria	6
Unrest 2011-12	s?		3.3-6.3	geodesy	7-9
Silicic melt generation	s	250-350	9.6-13.5*	Phase equilibria Fe/Mg ratios	10

1. Barton & Huijsmans (1986); 2. Huijsmans & Barton (1989); 3. Cottrell *et al.* (1999); 4. Gertisser *et al.* (2009) ; 5. Cadoux *et al.* (2014) ; 6. Andujar *et al.* (2015) ; 7. Newman *et al.* (2012) ; 8. Parks *et al.* (2013) ; 9. Papoutsis *et al.* (2013); 10. Andujar *et al.* (submitted).
m, mafic ; i, intermediate ; s, silicic ; mph, microphenocryst
Min, Minoan; CR, Cape Riva; LP2, Lower Pumice 2, LP1, Lower Pumice 1
ol, olivine; cpx, clinopyroxene; hb, hornblende; qz, quartz

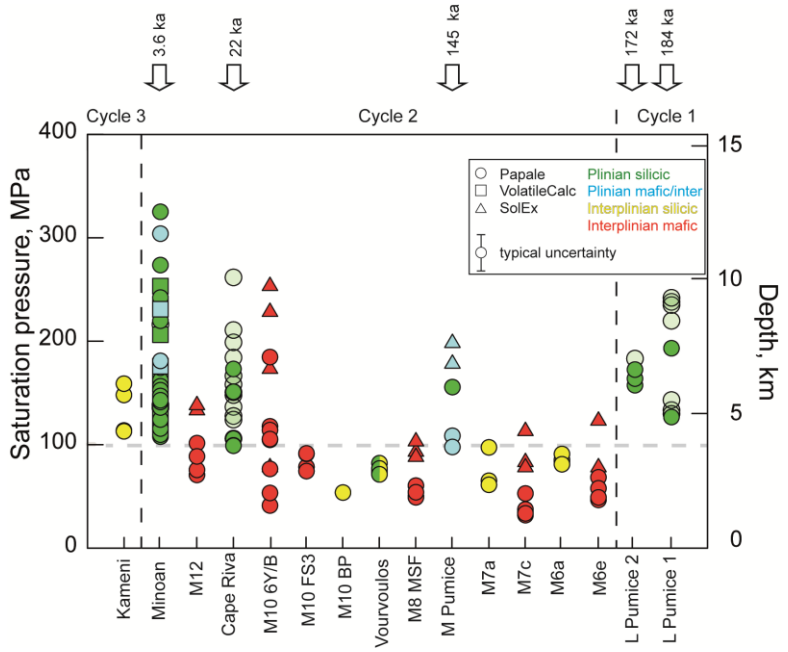

Figure 75. Magma pre-eruptive storage depths based on H2O + CO2 contents of melt inclusions (Druitt et al. submitted).

rims grew and from which the magma was erupted (Cottrell et al. 1999; Druitt et al. submitted).

Silicic magma reservoirs during cycle-2 interplinian periods were situated at depths of <4 km, systematically shallower than the tops of plinian reservoirs. This is attributed to the existence, prior to plinian eruptions, of large intracaldera edifices that then collapsed at the onset of the intraplinian periods. The presence of high intracaldera edifices prior to plinian eruptions probably caused ponding of silicic magma at depths >4 km, whereas stress release following caldera formation and edifice collapse allows interplinian silicic magmas to pond at higher (<4 km) levels (Pinel and Jaupart 2000).

The H_2O + CO_2 saturation depth of the magma reservoir(s) feeding the present-day Kameni edifice (3.9-6.2 km) is similar to those of pressure sources calculated by modelling of ground deformation during the 2011-2012 unrest period, lending support to a magmatic origin for the unrest. The bodies of dacitic magma that feed the Kameni eruptions are deeper than the reservoirs that fed earlier interplinian silicic eruptions, perhaps due to a change in crustal stress field following the Minoan eruption.

MAGMA PLUMBING SYSTEM

Basaltic melts with 6.5-7.5 wt% MgO, up to 4 wt% H_2O, ~2000 ppm CO_2, 1200 ppm S, 500 ppm Cl and 100 ppm F are intruded at the interface between the upper and lower crust (~15 km). Primary mantle-derived melts containing 9-12 wt% MgO, from which the basalts are derived by fractionation, may pond at deeper crustal levels or at the Moho. Repeated injection of basalt at ~15 km forms crystal mush zones in which intermediate to silicic residual melts are produced (Fig. 76). The melts are then extracted and transferred to higher levels as the mushes compact. Gabbros and diorites brought to the surface by erupting magmas are cumulates from which intermediate and silicic melts have been removed. MIs from cores of Minoan plagioclase crystals record pressures corresponding to this range and support the idea of mid-crustal generation and extraction of evolved melts. Ascent-driven decompression of volatile-saturated intermediate to silicic melts causes vesiculation and injection of foams into the shallow upper crust, where they either crystallise or accumulate to form reservoirs of eruptible magma. One factor controlling the depths of shallow injection may be the presence or absence of a high intracaldera edifice. The small reservoirs that fed interplinian eruptions are situated at shallower levels than those that fed large plinian eruptions. Basaltic magma rooted in the deep storage zones ascends through the upper crust to form shallow intrusions or to erupt.

The present-day crustal column beneath the caldera is the time-integrated product of more than half a million years of magmatism. It most probably consists of a plutonic complex zoned upwards from ultramafic cumulates, through gabbros and diorites, to granodiorites and overlain by a shallow, compositionally heterogeneous hyperbyssal or cupola complex corresponding to the magma bodies that fed

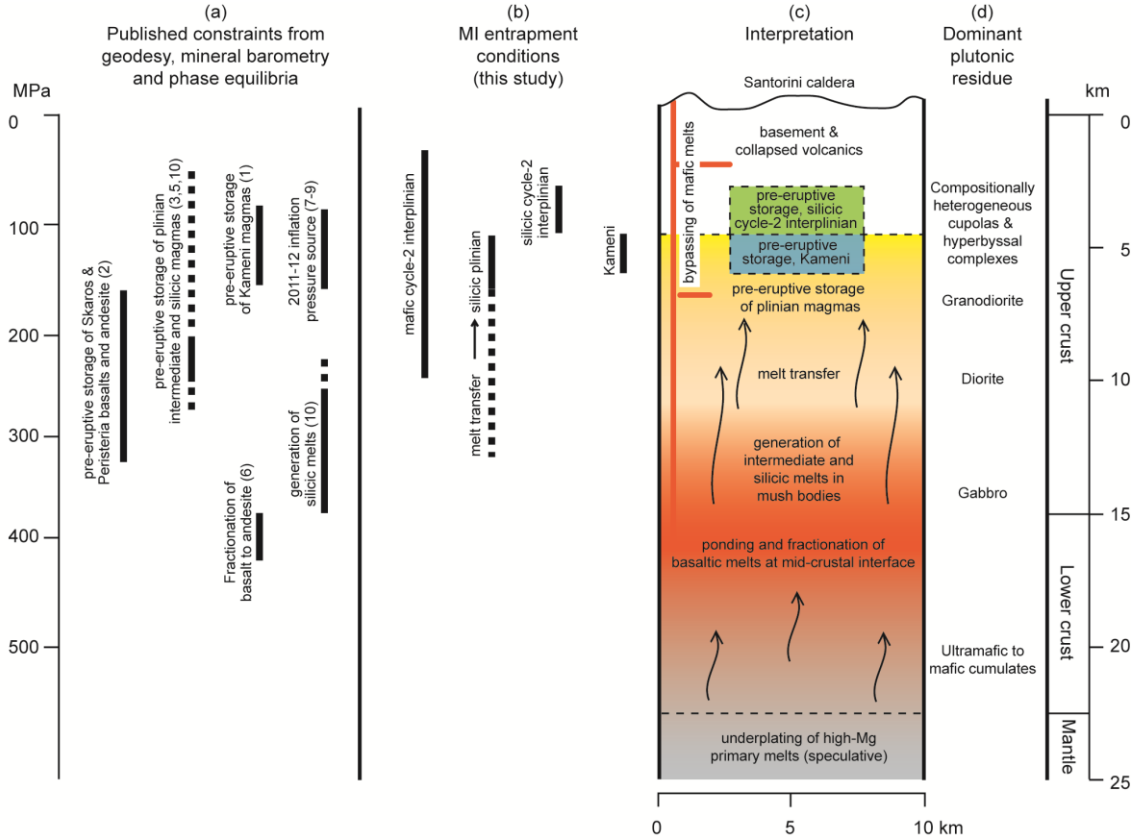

Figure 76. The magma storage system beneath Santorini (Druitt et al. submitted).

interplinian eruptions. The historically active Kameni Volcano is fed from one or more bodies of dacitic magma at 4-6 km within the largely crystallized remains of the Minoan reservoir (Fig. 76).

COMPOSITIONAL ZONING PATTERNS

The pyroclastic deposits of Santorini formed by eruption of water-rich silicic to intermediate magmas, with subordinate mafic components. Of the twelve main eruptions, ten exhibit some degree of chemical heterogeneity and/or zoning (Figs. 77 and 78). Two types of zoning are distinguished: (1) eruptions of predominantly silicic magma, with small amounts of mafic magma, that terminate each explosive cycle (Lower Pumice 1 – Lower Pumice 2; Cape Riva – Minoan), and (2) eruptions of predominantly dacitic-andesitic composition with relatively small compositional gaps (Fig. 77).

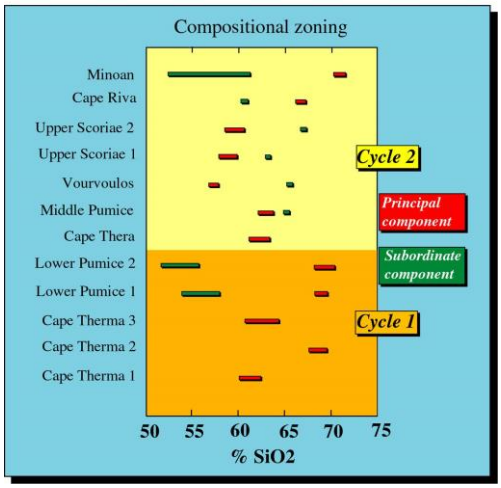

Figure 77. Compositional zoning in different eruptions of the pyroclastic succession (Druitt et al. 1999).

Pyroclastic eruptions of dominantly silicic composition

Each of these four eruptions is dominated by silicic pumice that displays only slight compositional spread beyond analytical error. In each case there is also a subordinate component of andesite or basalt. In Lower Pumice 1 the andesitic component appeared towards the end of the eruption and increased in abundance with time, as expected from the progressive tapping of a two-layer magma chamber. In Lower Pumice 2, Cape Riva and Minoan, andesite or basalt was erupted during the Plinian phase, but was absent during subsequent phases (Fig. 78), perhaps due to changes in vent configuration and withdrawal geometry during caldera collapse (Fig. 35).

Basaltic and andesitic scoria in the Lower Pumice 2 and Minoan deposits have distinctive cauliform surfaces, tabular shapes and microlitic groundmasses, possibly due to mingling and quenching at the mafic margins of composite dykes. They contain abundant fragments of cumulate gabbro and cognate crystal mush ripped up and entrained in andesitic liquids during magma chamber replenishment.

Cape Riva andesite has a disequilibrium phase assemblage caused by mixing of basaltic andesite into the host rhyodacite. Banded pumices occur abundantly in this deposit. Interbanding was probably syneruptive because the contacts between different magmas are sharp on the scale of the electron probe.

Pyroclastic eruptions of dominantly intermediate magma

The other pyroclastic units are characterized by large volumes of dacitic or andesitic magma. All except the Cape Thera Tuff contain two pumice types, the less evolved of the two being volumetrically dominant in

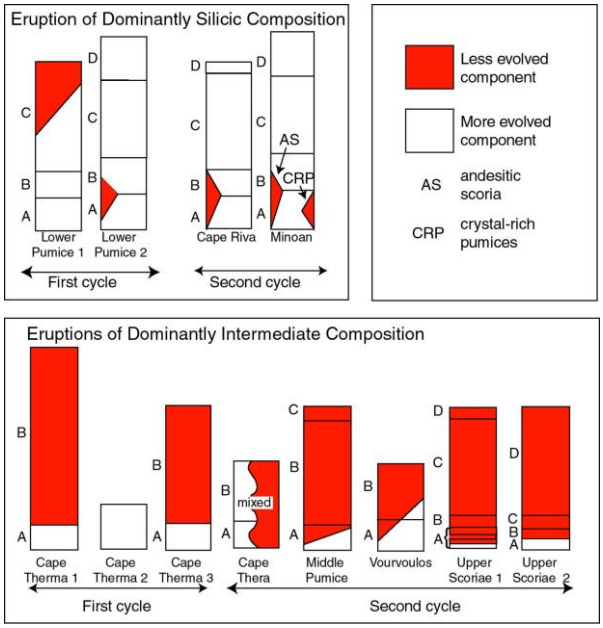

Figure 78. Compositional zoning patterns in different eruptions of the pyroclastic succession (Druitt et al. 1999).

each case. Compositional zoning is always of normal type; each eruption discharged first dacite, then a larger volume of less evolved dacite or andesite. The parent magma reservoirs are inferred to have contained a thin layer of lighter, more evolved magma overlying a larger volume of less evolved magma.

TIMESCALES OF MAGMATIC CYCLES

The magmatic cyclicity occurs on three timescales.

- Two long-term cycles are recognized in the pyroclastic sequence, each lasting about 170 ky. Each one started with a series of broadly andesitic eruptions, and terminated with a pair of large, dominantly silicic eruptions (Fig. 14).

- Individual pyroclastic units of the two 170 ky cycles alternate with lavas and associated interplinian tephra horizons. This alternation defines a second type of cycle of duration 20-40 ky in which large explosive eruptions are followed by prolonged periods of lava effusion, and the construction of cones and shields, until the next large explosive event. Construction of the Skaros lava shield following the Upper Scoria 1 explosive eruption lasted ~12 ky. Once the shield had reached ~300 m above present sea level, stresses exerted by the edifice on the plumbing system initiated repose, differentiation, and buildup to the next explosive eruption. The Kameni Islands are a modern, immature analogue of Skaros.

- Shorter-term compositional cycles occur within the lava sequences (Figs. 79 and 80). The Skaros shield contains three cycles, probably related to the repeated emptying and refilling of magma reservoirs (Huijsmans 1985).

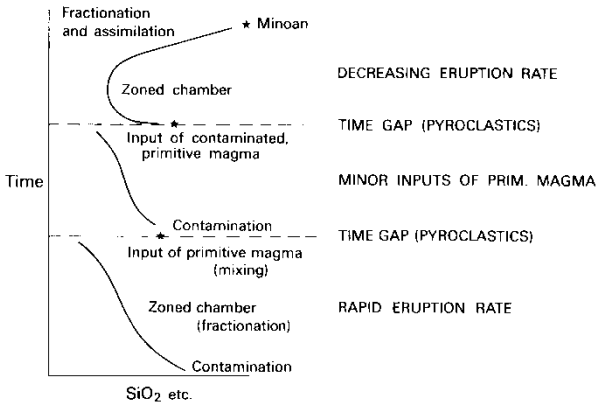

Figure 79. Schematic variation of SiO2 in the Skaros lava pile, with interpretation (Huijsmans 1985).

TIMESCALES OF MAGMA CHAMBER ASSEMBLY

Silicic melts at Santorini are generated in the lower to middle crust, then transferred as potentially eruptible batches to the upper crust (Fig. 76). New studies have placed constrains on the timescales of melt transfer and construction of upper crustal silicic magma chambers.

Therasia – Cape Riva

The Therasia and Cape Riva dacitic magmas are similar in their major element compositions (apart from K), so that the slow effusion of the Therasia lavas over 24 ky (from 48 to 24 ka) was previously interpreted as 'precursory leaks' from the growing 22 ka Cape Riva magma chamber (Druitt 1985). However, the two dacite series differ in their incompatible element contents and are unrelated by shallow processes. They are interpreted as distinct batches of silicic magma from depth (Fabbro et al. 2013). The jump in trace elements from Therasia to Cape Riva represents one increment in the long-term temporal depletion of incompatibles at the volcano (Fig. 69). Therasia lavas are about 2 km^3 and the Cape Riva at least 10 km^3 DRE. The last Therasia lava was erupted 2800 ± 1400 y prior to Cape Riva (Fig. 80), so that the >10 km^3 of incompatible-depleted dacite ascended into the upper crust in that time period at >0.004 km^3/y. Diffusion profiles of Mg in plagioclase and Mg-Fe in opx in Cape Riva dacite are consistent with a major growth phase of the Cape Riva chamber on timescales of only decades to years prior to the eruption (Fabbro 2014).

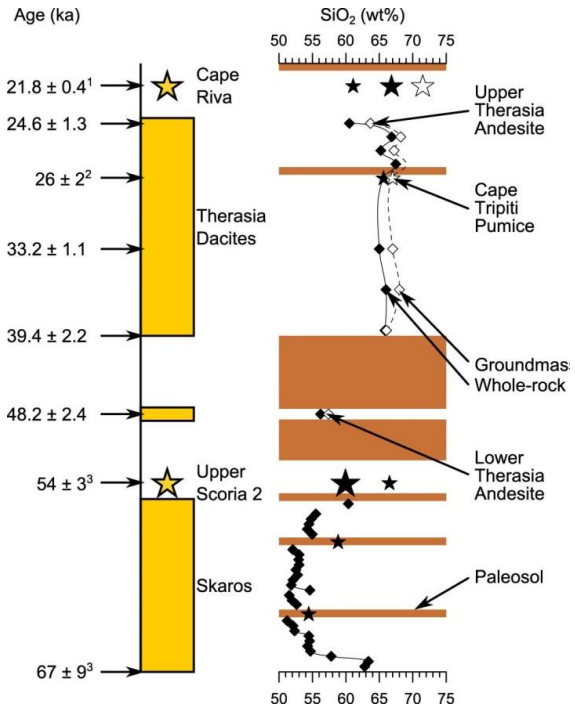

Figure 80. Compositional variations in the Skaros and Therasia lavas. Timescales of events leading up to the Cape Riva eruption at 21.8 ka (Fabbro et al. 2013).

Minoan

The Minoan eruption discharged three magma types: (1) the dominant crystal-poor rhyodacite, (2) a microphenocryst-rich andesitic pumice, and (3) mush-contaminated grey cauliform andesitic scoria. The two andesitic components derive from a radiogenic, high-Ba, low-Zr andesitic magma that is genetically unrelated to the rhyodacite (Figs. 81 and 82).

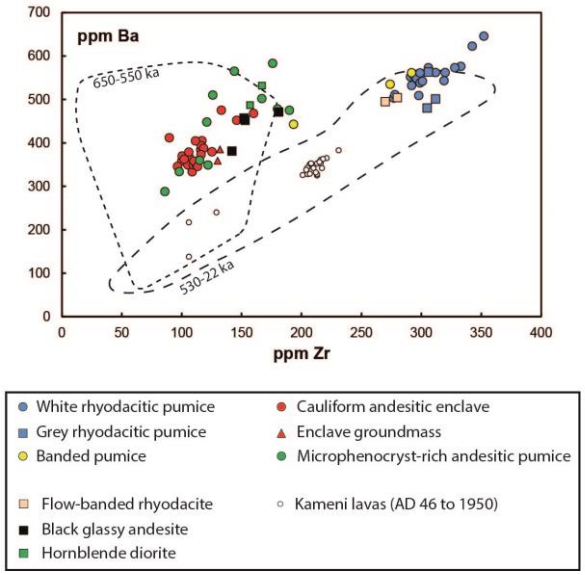

Figure 81. Ba-Zr plot of different components of the Minoan eruption (Druitt 2014).

The microphenocryst-rich pumice and associated plutonic nodules represent the contents of a shallow, variably crystallized intrusion, that was pushed out by the ascending rhyodacite, which probably exploited its pathway to reach the surface.

Plagioclase phenocrysts in the Minoan rhyodacite have cores of $An_{50\pm7}$ mantled by rims of $An_{40\pm3}$ (Cottrell et al., 1999; Druitt et al., 2012). Melt inclusions in the cores contain 6-7 wt% H_2O, whereas those in the rims contain 4-5 wt %. The cores derive from 10-12 km, and were then overgrown by the rims in a main pre-eruptive storage level at 4-6 km. Druitt et al. (2012) used Mg-in-plagioclase diffusion chronometry to show that this occurred within a few decades to a few months of the eruption.

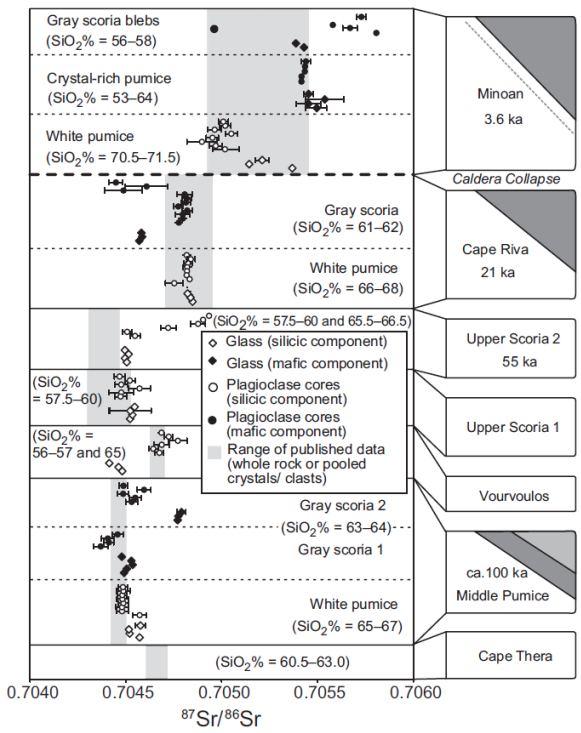

Figure 82. Single-crystal Sr isotopic data, showing the three isotopically distinct magmas of the Minoan products (Martin et al. 2010).

The data suggest that the upper crustal magma chamber underwent a major growth pulse in the few decades prior to eruption (Druitt et al. 2012) (Fig. 83). Mg-Fe diffusion profiles in opx give similar timescales (Flaherty 2015), yielding a story similar to that for the Cape Riva eruption.

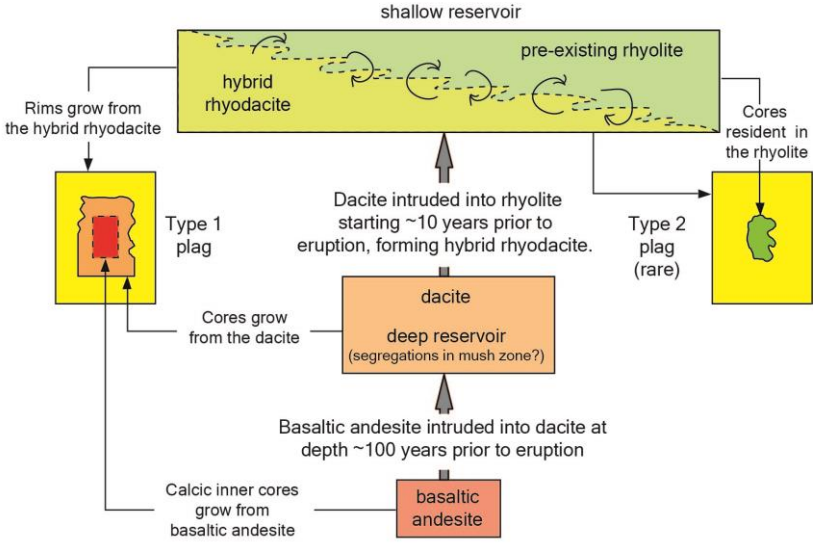

Figure 83. Interpretation of events leading up to the Minoan eruption (Druitt et al. 2012).

THE KAMENI MAGMATIC SYSTEM

The Kameni products are mainly dacitic lavas including different types of basaltic to andesitic magmatic enclaves (Fig. 84), varying from <1 cm to about 50 cm in diameter. Dacitic pumices related to the subplinian eruption of 726 AD are banded and contain mafic micro-enclaves.

Lavas contain 4-17 vol% phenocrysts of plagioclase (70-85 vol% on total phenocrysts; mainly An_{35-55}), clinopyroxene (Mg# = Mg/(Mg+Fe+Mn) = 0.43-0.74),

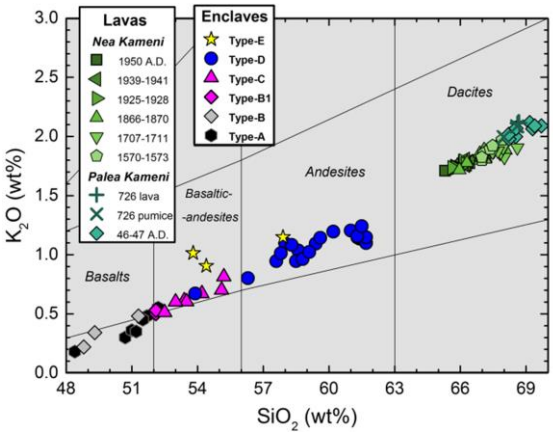

Figure 84. K_2O-SiO_2 classification diagram for Palea- and Nea Kameni mafic enclaves and relative host rocks (mainly lavas, except for the 726 pumices). Data are plotted on water-free bases.

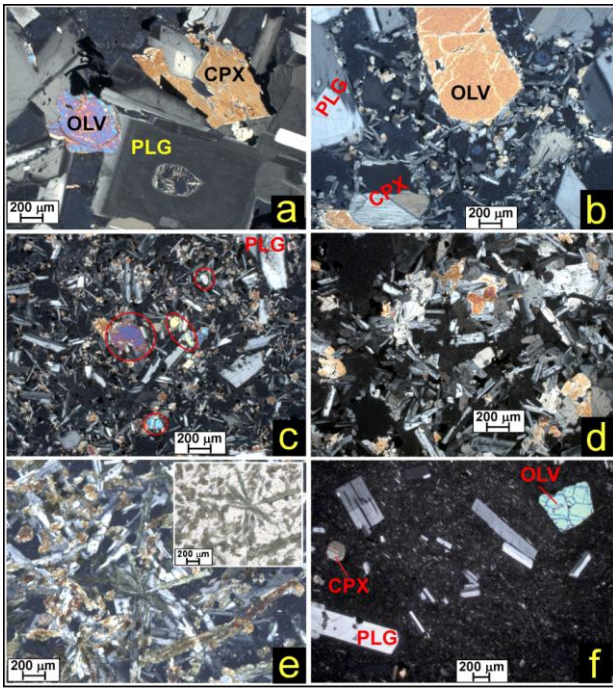

Figure 85. Photographs of the Kameni products in thin section. a) Type-A, b) Type-B, c) Type-C, d) Type-D, e) Type-E enclaves, f) 1925 lava (an olv xenocryst is shown). Pictures are taken under crossed polars, except for the inset photo in Type-E that is in plane-polarized light. Some crystals are named as examples: OLV, olivine; CPX, clinopyroxene; PLG, plagioclase. The mineral assemblages (phenocrysts and groundmass) of Type-C is olv + cpx + plg: some OLV crystals are red circled. In (d) and (e) plg + pyroxenes (green cpx in Type-E) are shown.

orthopyroxene (Mg# = 0.43-0.70), Ti-magnetite and ilmenite, with some xenocrysts of olivine (Fig. 85f). The whole-rock SiO_2 content ranges from 65 to 70 wt% decreasing from the 46-47 to 1950 lavas, with only some oscillations towards more evolved compositions (Fig. 84). A similar behaviour with time is observed for the other major and trace elements (Fig. 86) (Barton and Huijsmans, 1986; Francalanci et al., 1998).

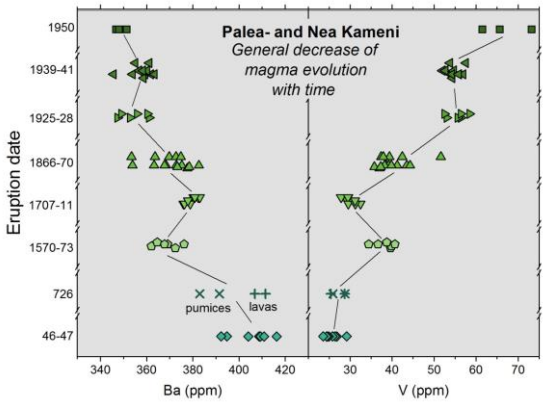

Figure 86. Variation with time of Ba and V contents in the Kameni lavas and pumices.

Most of the mafic enclaves have rounded shapes, with diktytaxitic vesicular groundmasses and frequent chilled margins, thus indicating they represent chilled portions of mafic magmas intruded and rapidly crystallized in contact with the cooler, more-silicic host magmas (Conticelli et al., 1998; Francalanci et al., 1998; Martin et al., 2006).

Six types of enclaves can be recognised on the bases of their different textural, mineralogical and chemical characteristics (Conticelli et al., 1998).

- Type-A basaltic enclaves are cumulates of olivine, pyroxenes, plagioclase and opaques with a crystal content > 80 vol% (Figs. 85a).
- Type-B basaltic enclaves are variably porphyritic (PI: 25-75 vol%), characterized by large resorbed xenocrysts of olivine, pyroxene and plagioclase representing fragments from disrupted gabbroic or troctolitic cumulates (Fig. 85b).
- Type-B1 is similar to the previous type, but with olivine among the groundmass crystals.
- Type-C basaltic-andesitic enclaves are porphyritic (PI: 5-30 vol%) with generally small (<1 mm) and zoned phenocrysts of clinopyroxene + plagioclase + skeletal olivine ± orthopyroxene and with olivine among the groundmass crystals (Fig. 85c).
- Type-D andesitic enclaves are nearly aphyric with different proportions of elongate plagioclase and pyroxene microlites (Fig. 85d).
- Type-E basaltic-andesitic to andesitic enclaves are slightly porphyritic with groundmasses mainly formed by elongate green clinopyroxene and plagioclase microlites and minor amounts of wollastonite resorbed xenocrysts (Fig. 85e).

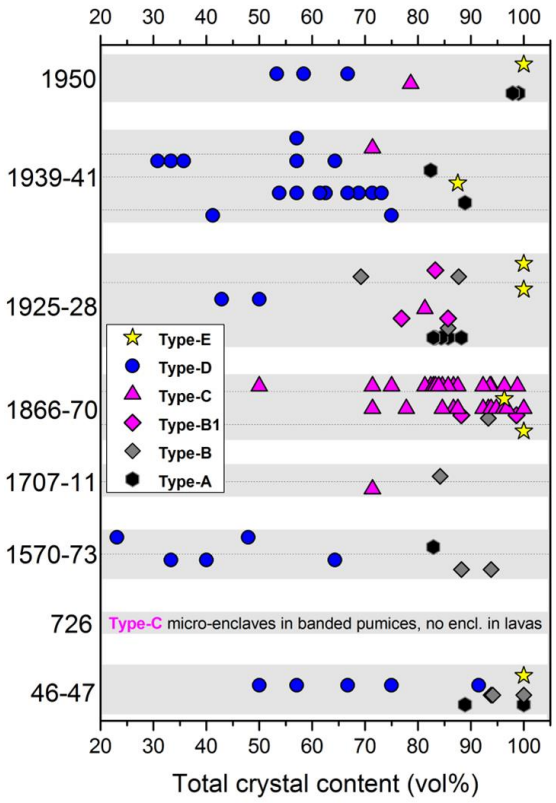

Figure 87. Distribution of the different enclave types in the products of all the subaerial Kameni eruptive events, with reported the enclave total crystal content variation (recalculated without vesicularity). Dashed horizontal lines divide the successive lavas of a single event.

Enclaves are variably distributed inside products of the different eruptive events (Fig. 87). The most common enclaves are those of Type-D (Martin et al. (2006), although they are lacking in the 1707-11 and 1866-70 lavas; the latter lavas, on the other hand, mainly contain Type-C enclaves (Francalanci et al., 1998).

Temperatures and crystallization depth of Kameni magmas were estimated on the bases of several geothermobarometers. Lavas show lower temperatures (970-1020 °C, similar to those directly measured during 1925-28 lava effusion; Washington, 1926) than mafic enclaves (1020-1150 °C) (Barton and Huijsmans, 1986; Conticelli et al., 1998). Slightly lower temperatures (900-930 °C) were found by touching mt-ilm pairs in AD 726 pumice (Druitt, 2014). Barton and Huijsmans (1986) estimated the reservoir depth at 2-4 km, whereas Druitt et al. (submitted) calculated reservoir depths of 3.9-6.2 km, based on H_2O + CO_2 contents of melt inclusions in the same pumices.

$^{87}Sr/^{86}Sr$ values increase with time both in lavas (0.70460–0.70482) and enclaves (0.70453–0.70490), with the exception of Type-E enclaves, having much higher $^{87}Sr/^{86}Sr$ values. $^{143}Nd/^{144}Nd$ negatively correlate with Sr-isotopes. The isotopic variations in mafic enclaves are ascribed to a small amount of limestone assimilation, whereas those in host lavas are due to interaction (mixing/mingling) between dacitic magmas and enclave melts (Francalanci et al., 1998).

Plagioclase residence times in dacitic magmas, estimated by Sr diffusion dating, are less than 100-450 y (Zellmer et al. 1999). Analysis of Mg-Fe diffusion profiles in olivine suggest that mingling of the mafic enclave magma into the host dacite took place 20-60 days prior to onset of the 1925-28 eruption (Martin et al. 2008).

The data are consistent with two hypotheses on the plumbing system dynamics. One hypothesis proposes the successive injection of small volumes of dacitic magma, with entrained enclaves, into the upper crust. Phenocrysts grow during vapour-saturated decompression during ascent. Each batch then either erupts or crystallizes at depth. Eruption follows several months to decades after arrival in the upper crust. The other model envisages a long-lived, upper-crustal volume of dacite that is periodically recharged by mafic magma, forming a zoned reservoir at the base. The unrest of 2011-12 may have been due to an injection of dacitic magmas (Parks et al. 2012), mafic magma (Rizzo et al. 2015), or both that then failed to cause eruption.

Books and geological map

Doumas, C.G. (1983). Thera. Pompeii of the ancient Aegean. Thames and Hudson, London, 168pp.

Druitt, T.H., Edwards, L., Mellors, R.M., Pyle, D.M., Sparks, R.S.J., Lanphere, M., Davies, M. and Barriero, B. (1999). Santorini Volcano. Geological Society of London Memoir 19: 165 pp.

Druitt, T.H. and Davies, M.A. (1999). Geological map of the Santorini Islands, Aegean Sea, Greece. Scale 1:20,000. In: Druitt, T.H., Edwards, L., Davies, M., Lanphere, M.A., Mellors, R., Pyle, D., Sparks, R.S.J. and Barreiro, B (1999). Santorini Volcano. Memoir of the Geological Society of London 19, 176 pp.

Fouqué F. (1879) Santorini and its eruptions (English translation, by A.R. McBirney), John Hopkins, 495pp.

Friedrich, W.L. (2000). Fire in the Sea: The Santorini Volcano. Cambridge University Press, 272 pp.

Manning, S.W. (1999). A test of time. The volcano of Thera and the chronology and history of the Aegean and east Mediterranean in the mid second millenium BC. Oxbow Books, Oxford, 494pp.

Thera and the Aegean World I (1978), C. Doumas (Ed.), London, 823p

Thera and the Aegean World II (1980), C. Doumas (Ed.), London, 427p

Thera and the Aegean World III (1990), Volume 2, Hardy D.A. (Ed.), The Thera Foundation, London, 487p

Vougioukalakis, G. (2005). Blue Volcanoes: Santorini. Geothira SA.

Geophysics and tectonics

Benetatos, C., Kiratzi, A., Papazachos, C. and Karakaisis, G. (2004). Focal mechanisms of shallow and intermediate depth earthquakes along the Hellenic arc. Journal of Geodynamics, 37(2):253–296. doi:10.1016/j.jog.2004.02.002.

Bohnhoff, M., Rische, M., Meier, T., Becker, D., Stavrakakis, G. and Harjes, H. (2006). Microseismic activity in the Hellenic Volcanic Arc, Greece, with emphasis on the seismotectonic setting of the Santorini-Amorgos zone. Tectonophysics, 423(1-4):17–33 doi:10.1016/j.tecto.2006.03.024.

Dimitriadis, I., Karagianni, E., Panagiotopoulos, D., Papazachos, C., Hatzidimitriou, P., Bohnhoff, M., Rische, M. and Meier, T. (2009). Seismicity and active tectonics at Coloumbo reef (Aegean Sea, Greece): Monitoring an active volcano at Santorini volcanic center using a temporary seismic network. Tectonophysics, 465(1-4):136–149. doi:10.1016/j.tecto.2008.11.005.

Dimitriadis, I., Papazachos, C., Panagiotopoulos, D., Hatzidimitriou, P., Bohnhoff, M., Rische, M. and Meier, T. (2010). P and S velocity structures of the Santorini–Coloumbo volcanic system (Aegean Sea, Greece) obtained by non-linear inversion of travel times and its tectonic implications. Journal of Volcanology and Geothermal Research, 195(1):13–30. doi:10.1016/j.jvolgeores.2010.05.013.

Feuillet, N. (2013). The 2011–2012 unrest at Santorini rift: Stress interaction between active faulting and volcanism. Geophysical Research Letters, 40(14):3532–3537. doi:10.1002/grl.50516.

Floyd, M. A., Billiris, H., Paradissis, D., Veis, G., Avallone, A., Briole, P., McClusky, S., Nocquet, J., Palamartchouk, K., Parsons, B. and England, P. C. (2010). A new velocity field for Greece: Implications for the kinematics and dynamics of the Aegean. Journal of Geophysical Research, 115(B10):B10403. doi:10.1029/2009JB007040.

Jackson, J. (1994). Active tectonics of the Aegean region. Annual Review of Earth and Planetary Sciences, 22(1):239–271. doi:10.1146/annurev.ea.22.050194.001323.

Jolivet, L. and Brun, J.-P. (2010). Cenozoic geodynamic evolution of the Aegean. International Journal of Earth Sciences, 99(1):109–138. doi:10.1007/s00531-008-0366-4.

Jolivet, L. and Faccenna, C. (2000). Mediterranean extension and the Africa-Eurasia collision. Tectonics, 19(6):1095–1106. doi:10.1029/2000TC900018.

Jolivet, L., Faccenna, C., Huet, B., Labrousse, L., Le Pourhiet, L., Lacombe, O., Lecomte, E., Burov, E., Denèle, Y., Brun, J.-P., Philippon, M., Paul, A., Salaün, G., Karabulut, H., Piromallo, C., Monié, P., Gueydan, F., Okay, A. I., Oberhänsli, R., Pourteau, A., Augier, R., Gadenne, L. and Driussi, O. (2013). Aegean tectonics: Strain localisation, slab tearing and trench retreat. Tectonophysics, 597–598:1–33. doi:10.1016/j.tecto.2012.06.011.

Karagianni, E. E. and Papazachos, C. B. (2007). Shear velocity structure in the Aegean region obtained by joint inversion of Rayleigh and Love waves. Geological Society, London, Special Publications, 291(1):159–181. doi:10.1144/SP291.8.

Karagianni, E. E., Papazachos, C. B., Panagiotopoulos, D. G., Suhadolc, P., Vuan, A. and Panza, G. F. (2005). Shear velocity structure in the Aegean area obtained by inversion of Rayleigh waves. Geophysical Journal International, 160(1):127–143. doi:10.1111/j.1365-246X.2005.02354.x.

Konstantinou, K. I. (2010). Crustal rheology of the Santorini–Amorgos zone: Implications for the nucleation depth and rupture extent of the 9 July 1956 Amorgos earthquake, southern Aegean. Journal of Geodynamics, 50(5):400–409. doi:10.1016/j.jog.2010.05.002.

Le Pichon, X. and Angelier, J. (1979). The Hellenic arc and trench system: A key to the neotectonic evolution of the eastern Mediterranean area. Tectonophysics, 60(1-2):1–42. doi:10.1016/0040- 1951(79)90131-8.
Lister, G. S., Banga, G. and Feenstra, A. (1984). Metamorphic core complexes of Cordilleran type in the Cyclades, Aegean Sea, Greece. Geology, 12(4):221–225. doi:10.1130/0091-7613(1984)12<221:MCCOCT>2.0.CO;2.
Nocquet, J.-M. (2012). Present-day kinematics of the Mediterranean: A comprehensive overview of GPS results. Tectonophysics, 579:220–242. doi:10.1016/j.tecto.2012.03.037.
Nyst, M. and Thatcher, W. (2004). New constraints on the active tectonic deformation of the Aegean. Journal of Geophysical Research, 109:B11406. doi:200410.1029/2003JB002830.
Okal, E. A., Synolakis, C. E., Uslu, B., Kalligeris, N. and Voukouvalas, E. (2009). The 1956 earthquake and tsunami in Amorgos, Greece. Geophysical Journal International, 178(3):1533–1554. doi:10.1111/j.1365-246X.2009.04237.x.
Papadopoulos, G. A. and Pavlides, S. B. (1992). The large 1956 earthquake in the south Aegean: Macroseismic field configuration, faulting and neotectonics of Amorgos island. Earth and Planetary Science Letters, 113(3):383–396. doi:16/0012-821X(92)90140-Q.
Papazachos, B. C. and Panagiotopoulos, D. G. (1993). Normal faults associated with volcanic activity and deep rupture zones in the southern Aegean volcanic arc. Tectonophysics, 220(1-4):301–308. doi:16/0040-1951(93)90237-E.
Papazachos, B. C., Karakostas, V. G., Papazachos, C. B. and Scordilis, E. M. (2000). The geometry of theWadati-Benioff zone and lithospheric kinematics in the Hellenic arc. Tectonophysics, 319(4):275–300. doi:10.1016/S0040-1951(99)00299-1.
Papazachos, C. and Nolet, G. (1997). P and S deep velocity structure of the Hellenic area obtained by robust nonlinear inversion of travel times. Journal of Geophysical Research, 102(B4):8349–8367. doi:199710.1029/96JB03730.
Pearce, F. D., Rondenay, S., Sachpazi, M., Charalampakis, M. and Royden, L. H. (2012). Seismic investigation of the transition from continental to oceanic subduction along the western Hellenic Subduction Zone. Journal of Geophysical Research, 117(B7):B07306. doi:10.1029/2011JB009023.
Piper DJW, Perissoratis C (2003) Quaternary neotectonics of the South Aegean arc. Marine Geology 198: 259–288.
Reilinger, R., McClusky, S., Paradissis, D., Ergintav, S. and Vernant, P. (2010). Geodetic constraints on the tectonic evolution of the Aegean region and strain accumulation along the Hellenic subduction zone. Tectonophysics, 488(1-4):22–30. doi:10.1016/j.tecto.2009.05.027.
Reilinger, R., McClusky, S., Vernant, P., Lawrence, S., Ergintav, S., Cakmak, R., Ozener, H., Kadirov, F., Guliev, I., Stepanyan, R., Nadariya, M., Hahubia, G., Mahmoud, S., Sakr, K., ArRajehi, A., Paradissis, D., Al-Aydrus, A., Prilepin, M., Guseva, T., Evren, E., Dmitrotsa, A., Filikov, S. V., Gomez, F., Al-Ghazzi, R. and Karam, G. (2006). GPS constraints on continental deformation in the Africa-Arabia-Eurasia continental collision zone and implications for the dynamics of plate interactions. Journal of Geophysical Research, 111:26 PP. doi:200610.1029/2005JB004051.
Tirel, C., Gueydan, F., Tiberi, C. and Brun, J.-P. (2004). Aegean crustal thickness inferred from gravity inversion. Geodynamical implications. Earth and Planetary Science Letters, 228(3-4):267– 280. doi:10.1016/j.epsl.2004.10.023.
Zhu, L., Mitchell, B. J., Akyol, N., Cemen, I. and Kekovali, K. (2006). Crustal thickness variations in the Aegean region and implications for the extension of continental crust. Journal of Geophysical Research, 111(B1), B01301. doi:10.1029/2005JB003770

General geology and eruption dynamics

Asku, A. E., Jenner, G., Hiscott, R. N. and Isler, E. B. (2008). Occurrence, stratigraphy and geochemistry of Late Quaternary tephra layers in the Aegean Sea and the Marmara Sea. Marine Geology, 252(3-4):174–192. doi:10.1016/j.margeo.2008.04.004.
Bardot L (2000) Emplacement temperature determinations of proximal pyroclastic deposits on Santorini, Greece and their implications. Bulletin of Volcanology 61: 450–467
Bardot, L. and McClelland, E. (2000). The reliability of emplacement temperature estimates using palaeomagnetic methods: a case study from Santorini, Greece. Geophysical Journal International, 143(1), 39–51. doi:10.1046/j.1365-246x.2000.00186.x
Budetta, G., Condarelli, D., Fytikas, M., Kolios, N., Pascare, G., Rapolla, A. and Pinna, E. 1984. Geophysical prospecting on the Santorini Islands. Bulletin of Volcanology. 47, 447-466
Davis, E.N. and Bastas, C. (1980). Petrology and geochemistry of the metamorphic system of Santorini. Thera and the Aegean World II , C. Doumas (Ed.), London: 61-79

Druitt T.H. and Sparks R.S.J. (1982) A proximal ignimbrite breccia facies on Santorini, Greece Journal of Volcanology and Geothermal Research 13: 147-171
Druitt T.H., Mellors R.A., Pyle D.M. and Sparks R.S.J. (1989). Explosive volcanism on Santorini, Greece. Geological Magazine 126: 95-126.
Druitt, T. H. (1985). Vent evolution and lag breccia formation during the Cape Riva eruption of Santorini, Greece. The Journal of Geology, 93(4):439–454. doi:10.1086/628965.
Druitt, T. H. and Francaviglia, V. (1992). Caldera formation on Santorini and the physiography of the islands in the late Bronze Age. Bulletin of Volcanology, 54(6):484–493 doi:10.1007/BF00301394.
Gardner, J.E., Thomas, R.M.E., Jaupart, C. and Tait, S.R. (1996). Fragmentation of magma during Plinian volcanic eruptions. Bulletin of Volcanology 58, 144-162.
Keller, J., Ryan, W. B. F., Ninkovich, D. and Altherr, R. (1978). Explosive volcanic activity in the Mediterranean over the past 200,000 yr as recorded in deep-sea sediments. Geological Society of America Bulletin, 89(4):591–604. doi:10.1130/0016-7606(1978)89<591:EVAITM>2.0.CO;2.
Margari, V., Pyle, D. M., Bryant, C. and Gibbard, P. L. (2007). Mediterranean tephra stratigraphy revisited: Results from a long terrestrial sequence on Lesvos Island, Greece. Journal of Volcanology and Geothermal Research, 163(1-4):34–54. doi:10.1016/j.jvolgeores.2007.02.002.
Keller, J., Gertisser, R., Reusser, E. and Dietrich, V. (2014). Pumice deposits of the Santorini Lower Pumice 2 eruption on Anafi island, Greece: Indications for a Plinian event of exceptional magnitude. Journal of Volcanology and Geothermal Research, 278-279, 120–128. doi:10.1016/j.jvolgeores.2014.04.009
McClelland E.A. and Druitt T.H. (1989) Palaeomagnetic estimates of emplacement temperatures of pyroclastic deposits on Santorini, Greece Bulletin of Volcanology 51: 16-27
Mellors, R. A. and Sparks, R. S. J. (1991). Spatter-rich pyroclastic flow deposits on Santorini, Greece. Bulletin of Volcanology, 53(5):327–342. doi:10.1007/BF00280225.
Narcisi, B. and Vezzoli, L. (1999). Quaternary stratigraphy of distal tephra layers in the Mediterranean—an overview. Global and Planetary Change, 21(1-3):31–50. doi:10.1016/S0921- 8181(99)00006-5.
Pyle, D.M. and Elliot, J.R. (2010). Quantitative morphology, recent evolution and future activity of the Kameni Islands Volcano, Santorini, Greece. Geosphere 2: 253-268.
Sparks R.S.J. and Wright J.V. (1979). Welded air-fall tuffs. Geological Society of America Bulletin180: 155-166.
Vespa, M., Keller, J. and Gertisser, R. (2006). Inter-Plinian explosive activity of Santorini volcano (Greece) during the past 150,000 years. Journal of Volcanology and Geothermal Research 153, 262-286.
Wulf, S., Kraml, M., Kuhn, T., Schwarz, M., Inthorn, M., Keller, J., Kuscu, I. and Halbach, P. (2002). Marine tephra from the Cape Riva eruption (22 ka) of Santorini in the Sea of Marmara. Marine Geology, 183(1-4):131–141. doi:10.1016/S0025-3227(01)00302-4.

Minoan eruption and Bronze-Age Thera

Anadón P, Canet C, Friedrich W (2013) Aragonite stromatolitic buildups from Santorini (Aegean Sea, Greece): Geochemical and palaeontological constraints of the caldera palaeoenvironment prior to the Minoan eruption (ca 3600 yr bp). Sedimentology 60: 1128-1155
Badertscher, S., Borsato, a., Frisia, S., Cheng, H., Edwards, R. L., Tüysüz, O. and Fleitmann, D. (2014). Speleothems as sensitive recorders of volcanic eruptions – the Bronze Age Minoan eruption recorded in a stalagmite from Turkey. Earth and Planetary Science Letters, 392, 58–66. doi:10.1016/j.epsl.2014.01.041
Baillie, M.G.L. and Munro, M.A.R. 1988. Irish tree rings, Santorini and volcanic dust veils. Nature 332: 344-346
Bond A. and Sparks. R.S.J. (1976) The Minoan eruption of Santorini, Greece Journal of the Geological Society of London 132: 1-16
Bruins, H. J., MacGillivray, J. A., Synolakis, C. E., Benjamini, C., Keller, J., Kisch, H. J., Klügel, A. and van der Plicht, J. (2008). Geoarchaeological tsunami deposits at Palaikastro (Crete) and the Late Minoan IA eruption of Santorini. Journal of Archaeological Science, 35(1):191–212. doi:16/j.jas.2007.08.017.
Cadoux, A., Scaillet, B., Bekki, S., Oppenheimer, C., Druitt, T.H. (2015). Stratospheric Ozone destruction by the Bronze-Age Minoan eruption (Santorini Volcano, Greece). Scientific Reports, 5, 12243; doi: 10.1038/srep12243 (2015).
Cioni, R., Gurioli, L., Sbrana, A. and Vougioukalakis, G. (2000). Precursory phenomena and destructive events related to the Late Bronze Age Minoan (Thera, Greece) and AD 79 (Vesuvius, Italy) Plinian eruptions; inferences from the stratigraphy in the archaeological areas. Geological Society of London Special Publication 171: 123-141.

Cioni, R., Gurioli, L., Sbrana, A. and Vougioukalakis, G. (2000). Precursors to the Plinian eruptions of Thera (Late Bronze Age) and Vesuvius (AD 79): Data from archaeological areas. Physics and Chemistry of the Earth, Part A: Solid Earth and Geodesy, 25(9-11):719–724. doi:10.1016/S1464- 1895(00)00111-3.

Cottrell, E., Gardner, J.E. and Rutherford, M.J. (1999). Petrologic and experimental evidence for the movement and heating of the pre-eruptive Minoan rhyodacite (Santorini, Greece). Contributions to Mineralogy and Petrology 135: 315-331.

Dominey-Howes, D. (2004). A re-analysis of the Late Bronze Age eruption and tsunami of Santorini, Greece and the implications for the volcano-tsunami hazard. Journal of Volcanology and Geothermal Research 130 : 107-132.

Druitt T.H. and Francaviglia V. (1992) Caldera formation on Santorini and the physiography of the islands in the late Bronze Age. Bulletin of Volcanology 54: 484-493

Druitt TH, Sparks RSJ (1982) A proximal ignimbrite breccia facies on Santorini, Greece. Journal of Volcanology and Geothermal Research 13: 147-171

Druitt, T. H., Costa, F., Deloule, E., Dungan, M. and Scaillet, B. (2012). Decadal to monthly timescales of magma transfer and reservoir growth at a caldera volcano. Nature, 482(7383), 77–80. doi:10.1038/nature10706

Druitt, T.H. (2014). New insights into the initiation and venting of the Bronze-Age eruption of Santorini (Greece), from component analysis. Bulletin of Volcanology 76, 794. doi:10.1007/s00445-014-0794-x

Eriksen U, Friedrich WL, Buchardt B, Tauber H, Thomsen MS (1990) The Stronghyle caldera: geological, palaeontological and stable isotope evidence from radiocarbon dated stromatolites from Santorini. In: Hardy DA (ed.) Thera and the Aegean World III, vol 2. Thera Foundation, London, pp 139-150

Friedrich W, Kromer B, Friedrich M, Heinemeier J, Pfeiffer T, Talamo S (2006) Santorini eruption radiocarbon dated to 1627-1600 B.C. Science 312: 548

Friedrich, W. L., Eriksen, U., Tauber, H., Heinemeier, J., Rud, N., Thomsen, M. S. and Buchardt, B. (1988). Existence of a water-filled caldera prior to the Minoan eruption of Santorini, Greece. Naturwissenschaften, 75(11):567–569. doi:10.1007/BF00377720.

Goodman-Tchernov, B. N., Dey, H. W., Reinhardt, E. G., McCoy, F. and Mart, Y. (2009). Tsunami waves generated by the Santorini eruption reached Eastern Mediterranean shores. Geology, 37(10), 943–946. doi:10.1130/G25704A.1

Heiken G. and McCoy F.Jr. (1990) Precursory activity to the Minoan eruption, Thera, Greece. Thera and the Aegean World III (1990), Volume 2, Hardy D.A. (Ed.), The Thera Foundation, London 79-88

Heiken, G. and McCoy, F. (1984). Caldera development during the Minoan eruption, Thira, Cyclades, Greece. Journal of Geophysical Research, 89(B10):8441–8462. doi:10.1029/JB089iB10p08441.

Johnston EN, Phillips JC, Bonadonna C, Watson IM (2012) Reconstructing the tephra dispersal pattern from the Bronze Age eruption of Santorini using an advection–diffusion model. Bulletin of Volcanology 74 : 1485–150

Johnston, E. N., Sparks, R. S. J., Phillips, J. C. and Carey, S. (2014). Revised estimates for the volume of the Late Bronze Age Minoan eruption , Santorini , Greece. Journal of the Geological Society of London, 171, 583–590.

LaMarche, V.C. and Hirschboeck, K.K. 1984. Frost rings in trees as records of major volcanic eruptions. Nature 307: 121-126

Manning SW, Ramsey CB, Kutschera W, Higham T, Kromer B, Steier P, Wild EM (2006) Chronology for the Aegean Late Bronze Age 1700-1400 B.C. Science 312, 565–9

Manning, S.W., Ramsay, C.B., Kutschera, W., Higham, T., Kromer, B., Steier, P. and Wild, E.V. (2006). Chronology for the Aegean Late Bronze Age 1700 – 1400. Science 312 :565-569.

McClelland E, Thomas R (1990) A palaeomagnetic study of Minoan age tephra from Thera. In: Hardy DA (ed.) Thera and the Aegean World III, vol 2. Thera Foundation, London, pp 129-138.

McCoy, F. W. (2000). Tsunami Generated by the Late Bronze Age Eruption of Thera (Santorini), Greece. Pure and Applied Geophysics, 157(6-8), 1227–1256. doi:10.1007/s000240050024

Minoura, K., Imamura, F. and Kuran, U. (2000). Discovery of Minoan tsunami deposits. Geology, 59–62.

Novikova, T., Papadopoulos, G. A. and McCoy, F. W. (2011). Modelling of tsunami generated by the giant Late Bronze Age eruption of Thera, South Aegean Sea, Greece. Geophysical Journal International, 186(2), 665–680. doi:10.1111/j.1365-246X.2011.05062.x

Panagiotakopulu E, Higham T, Sarpaki A, Buckland P, Doumas C (2013) Ancient pests: the season of the Santorini Minoan volcanic eruption and a date from insect chitin. Die Naturwissenschaften, 100 : 683–689

Pareschi, M. T., Favalli, M. and Boschi, E. (2006). Impact of the Minoan tsunami of Santorini: Simulated scenarios in the eastern Mediterranean. Geophysical Research Letters, 33(18), L18607. doi:10.1029/2006GL027205

Pearce, N.J.G., Westgate, J.A., Preece, S.J., Eastwood, W.J. and Perkins, W.T. (2004). Identification of Aniakchak (Alaska) tephra in Greenland ice core challenges the 1645 BC date for Minoan eruption of Santorini. G cubed 5: 3, 10pp.
Pearson, C. L., Dale, D. S., Brewer, P. W., Kuniholm, P. I., Lipton, J. and Manning, S. W. (2009). Dendrochemical analysis of a tree-ring growth anomaly associated with the Late Bronze Age eruption of Thera. Journal of Archaeological Science, 36(6), 1206–1214. doi:10.1016/j.jas.2009.01.009
Pfeiffer T (2001) Vent development during the Minoan eruption (1640 BC) of Santorini, Greece, as suggested by ballistic blocks. Journal of Volcanology and Geothermal Research 106: 229-242
Pyle D (1997) The global impact of the Minoan eruption of Santorini, Greece. Environmental Geology 30: 59–61
Pyle DM (1990) New estimates for the volume of the Minoan eruption. In: Hardy DA (ed.) Thera and the Aegean World III, vol 2. Thera Foundation, London, pp 113-121
Scheffers, A., Kelletat, D., Vött, A., May, S. M. and Scheffers, S. (2008). Late Holocene tsunami traces on the western and southern coastlines of the Peloponnesus (Greece). Earth and Planetary Science Letters, 269(1-2), 271–279. doi:10.1016/j.epsl.2008.02.021
Sigurdsson H, Carey S, Devine JD (1990) Assessment of the mass, dynamics and environmental effects of the Minoan eruption of Santorini Volcano. In: Hardy DA (ed.) Thera and the Aegean World III, vol 2. Thera Foundation, London, pp 100-112
Sparks R.S.J. and Wilson C.J.N. (1990) The Minoan deposits: a review of their characteristics and interpretation Thera and the Aegean World III (1990), Volume 2, Hardy D.A. (Ed.), The Thera Foundation, London 89-99
Sparks R.S.J., Brazier S., Huang T.C. and Muerdter D. (1983) Sedimentology of the Minoan deep-sea tephra layer in the Aegean and Eastern Mediterranean Marine Geology 54: 131-167
Sparks RSJ, Wilson CJN (1990) The Minoan deposits: a review of their characteristics and interpretation In: Hardy DA (ed.) Thera and the Aegean World III, vol 2. Thera Foundation, London, pp 89-99
Sparks SRJ, Sigurdsson H (1977) Magma mixing: a mechanism for triggering acid explosive eruptions. Nature 267: 315-318
Sulpizio, R., Alçiçek, M. C., Zanchetta, G. and Solari, L. (2013). Recognition of the Minoan tephra in the Acigöl Basin, western Turkey: implications for inter-archive correlations and fine ash dispersal. Journal of Quaternary Science, 28(4), 329–335. doi:10.1002/jqs.2630
Taddeucci J, Wohletz KH (2001) Temporal evolution of the Minoan eruption (Santorini, Greece), as recorded by its Plinian fall deposit and interlayered ash flow beds. Journal of Volcanology and Geothermal Research 109: 299-317
Urbanski N-A (2003) Eruption dynamics during Plinian eruptions: Insights from the stratigraphic variations of deposit structures and pumice textures of the Minoan eruption (Santorini, Greece) and the Laacher See eruption (East Eifel, Germany). Unpublished dissertation, University of Kiel.
Wilson CJN, Houghton BF (1990) Eruptive mechanisms in the Minoan eruption: evidence from pumice vesicularity. In: Hardy DA (ed.) Thera and the Aegean World III, vol 2. Thera Foundation, London, pp 122-128

Historical activity and marine

Barton, M. and Huijsmans, J. P. P. (1986). Post-caldera dacites from the Santorini volcanic complex, Aegean Sea, Greece: an example of the eruption of lavas of near-constant composition over a 2,200 year period. Contributions to Mineralogy and Petrology, 94(4):472–495. doi:10.1007/BF00376340.
Bell, K. L. C., Carey, S. N., Nomikou, P., Sigurdsson, H. and Sakellariou, D. (2013). Submarine evidence of a debris avalanche deposit on the eastern slope of Santorini volcano, Greece. Tectonophysics, 597-598, 147-160.
Cantner, K., Carey, S. and Nomikou, P. (2014). Integrated volcanologic and petrologic analysis of the 1650AD eruption of Kolumbo submarine volcano, Greece. Journal of Volcanology and Geothermal Research, 269:28–43. doi:10.1016/j.jvolgeores.2013.10.004.
Carey, S., Nomikou, P., Croff Bell, K. L., Lilley, M., Lupton, J., Roman, C., Stathopoulou, E., Bejelou, K. and Ballard, R. (2013). CO2 degassing from hydrothermal vents at Kolumbo submarine volcano, Greece and the accumulation of acidic crater water. Geology, 41(9):1035–1038. doi:10.1130/G34286.1.
Chouliaras, G., Drakatos, G., Makropoulos, K. and Melis, N. S. (2012). Recent seismicity detection increase in the Santorini volcanic island complex. Natural Hazards and Earth System Science, 12(4), 859–866. doi:10.5194/nhess-12-859-2012

Condomines, M., Sigmarsson, O. and Gauthier, P. J. (2010). A simple model of 222Rn accumulation leading to 210Pb excesses in volcanic rocks. Earth and Planetary Science Letters, 293(3-4), 331–338. doi:10.1016/j.epsl.2010.02.048

Dominey-Howes, D. T. M., Papadopoulos, G. A. and Dawson, A. G. (2000). Geological and historical investigation of the 1650 Mt. Columbo (Thera island) eruption and tsunami, Aegean Sea, Greece. Natural Hazards, 21(1):83–96. doi:10.1023/A:1008178100633.

Feuillet, N. (2013). The 2011–2012 unrest at Santorini rift: stress interaction between active faulting and volcanism. Geophysical Research Letters 40, 3532-3537. doi:10.1002/grl.50516

Foumelis, M., Trasatti, E., Papageorgiou, E., Stramondo, S. and Parcharidis, I. (2013). Monitoring Santorini volcano (Greece) breathing from space. Geophysical Journal International, 193(1):161– 170. doi:10.1093/gji/ggs135.

Fytikas M, Kolios N, Vougioukalakis G (1990) Post-Minoan volcanic activity of the Santorini volcano. Volcanic hazard and risk, forecasting possibilities. In: Hardy DA (ed.) Thera and the Aegean World III, vol 2. Thera Foundation, London pp 183-198

Gregg, P. M., de Silva, S. L. and Grosfils, E. B. (2013). Thermomechanics of shallow magma chamber pressurization: Implications for the assessment of ground deformation data at active volcanoes. Earth and Planetary Science Letters, 384, 100–108. doi:10.1016/j.epsl.2013.09.040

Higgins, M.D. (1996). Magma dynamics beneath Kameni Volcano, Thera, Greece, as revealed by crystal size and shape measurements. J. Volcanol. Geotherm. Res. 70: 37-48.

Holness, M. B., Martin, V. M. and Pyle, D. (2005). Information about open-system magma chambers derived from textures in magmatic enclaves: the Kameni Islands, Santorini, Greece. Geological Magazine, 142(6):637–649. doi:10.1017/S0016756805001172.

Kilias, S. P., Nomikou, P., Papanikolaou, D., Polymenakou, P. N., Godelitsas, A., Argyraki, A., Carey, S., Gamaletsos, P., Mertzimekis, T. J., Stathopoulou, E., Goettlicher, J., Steininger, R., Betzelou, K., Livanos, I., Christakis, C., Croff Bell, K. L. and Scoullos, M. (2013). New insights into hydrothermal vent processes in the unique shallow-submarine arc-volcano, Kolumbo (Santorini), Greece. Scientific Reports, 3:2421. doi:10.1038/srep02421.

Konstantinou, K. I. (2015). Maximum horizontal range of volcanic ballistic projectiles ejected during explosive eruptions at Santorini caldera. Journal of Volcanology and Geothermal Research, 301, 107–115. doi:10.1016/j.jvolgeores.2015.05.012

Lagios, E., Sakkas, V., Parcharidis, I. and Dietrich, V. (2005). Ground deformation of Nisyros Volcano (Greece) for the period 1995–2002: Results from DInSAR and DGPS observations. Bulletin of Volcanology, 68:201–214. doi:10.1007/s00445-005-0004-y.

Martin, V. M., Holness, M. B. and Pyle, D. M. (2006). Textural analysis of magmatic enclaves from the Kameni Islands, Santorini, Greece. Journal of Volcanology and Geothermal Research, 154(1-2):89–102. doi:10.1016/j.jvolgeores.2005.09.021.

Martin, V. M., Morgan, D. J., Jerram, D. A., Caddick, M. J., Prior, D. J. and Davidson, J. P. (2008). Bang! Month-scale eruption triggering at Santorini volcano. Science, 321(5893):1178. doi:10.1126/science.1159584.

Newman, A.V., Stiros, S., Feng, L., Psimoulis, P., Moschas, F., Saltogianni, V. and others (2012). Recent geodetic unrest at Santorini Caldera, Greece. Geophysical Research Letters 39 (L06309). doi:10.1029/2012GL051286

Nomikou P, Carey S, Papanikolaou D, Croff Bell K, Sakellariou D, Alexandri M, Bejelou K (2012) Submarine volcanoes of the Kolumbo volcanic zone NE of Santorini Caldera, Greece. Global and Planetary Change 90-91: 135–151

Nomikou, P., Carey, S., Croff Bell, K. L., Papanikolaou, D., Bejelou, K., Alexandri, M., Cantner, K. and Martin, J. F. (2013a). Morphological analysis and related volcanic features of the Kolumbo submarine volcanic chain (NE of Santorini Island, Aegean Volcanic Arc). Zeitschrift für Geomorphologie, Supplementary Issues, 57(3):29–47. doi:10.1127/0372-8854/2013/S-00142.

Nomikou, P., Carey, S., Croff Bell, K. L., Papanikolaou, D., Bejelou, K., Cantner, K., Sakellariou, D. and Perros, I. (2012a). Tsunami hazard risk of a future volcanic eruption of Kolumbo submarine volcano, NE of Santorini Caldera, Greece. Natural Hazards. doi:10.1007/s11069-012-0405-0.

Nomikou, P., Papanikolaou, D., Alexandri, M., Sakellariou, D. and Rousakis, G. (2013b). Submarine volcanoes along the Aegean volcanic arc. Tectonophysics, 597-598:123–146. doi:10.1016/j.tecto.2012.10.001.

Nomikou, P., Parks, M. M., Papanikolaou, D., Pyle, D. M., Mather, T. A., Carey, S., Watts, A. B., Paulatto, M., Kalnins, M. L., Livanos, I., Bejelou, K., Simou, E. and Perros, I. (2014). The emergence and growth of a submarine volcano: The Kameni islands, Santorini (Greece). GeoResJ, 1–2:8–18. doi:10.1016/j.grj.2014.02.002.

Papoutsis, I., Papanikolaou, X., Floyd, M., Ji, K. H., Kontoes, C., Paradissis, D. and Zacharis, V. (2012). Mapping inflation at Santorini volcano, Greece, using GPS and InSAR. Geophysical Research Letters, 40, 267–272. doi:10.1029/2012GL054137

Parks, M.M., Biggs, J., England, P., Mather, T.A., Nomikou, P., Palamartchouk, K. and others (2012). Evolution of Santorini Volcano dominated by episodic and rapid fluxes of melt from depth. Nature Geoscience 5, 749–754. doi:10.1038/ngeo1562

Parks, M. M., Caliro, S., Chiodini, G., Pyle, D. M., Mather, T. a., Berlo, K., … Raptakis, C. (2013). Distinguishing contributions to diffuse CO2 emissions in volcanic areas from magmatic degassing and thermal decarbonation using soil gas 222Rn–δ13C systematics: Application to Santorini volcano, Greece. *Earth and Planetary Science Letters*, *377-378*, 180–190. doi:10.1016/j.epsl.2013.06.046

Parks, M. M., Moore, J. D. P., Papanikolaou, X., Biggs, J., Mather, T. a, Pyle, D. M., … Nomikou, P. (2015). From quiescence to unrest: 20years of satellite geodetic measurements at Santorini volcano, Greece. *Journal of Geophysical Research*, 1–20. doi:10.1002/2014JB011540.

Pyle, D.M. and Elliott, J.R. (2006). Quantitative morphology, recent evolution and future activity of the Kameni Islands volcano, Santorini, Greece. Geosphere 2, 253-268.

Rizzo, A. L., Barberi, F., Carapezza, M. L., Di Piazza, A., Francalanci, L., Sortino, F. and D'Alessandro, W. (2015). New mafic magma refilling a quiescent volcano: Evidence from He-Ne-Ar isotopes during the 2011–2012 unrest at Santorini, Greece. Geochemistry, Geophysics, Geosystems, 16(3), 798–814. doi:10.1002/2014GC005653.Received

Sakellariou, D., Sigurdsson, H., Alexandri, M., Carey, S., Rousakis, G., Nomikou, P., Georgiou, P. and Ballas, D. (2010). Active tectonics in the Hellenic Volcanic Arc: the Kolumbo submarine volcanic zone. Bulletin of the Geological Society of Greece, 43(2):1056–1063.

Saltogianni, V., Stiros, S. C., Newman, A. V., Flanagan, K. and Moschas, F. (2014). Time-space modelling of the dynamics of Santorini Volcano (Greece) during the 2011-2012 unrest. Journal of Geophysical Research, 119. doi:10.1002/2014JB011409.

Sigurdsson, H., Carey, S., Alexandri, M., Vougioukalakis, G., Croff, K., Roman, C., Sakellariou, D., Anagnostou, C., Rousakis, G., Ioakim, C., Gogou, A., Ballas, D., Misaridis, T. and Nomikou, P. (2006). Marine investigations of Greece's Santorini volcanic field. Eos, 87(34):337–348. doi:200610.1029/2006EO340001.

Tassi, F., Vaselli, O., Papazachos, C.B., Giannini, L., Chiodini, G., Vougioukalakis, G.E., Karagianni, E., Vamvakaris, D. and Panagiotopoulos, D. (2013). Geochemical and isotopic changes in the fumarolic and submerged gas discharges during the 2011–2012 unrest at Santorini caldera (Greece). Bulletin of Volcanology 75, 711. doi:10.1007/s00445-013-0711-8

Ulvrová, M., Paris, R., Kelfoun, K. and Nomikou, P. (2013). Numerical simulations of tsunami generated by underwater volcanic explosions at Karymskoye lake (Kamchatka, Russia) and Kolumbo volcano (Aegean Sea, Greece). Natural Hazards and Earth System Sciences Discussions, 1(6), 6399–6432. doi:10.5194/nhessd-1-6399-2013

Vougioukalakis, G.E. and Fytikas, M. (2005). Volcanic hazards in the Aegean area, relative risk evaluation, monitoring and present state of the active volcanic centers. Developments in Volcanology 7, 2005, 161–183.

General petrology and geochemistry

Andújar, J., Scaillet, B., Pichavant, M., Druitt, T.H. (2015). Differentiation conditions of a basaltic magma from Santorini and its bearing on basalt-andesite to andesite magma production in arc settings. Journal of Petrology 56, 765-794.

Andújar, J., Scaillet, B., Druitt, T.H. (submitted). Generation conditions of dacites and rhyodacites by the crystallization of an andesitic magma. Implications for the plumbing system at Santorini (Greece). Journal of Petrology.

Bailey, J.C., Jensen, E.S., Hansen, A., Kann, A.D. J. and Kann K. (2009) Formation of heterogeneous magmatic series beneath North Santorini, South Aegean island arc. Lithos 110, 20-36. doi:10.1016/j.lithos.2008.12.002

Barton, M., Salters V.J.M. and Huijsmans J.P.P. (1983) Sr isotope and trace element evidence for the role of continental crust in calc-alkaline volcanism on Santorini and Milos, Aegean Sea, Greece. Earth and Planetary Science Letters 63, 273-291. doi:10.1016/0012-821X(83)90042-0

Briqueu, L., Javoy, M., Lancelot, J. R. and Tatsumoto, M. (1986). Isotope geochemistry of recent magmatism in the Aegean arc: Sr, Nd, Hf and O isotopic ratios in the lavas of Milos and Santorini— geodynamic implications. Earth and Planetary Science Letters, 80(1-2):41–54. doi:10.1016/0012-821X(86)90018-X.

Cadoux, A., Scaillet, B., Druitt, T.H. and Deloule, E. (2014). Magma Storage Conditions of Large Plinian Eruptions of Santorini Volcano (Greece). Journal of Petrology 55, 1129-1171. doi:10.1093/petrology/egu02

Conticelli, S., Francalanci, L., Santo, A.P. and Petrone C. (1998). Petrographic, chemical and isotopic variations in the intra-caldera post-Minoan rocks of the Santorini volcanic field. Proc. second workshop, Santorini, Greece, European Commission pp157-174.

Druitt, T.H., Mercier, M., Florentin, L., Deloule, E., Cluzel, N., Medard, E., Cadoux, A. (submitted). Magma storage and extraction during plinian and interplinian periods at Santorini caldera (Greece). Journal of Petrology.

Fabbro, G. N., Druitt, T. H. and Scaillet, S. (2013). Evolution of the crustal magma plumbing system during the build-up to the 22-ka caldera-forming eruption of Santorini (Greece). Bulletin of Volcanology, 75(12):1–22. doi:10.1007/s00445-013-0767-5.

Francalanci, L., Vougioukalakis, G. and 5 others (1998). Petrographic, chemical and isotopic variations in the intra-caldera post-Minoan rocks of the Santorini volcanic field. Proceedings of the second workshop, Santorini, Greece, European Commission pp175-186.

Francalanci, L., Vougioukalakis, G.E., Perini, G. and Manetti, P. (2005). A west-east traverse along the magmatism of the south Aegean volcanic arc in the light of volcanological, chemical and isotope data. In: Fytikas, M. and Vougioukalakis, G.E. (eds) The South Aegean active volcanic arc: present knowledge and future perspectives. Developments in Volcanology, Elsevier, 65–111

Gertisser, R., Preece, K. and Keller, J. (2009). The Plinian Lower Pumice 2 eruption, Santorini, Greece: magma evolution and volatile behaviour. Journal of Volcanology and Geothermal Research 186, 387-406.

Huijsmans, J. Calc-alkaline lavas from the volcanic complex of Santorini, Aegean Sea, Greece. Geologica Ultraiectina 41, 316 pp (1985).

Huijsmans, J.P.P. and Barton, M. (1989). Polybaric Geochemical Evolution of Two Shield Volcanoes from Santorini, Aegean Sea, Greece: Evidence for Zoned Magma Chambers from Cyclic Compositional Variations. Journal of Petrology 30, 583–625. doi:10.1093/petrology/30.3.583

Huijsmans, J.P.P., Barton, M. and Salters, V.J.M. (1988). Geochemistry and evolution of the calc-alkaline volcanic complex of Santorini, Aegean Sea, Greece. Journal of Volcanology and Geothermal Research 34, 283-306. doi:10.1016/0377- 0273(88)90039-X

Mann, A.C. (1983). Trace Element Geochemistry of High Alumina Basalt- Andesite- Dacite- Rhyodacite Lavas of the Main Volcanic Series of Santorini Volcano , Greece. Contributions to Mineralogy and Petrology 395, 43–57.

Martin, V.M, Davidson, J., Morgan, D and Jerram, D.A. (2010). Using the Sr isotope compositions of feldspars and glass to distinguish magma system components and dynamics Geology 38: 539-542.

Michaud, V., Clocchiatti, R. and Sbrana, S. (2000). The Minoan and post-Minoan eruptions, Santorini (Greece), in the light of melt inclusions: chlorine and sulphur behavior. Journal of Volcanology and Geothermal Research 99, 195-214.

Mortazavi, M. and Sparks, R. S. J. (2004). Origin of rhyolite and rhyodacite lavas and associated mafic inclusions of Cape Akrotiri, Santorini: the role of wet basalt in generating calcalkaline silicic magmas. Contributions to Mineralogy and Petrology, 146(4), 397–413. doi:10.1007/s00410-003-0508-4

Nicholls I.A. (1978) Primary basaltic magmas for the pre-caldera volcanic rocks of Santorini. Thera and the Aegean World I, C. Doumas (Ed.), London: 109-120

Nicholls, I. A. (1971). Petrology of Santorini Volcano, Cyclades, Greece. Journal of Petrology, 12(1):67–119. doi:10.1093/petrology/12.1.67.

Santo, A.P. (2005). Magmatic evolution processes as recorded in plagioclase phenocrysts of Nea Kameni rocks (Santorini Volcano, Greece). Developments in Volcanology 7, 139-160.

Stamatelopoulou, K., Vlassopoulos, D., Pearce, T.H. and Rice, C. (1990). The record of magma chamber processes in plagioclase phenocrysts at Thera Volcano, Aegean volcanic arc, Greece. Contributions to Mineralogy and Petrology 104: 73-84.

Vaggelli, M., Pellegrini, M., Vougioukalakis, G., Innocenti, S. and Francalanci, I. (2009). Highly Sr radiogenic tholeiitic magmas in the latest inter-Plinian activity of Santorini volcano, Greece. Journal of Geophyical Research 114, 1-21.

Zellmer, G. F., Blake, S., Vance, D., Hawkesworth, C. and Turner, S. (1999). Plagioclase residence times at two island arc volcanoes (Kameni Islands, Santorini and Soufriere, St. Vincent) determined by Sr diffusion systematics. Contributions to Mineralogy and Petrology, 136(4):345–357. doi:10.1007/s004100050543.

Zellmer, G., Turner, S. and Hawkesworth, C. (2000). Timescales of destructive plate margin magmatism: new insights from Santorini, Aegean volcanic arc. Earth and Planetary Science Letters 174, 265-281. doi:10.1016/S0012-821X(99)00266-6